Restoring Fine Motor Prosthetic Hand Control via Peripheral Neural Technology

by

Philip Vu

A dissertation submitted in partial fulfillment
of the requirements for the degree of
Doctor of Philosophy
(Biomedical Engineering)
in The University of Michigan
2019

Doctoral Committee:

Associate Professor Cynthia A. Chestek, Chair
Assistant Professor Timothy M. Bruns
Professor R. Brent Gillespie
Associate Professor Parag G. Patil

Philip Vu

philipv@umich.edu

ORCID iD: 0000-0001-7646-7481

DEDICATION

For my family and friends

ACKNOWLEDGEMENTS

Oh man. This has been one hectic journey of many emotions. Many new emotions I did not know I was capable of feeling, but in the end everything led to one final emotion, gratitude. There are so many people to thank for their invaluable advice, inspiration, and guidance throughout my entire life leading up to this moment, so no acknowledgments section will do them justice but I will certainly give it a shot.

First, I would like to thank my family. In particular, I would like to thank my parents who have supported and continue to support me throughout my life. Their guidance and encouragement have shaped and molded the person I am today, and I will be forever grateful for their kind and loving support. I only hope that I can repay their everlasting support in kind. I would like to thank my brother, who has been a significant role model for me during my childhood. I always looked up to you for advice and how to be cool since you were already much older than me and doing cool things. I will continue to look up to you no matter how old we get.

None of this work could have been accomplish without tremendous help from my advisor, Cindy Chestek. Cindy, you have given me so much quality advice that I hope I'll be able to retain all of it. You have encouraged and driven me to achieve far greater than I could have imagined and I will always be thankful. I would also like to thank the rest of my committee, Tim Bruns, Parag Patil, Brent Gillespie, for their ongoing help and advice. I only hope to meet your expectations and continue to learn and grow from your constructive criticisms.

Second to last, I would like to thank the Chestek lab, both former and current members. All of you have made my time in the lab awesome with many moments of laughter, joy, and even

sadness. We've formed unbreakable bonds and I hope that we all see each other in the near future, hopefully at a Waffle House.

Lastly, I would like to acknowledge my family's posterity, currently living and those that have yet to be born. If you happen to come across reading this dissertation when you're older, I hope this work will inspire you to pursue work that you think is worthwhile and beneficial to humanity, but most importantly work that will bring you joy.

TABLE OF CONTENTS

LIST OF TABLES

LIST OF FIGURES

ABSTRACT

Losing a limb can drastically alter a person's way of life, and in some cases, brings great financial and emotional burdens. In particular, upper-limb amputations means losing the ability to do many daily activities that are normally simple with intact hands. Prosthesis technology has significantly advanced in the past decade to replicate the mechanical complexity of the human hand. However, current commercial user-to-prosthesis interfaces fail to provide users with full intuitive control over the many functionalities advanced prosthetic hands can offer. Research in developing new interfaces for better motor control has been on the rise, focusing on tapping directly into the peripheral nervous system. The aim of this work is to characterize and validate the properties of a novel peripheral interface called the Regenerative Peripheral Nerve Interface (RPNI) to improve fine motor skills for prosthetic hand control.

The first study characterizes the use of RPNI signals for continuous hand control in non-human primates. In two rhesus macaques, we were able to reconstruct continuous finger movement offline with an average correlation of $\rho = 0.87$ and root mean squared error (RMSE) of 0.12 between actual and predicted position across both macaques. During real-time control, neural control performance was slightly slower but maintained an average target hit success rate of 96.7% compared to physical hand control.

The second study presents the viability of the RPNI in humans who have suffered from upper-limb amputations. Three participants with transradial amputations, P1, P2 and P3, underwent surgical implantation of nine, three, and four RPNIs for the treatment of neuroma pain, respectively. In P1 and P2, ultrasound demonstrated strong contractions of P1 and P2's median

RPNIs during flexion of the phantom thumb, and of P1's ulnar RPNIs during small finger flexion. In P1, the median RPNI and ulnar RPNIs produced electromyography (EMG) signals with a signal-to-noise ratio (SNR) of 4.62 and 3.80 averaged across three recording sessions, respectively. In P2, the median RPNI and ulnar RPNI had an average SNR of 107 and 35.9, respectively, while P3's median RPNI and ulnar RPNIs had an average SNR of 22.3 and 19.4, respectively.

The final study characterizes the capabilities of RPNI signals to predict continuous finger position in human subjects. Two participants, P2 and P3, successfully hit targets during a center-out target task with 92.4 ± 2.3% accuracy, controlling RPNI-driven one DOF finger movements. Comparably, non-RPNI driven finger movement had similar accuracy and performance. Without recalibrating parameter coefficients, no decreasing trend in motor performance was seen for all one DOF finger control across 300 days for P2 and 40 days for P3, suggesting that RPNIs can generate robust control signals from day to day. Lastly, using RPNI-driven control, P2 and P3 successfully manipulated a two DOF virtual and physical thumb with 96.4 ± 2.5% accuracy.

These three studies demonstrated: (1) RPNIs provided robust continuous control of one DOF hand movement in non-human primates, an important step for human translation, (2) RPNIs were safely implemented in three participants, showing evidence of contraction and generation of EMG, and (3) in two participants, RPNIs can provide continuous control of one DOF finger movements and two DOF thumb movements. The results presented in this dissertation suggest RPNIs may be a viable option to advance peripheral nerve interfaces into clinical reality and enhance neuroprosthetic technology for people with limb loss.

CHAPTER I

Introduction

Limb loss can significantly alter a person's way of life, forcing many new physical and emotional burdens that can last a lifetime. In the United Sates alone, approximately 2 million people live with limb loss (Ziegler-Graham, MacKenzie, Ephraim, Travison, & Brookmeyer, 2008). Of the 2 million people, ~500,000 people underwent upper-extremity amputations. Many prosthetic options exist to replace upper-extremity amputations, from passive prostheses used for cosmetic purposes to active prostheses that can be controlled electronically. In fact, the past two decades have seen an expansion of more articulated, life-like prosthetic hands (DEKA LUKE arm, bebionic, i-limb ultra) in the commercial sector. However, there is not yet a proper interface for the user to actively control all functionalities of the prosthetic in a natural and intuitive manner.

Current body-powered or myoelectric controllers are limited to performing only a single hand posture or movement at a time (Roche, Rehbaum, Farina, & Aszmann, 2014). The control of multiple hand postures or movements with these basic controllers leads to unintuitive control or induces a learning curve. These complications may lead to overall reduction in use or abandonment of the prosthesis (Biddiss & Chau, 2007). The limited number of control signals is the underlying problem for users not achieving full autonomy of their prosthesis.

1.1 Prosthesis to User Interfaces

1.1.1 Commercial Myoelectric Interfaces

The human upper limb is composed of an intricate combination of muscles and tendons, providing people with fine control over their fingers or digits. Nerve fibers, specifically alpha motor neurons, innervate the muscles and send electrical pulses to induce muscle contractions. These contractions produce electromyography (EMG) signals, electrical activity emitted from muscle tissue, and are the main signal source used to control commercial myoelectric prostheses. Myoelectric prostheses technology was first introduced in the 1950s following World War II (Battye, Nightingale, & Whillis, 1955). In the most basic setup, EMG is recorded from a muscle group with one or two surface electrodes placed on the skin. The recorded activity is then used to control one or two simple movements, e.g. hand open/close, either via a discrete or continuous control scheme (details in section 1.2). This setup has been sufficiently reliable in a clinical setting (Roche et al., 2014; Schultz & Kuiken, 2011). However, commercial myoelectric interfaces are strictly limited to gross movements, and lack the ability to control multiple independent finger movements.

This limitation is due to several factors regarding the characteristics of surface electrodes. Ideally, one surface electrode records from one muscle group to control a specific finger joint or degree of freedom, providing a one to one mapping of EMG activity to finger movement. In practice, surface electrodes pick up EMG activity from multiple nearby muscle groups. Also known as cross-talk, this consequently limits the number of independent signals available for multi-functional movements. Additionally, surface EMG activity is highly sensitive to electrode shift and repositioning, which can negatively impact the performance of myoelectric control systems (Fougner, Scheme, Chan, Englehart, & Stavdahl, 2011; Young, Hargrove, & Kuiken,

2011). Other factors of influence include electrode impedance changes due to perspiration and muscle shifts relative to electrode placement (Farina et al., 2014).

Several solutions, both hardware and software, have been proposed to resolve some of these challenges mentioned above. High-density surface EMG electrodes have been shown to have feature properties robust against electrode count and shift (Muceli, Jiang, & Farina, 2014; Stango, Negro, & Farina, 2015). In terms of software, a rapid re-calibration algorithm has been proposed to alleviate electrode shift that has occurred during donning/doffing of the prosthetic limb (Prahm, Paassen, Schulz, Hammer, & Aszmann, 2017; Vidovic et al., 2016). Although these advances have shown progress in improving myoelectric technology, there still remains a fundamental problem. The number of available control sites is inversely proportional to the degree of amputation. In other words, the higher the amputation the fewer control sites. As amputation eliminates control sites, providing natural, intuitive prosthesis control becomes more difficult. In order to gain access to more control sites, interfacing directly with the peripheral nervous system is required.

1.1.2 Peripheral Nerve Interfaces

In the past two decades, many peripheral nerve interface methods have been developed in academic research. One of the reasons for this proliferation of nerve interface technology is that peripheral nerves still carry volitional commands to the intended absent limb, even decades, following amputation (Dhillon, Lawrence, Hutchinson, & Horch, 2004; Jia et al., 2007). Thus, the peripheral nerve is a rich signal source that could provide the necessary number of control sites for intuitive prosthesis control. These methods aim to record either spike waveforms, measured extracellular action potentials from alpha motor neuron fascicles, or electroneurogram (ENG) signals, activity arising from populations of alpha motor neuron fascicles. To gain access to these

types of signals, an entirely new type of electrode hardware is required. Peripheral nerve electrodes are split between two main categories, intraneural electrodes and epineural electrodes. Intraneural electrodes have contacts that penetrate into the peripheral nerve, while epineural electrodes have contacts that wrap around the surface of the nerve or just placed on top of the nerve.

The most common epineural electrode is the cuff electrode, which has two or more contacts placed around a flexible structure and wrapped around the nerve (Naples, Mortimer, Scheiner, & Sweeney, 1988; Sahin & Durand, 1998). Another epineural electrode is the flat interface nerve electrode (FINE), which wraps around and flattens the nerve so that its contacts are closer to the fascicles (Tyler & Durand, 2002). Unfortunately, ENG amplitudes are much smaller in scale compared to EMG activity (Popovic et al., 1993; Sahin, Haxhiu, Durand, & Dreshaj, 1997). Additionally, ENG faces the same problems of cross-talk as surface EMG, recording neural activity from a population of fascicles instead of just a single fascicle. To address this, beamforming algorithms have been proposed to localize and separate ENG activity (Calvetti, Wodlinger, Durand, & Somersalo, 2011; Tang, Wodlinger, & Durand, 2014; Wodlinger & Durand, 2009). More recently, these methods have been tested in chronic animal studies and show promise in separating and recovering fascicle signal sources reliably (Dweiri et al., 2017; Eggers, Dweiri, McCallum, & Durand, 2017). However, further studies are needed to determine if these methods can be translated and effectively utilized with human nerves. Overall, epineural electrodes have found more use as stimulating devices than recording devices for intuitive prosthetic control (Tan et al., 2014).

Intraneural electrodes, on the other hand, have had more success in recording higher amplitude signals because of their direct contact with the fascicles. A few examples of intraneural electrodes are the longitudinal intrafascicular electrode (LIFE; [Lawrence, Dhillon, Jensen,

Yoshida, & Horch, 2004]), transverse intrafascicular multichannel electrode (TIME; [Boretius et al., 2010]), and the Utah slanted electrode array (USEA; [Branner, Stein, & Normann, 2001]). The LIFE has been used in multiple human studies including: real-time control of grip force and elbow position, offline classification of three different grasps, and evoking sensory percepts via stimulation for object discrimination (Dhillon & Horch, 2005; Horch, Meek, Taylor, & Hutchinson, 2011; Micera et al., 2011; Rossini et al., 2010). Comparably, the TIME has been used to provide sensory feedback to human patients during a bi-directional prosthesis control task (Raspopovic et al., 2014). Similarly, the USEA has been implanted in humans up to 30 days, providing tactile sensory feedback and intuitive finger movement to amputee patients (Davis et al., 2016; Wendelken et al., 2017).

Although intraneural electrodes have been heavily tested in human subjects, their expected longevity and durability is still in question. Recent studies have reported degradation in signal amplitude and increased electrode impedance in USEAs over the course of four weeks (Davis et al., 2016; Wendelken et al., 2017). A histological analysis has shown that inserting these electrode tips into the nerve causes an inflammatory response with an increase of macrophages surrounding and attached to the device (Christensen, Wark, & Hutchinson, 2016). In other intraneural electrodes, there has been no similar reporting of signal degradation. However, these studies are also short-lived, lasting only a few weeks or less. The longest reported use of intraneural electrodes has been three months (Gasson, Hutt, Goodhew, Kyberd, & Warwick, 2005). Because of the short periods of implantation in these studies, the signal recording robustness of intraneural electrodes remains unproven.

An alternative peripheral interface, targeted muscle reinnervation (TMR; [Kuiken, Dumanian, Lipschutz, Miller, & Stubblefield, 2004]), has shown promise in the past two decades

to becoming a translatable technology into the clinical setting. TMR is a surgical technique that reroutes a transected nerve ending to a partially denervated intact muscle. After a few months, the nerve reinnervates the muscle, and the muscle can now contract normally under the efferent commands sent from the rerouted nerve. This in turn transforms the intact muscle to act as a biological amplifier for the once severed nerve, creating a new myoelectric site for prosthesis control. As reported in 2013, over 60 TMR procedures have been performed worldwide on shoulder disarticulation and transhumeral amputees (Miller, Feuser, & Kuiken, 2013). Since then, TMR continues to gain popularity as a surgical option for proximal amputee patients as it has also shown to treat neuroma and phantom limb pain (Dumanian et al., 2019). In the early days of TMR, a bilateral shoulder disarticulate amputee was able to control the elbow position, and hand open/close or wrist rotation using simultaneous proportional control (Kuiken et al., 2004). In 2007, Zhou et al. combined TMR signals with pattern recognition techniques, enabling users to control up to seven hand and arm postures (Kuiken, Li G, Lock BA, & et al, 2009; Zhou et al., 2007). More recently, a take home randomized clinical trial of eight TMR participants showed that pattern recognition control outperformed the conventional direct control (Hargrove, Miller, Turner, & Kuiken, 2017).

Although TMR has expanded the capabilities of traditional myoelectric interfaces to control more advanced prosthetic technology, the spatial distribution of the rerouted nerves is limited. The technique requires the whole nerve to be transferred to a whole muscle. At more proximal levels of amputation, the organization of fascicles in the nerve are disorganized (Delgado-Martínez, Badia, Pascual-Font, Rodríguez-Baeza, & Navarro, 2016). This prevents the different functions of the nerve to be equally distributed, and not all functions are guaranteed to be represented at the reinnervation site (Stubblefield, Miller, Lipschutz, & Kuiken, 2009). Since TMR

uses surface electrodes to record EMG signals, the maximum number of independent control sites is three, one for each nerve. This limitation is reflected in clinical practice, where users are only able to control three to four basic movements (Cheesborough, Smith, Kuiken, & Dumanian, 2015). Additionally, TMR adopts the challenges of surface electrodes mentioned previously.

These novel peripheral nerve interfaces have made great strides in improving the technology for advanced prosthesis control. However, further research must be conducted to resolve stability and longevity issues as well as increase the number of independent control sites.

1.2 Prosthesis Control methods

1.2.1 Commercial and Discrete Decoders

Building an interface that effectively extracts intuitive signals for prosthesis control represents one side of an elaborate equation. The other side is the interpretation and prediction of these signals and the user's intention. Conventional myoelectric controllers can either function in a discrete or continuous mode. In the discrete mode, a single channel or muscle group's amplitude must reach a fixed threshold to activate a single hand movement (e.g. hand open). Subsequently, the channel amplitude would then need to reach a higher fixed threshold to close the hand (Battye et al., 1955). The prosthetic hand moves at a pre-defined fixed velocity for both open and close states. This control scheme is known as on/off control, and a variant can be applied to two muscle groups (Popov, 1965). In the continuous mode, the EMG change in amplitude over time is used to control the velocity or force output of the prosthetic hand. Defined as proportional control, a user could use one muscle group to control how fast the hand closes, and a second muscle group to control how fast the hand opens. Both discrete and continuous methods become harder and

unintuitive to use with increasing number of limb movements or degrees of freedom (DoF). This is mainly due to the limited number of independent control sites (see section 1.1.1).

To gain more intuitive control of multifunctional prosthetic limbs, researchers have focused their attention on pattern recognition or discrete algorithms as a possible replacement for conventional control. In this control scheme, multiple recording electrodes capture the natural generation of muscle activity, which can be classified to a specific hand posture or grasp (Hudgins, Parker, & Scott, 1993). As different patterns arise, multiple postures or complex movements can be classified. Users can then naturally switch between movements by just activating the desired posture with their phantom limb. Multiple pattern recognition algorithms have been tested in a laboratory setting (Ajiboye & Weir, 2005; Kuiken et al., 2009; Tsenov, Zeghbib, Palis, Shoylev, & Mladenov, 2006), while one company (Coapt LLC, Chicago, IL) has commercialized the technology. Researchers continue to test pattern recognition algorithms in both the laboratory and clinical setting, further improving the technology for conventional use (Hargrove et al., 2017). Pattern recognition has taken one step further in providing prosthetic users intuitive and natural control. However, this technique is characteristically discrete, meaning that movements are chosen sequentially, and cannot be proportionally controlled. This is far from the golden standard of the natural human hand.

1.2.2 Neuromuscular Skeletal Models and Continuous Decoders

In order to reach the gold standard of the human hand, novel controller algorithms must be able to simultaneously and proportionally control multiple degrees of freedom at a time. One approach to reaching this standard is to mathematically determine the relationships between joint finger moments, muscle activations, and motor neuron spike trains.

Upper-limb movement forces are generated from muscles innervated by pools of firing alpha motor neurons (Farina & Negro, 2012; Heckman & Enoka, 2004). The relationships between these components are non-linear and neuromusculoskeletal modeling has shown promise in understanding the transformations between these components (Buchanan, Lloyd, Manal, & Besier, 2004). Surface EMG has been commonly used as the neural drive for neuromusculoskeletal models to predict joint moments, since it can be easily recorded (Manal, Gonzalez, Lloyd, & Buchanan, 2002; Sartori, Reggiani, Farina, & Lloyd, 2012). Often these models need to be scaled and calibrated to an individual's limb shape, size, and EMG-force properties (Sartori, Farina, & Lloyd, 2014). Although these surface-EMG driven models can accurately predict one DoF moments, they do not scale well to predicting multiple DoF moments (Sartori et al., 2012). This is mainly due to the limitations of surface EMG mentioned earlier: signal cross-talk, deep muscle signal attenuation, etc.. Thus, a neural drive with higher resolution is needed as inputs to these EMG-driven models.

To achieve higher resolution neural drive, several studies have proposed to use semi-supervised signal separation algorithms to decompose recorded EMG into its motor unit components (Florestal, Mathieu, & Malanda, 2006; Marateb, Muceli, McGill, Merletti, & Farina, 2011; McGill, Lateva, & Marateb, 2005). More recently, blind source separation has become a more popular tool for EMG decomposition due to its automation and high accuracy (Holobar, Minetto, Botter, Negro, & Farina, 2010; Holobar & Zazula, 2007; Negro, Muceli, Castronovo, Holobar, & Farina, 2016). In one study, signals from TMR patients were decomposed using blind source separation (Negro et al., 2016) and subsequently fed into a neuromusculoskeletal model (Sartori et al., 2014) to predict simultaneous and proportional control of multiple degrees of freedom, i.e. elbow flexion, forearm pronation ,and wrist flexion (Farina et al., 2017). In an effort

to combine three promising technologies, this is the first most physiologically-based neural interface tested in humans. However, since all predictions were performed offline, the success and practicality of this method during real-time control has yet to be determined. Some limitations lie in the computational complexity of the neuromusculoskeletal models and the decomposition algorithms, but current development in real-time neuromusculoskeletal models and EMG decomposition systems have shown progress in keeping under the maximum 200 ms delay specification for prosthesis response time (Barsakcioglu & Farina, 2018; Sartori, Durandau, Došen, & Farina, 2018).

Less computationally heavy methods, such as regression-based algorithms, have been proposed as an alternative to simultaneous and proportional control. Unlike discrete algorithms, regression algorithms can continuously and simultaneously estimate multiple control signals directly from EMG signals (Barsotti et al., 2019; Hahne et al., 2014; Jiang, Rehbaum, Vujaklija, Graimann, & Farina, 2014; Nielsen et al., 2011; Smith, Kuiken, & Hargrove, 2015). Although these algorithms show promise in accelerating the progress of reaching the gold standard for prosthesis control, there still remains some limitations. Muscle synergies play a large role in natural limb movement (d'Avella, Portone, Fernandez, & Lacquaniti, 2006; Lee, 1984; Ting & Macpherson, 2005). These muscle synergies have a clear representation in EMG data and heavily affect the parameter training of regression algorithms. These effects can be seen in studies where unintended movement has been reported during online testing of multiple degrees of freedom control (Smith et al., 2015; Wendelken et al., 2017). Little progress has been made in addressing this issue with one study showing a possible solution using sparse non-negative matrix factorization (Lin, Wang, Jiang, & Farina, 2018).

In the age of information and artificial intelligence, significant progress has been made in developing elegant control algorithms for myoelectric prosthesis control. However, further progress is needed to reach the ultimate goal of providing upper-limb prosthesis users intuitive and natural control of their prosthetic hand.

1.3 Summary of Thesis

This thesis addresses several of the limitations of peripheral nerve interfaces described above, and aims to present a viable option for long-term extraction of peripheral motor control signals for dexterous finger movement in humans with upper limb amputation.

Chapter 2 aims to characterize the usability of a novel peripheral interface for continuous and proportional control of hand movement in non-human primates. The regenerative peripheral nerve interface (RPNI), is a free muscle graft that has been reinnervated by a transected peripheral nerve. Previously developed and tested in animal models (Irwin et al., 2016; Kung et al., 2014; Ursu, Urbanchek, Nedic, Cederna, & Gillespie, 2016), the RPNI acts as a bioamplifier for efferent motor nerves. In this study, RPNI signals were successfully used in a regression-based Kalman filter to decode hand movement with high accuracy both offline and online. This demonstrates that RPNI signals can be decoded and used for simultaneous and proportional control of a prosthetic hand.

In Chapters 3, we present the efficacy and viability of RPNIs in human participants. Three transradial amputees, one proximal and two distal, were implanted with RPNI grafts. Under ultrasound, RPNI grafts were viewed contracting during cued finger movements. Additionally, EMG signals were recorded with one RPNI graft having a maximum SNR of 107. These results demonstrate that the RPNI surgical technique is translatable to human nerves and musculature, creating potential new control sites for myoelectric prosthesis control.

Chapter 4 demonstrates the utilization of recorded RPNI signals for continuous control of individuated fingers. Participants moved single degree of freedom individuated fingers in real-time with precision and accuracy, controlling both a virtual and physical prosthetic hand. Additionally, with no retraining of the algorithm, no significant change in performance was seen over the course of multiple sessions. This suggests that RPNI signals are a viable option in a clinical setting for long-term, fine motor prosthesis control.

Lastly, chapter 5 will discuss the results of each study and expand upon the impact RPNIs could have on myoelectric prosthetic technology.

1.3.1 Thesis Contributions

Previous work have shown that RPNIs can be successfully reinnervated and maintain a healthy electrical response up to 7 months post-implantation in rats (Kung et al., 2014). A further study has shown that RPNIs can generate high-amplitude EMG signal during volitional movements in walking rats (Ursu et al., 2016). As the next step to translating RPNIs into humans, Irwin et al., showed that RPNIs can be successfully reinnervated and maintain a heathy electrical response up to 20+ months in non-human primates. Additionally, the recorded RPNI signals can be used to predict hand flexion and extension movements using a classifier in real-time (Irwin et al., 2016). This thesis aims to continue the characterization of RPNIs started in the previous studies. In particular, aim 1 takes the discrete classification results in Irwin et al., one step further and determines if RPNIs can provide and maintain the appropriate EMG signals for hand-level prosthetic continuous control in non-human primates. Aim 2 then assesses if the RPNI viability and stability found in Irwin et al., is transferrable to humans with amputations. Finally, aim 3 continues the RPNI validation in humans from aim 2, and evaluates if the efficacy of RPNIs for continuous prosthetic control found in aim 1 can also be transferrable to humans with amputations.

CHAPTER II

Closed-loop continuous hand control via chronic recording of regenerative peripheral nerve interfaces

A version of this work has been accepted to IEEE Transactions on Neural Systems and Rehabilitation Engineering, and is currently published online (Vu et al., 2018).

2.1 Abstract

Loss of the upper limb imposes a devastating interruption to everyday life. Full restoration of natural arm control requires the ability to simultaneously control multiple degrees of freedom (DOFs) of the prosthetic arm and maintain that control over an extended period of time. Current clinically available myoelectric prostheses do not provide simultaneous control or consistency for transradial amputees. To address this issue, we have implemented a standard Kalman filter for continuous hand control using intramuscular electromyography (EMG) from both regenerative peripheral nerve interfaces (RPNI) and an intact muscle within non-human primates. Seven RPNIs and one intact muscle were implanted with indwelling bipolar intramuscular electrodes in two rhesus macaques. Following recuperations, function-specific EMG signals were recorded and then fed through the Kalman filter during a hand-movement behavioral-task to continuously predict the monkey's finger position. We were able to reconstruct continuous finger movement offline with an average correlation of $\rho = 0.87$ and root mean squared error (RMSE) of 0.12 between actual

and predicted position from two macaques. This finger movement prediction was also performed in real-time to enable closed-loop neural control of a virtual hand. Compared to physical hand control, neural control performance was slightly slower but maintained an average target hit success rate of 96.70%. Recalibration longevity measurements maintained consistent average correlation over time but had a significant change in RMSE ($p < 0.05$). Additionally, extracted single units varied in amplitude by a factor of +18.65% and –25.85% compared to its mean. This is the first demonstration of chronic indwelling electrodes being used for continuous position control via the Kalman filter. Combining these analyses with our novel peripheral nerve interface, we believe that this demonstrates an important step in providing patients with more naturalistic control of their prosthetic limbs.

2.2 Introduction

Limb loss can have a significant negative impact on a person's daily life. Every year, around 185,000 people will undergo some sort of amputation, (Dillingham, Pezzin, & Mackenzie, 2002) and the current number of people living with an amputation may increase by a factor of 10 within the next 3-4 years (Ziegler-Graham et al., 2008). The loss is particularly devastating in the case of upper limb amputation. As one possible solution, myoelectric prosthesis technology can help assist these people and alleviate their daily struggles. Myoelectric prostheses work by using electromyogram (EMG) signals from residual muscle to control prosthetic hand movements. However, despite the improved hardware and functionality of prosthesis technology within the past decade, an adequate control strategy is ultimately lacking (Roche et al., 2014; Schultz & Kuiken, 2011). Current control strategies involve two muscle activations controlling multiple functions of the prosthetic hand. For example, flexing and extending the wrist muscle would control the prosthetic wrist flex/extend function and also the hand open/close function. Users

would switch between functions through co-contracting the flexion and extension muscles, or another mode selection mechanism. Three main components of this current control strategy make clinical myoelectric prosthetics unappealing to patients: the unintuitive feeling of control, the low level of performance and movement complexity compared to the natural hand, and the amount of training time it takes to achieve even that limited amount of performance.

To address some of these issues, current research has focused on improving these discrete classification algorithms to achieve higher performance and provide a more intuitive control mechanism. Discrete machine learning algorithms classify different movements based on patterns of EMG signal features, allowing users to directly select a movement to perform rather than having to switch modes. Recent advancements have led to an increased number of classified posture movements, i.e. wrist flex/extend, forearm pronation/supination, and radial/ulnar deviation (Englehart, Hudgin, & Parker, 2001; Jun-Uk Chu, Inhyuk Moon, & Mu-Seong Mun, 2006; Saridis & Gootee, 1982) with further studies using EMG feature patterns to control individual fingers and finger combinations (Khushaba, Kodagoda, Takruri, & Dissanayake, 2012; Tenore et al., 2009; Tsenov et al., 2006). Discrete classifiers have achieved > 90% decoding accuracy in both able-bodied participants (Englehart et al., 2001; Jun-Uk Chu et al., 2006) and transradial amputee subjects (Ajiboye & Weir, 2005; Cipriani et al., 2011; Kuiken et al., 2009; Tenore et al., 2009). This has overall granted myoelectric users with multi-functionality and a slightly more intuitive control scheme.

Despite the high classification accuracy, certain characteristics of discrete classifiers prevent them from becoming the end-all solution for myoelectric prosthetic control. Classifiers can only operate sequentially and cannot provide simultaneous control for more complex movements. If the user desired to rotate the wrist and open the hand at the same time, an additional

class would need to be trained. This would result in increased training time and may be impractical in a clinical setting. Additionally, classifiers inherently do not provide proportional control, acting only in a binary on/off basis. The ability to control the speed and strength of the prosthesis is necessary for more refined tasks. Thus, the absence of simultaneous and proportional characteristics limits the overall level of natural control a discrete classifier can provide.

Regression algorithms, on the other hand, can offer both proportional and simultaneous control. They have the ability to continuously predict the output of multiple movement signals and provide users with a more intuitive control scheme. Several groups have demonstrated simultaneous and proportional control of wrist flex/extend, wrist supination/pronation, ulnar and radial deviation and hand open/close from EMG signals in both able-bodied and transradial amputee subjects (Hahne et al., 2014; Jiang et al., 2014; Muceli & Farina, 2012). However, very few studies have focused on restoring continuous control of individuated fingers using EMG, with the exception of those using neural networks to estimate joint finger angles in able-bodied subjects (Ngeo, Tamei, & Shibata, 2014; Smith, Huberdeau, Tenore, & Thakor, 2009). More investigation is needed in improving regression algorithms to control finger movements using EMG signals. In addition, the regression studies mentioned above used surface EMG signals, which cannot record EMG from specific muscles and has signal stability challenges such as movement artifacts, skin impedance changes, and electrode shifts. To overcome these issues, intramuscular EMG recordings may provide a more stable and more localized signal for regression algorithms. Smith et al. (Smith, Kuiken, & Hargrove, 2016), has demonstrated that intramuscular EMG can be used in regression algorithms to control wrist flex/extend, wrist supination/pronation, and hand open/close in able-bodied and amputee subjects. This holds promise for future studies to explore the specificity of intramuscular EMG for fine finger movements.

However, an additional concern for these novel regression algorithms is that they cannot be used when the necessary muscles are missing. Every person with an amputation is missing some amount of muscle, whether it is intrinsic hand function alone for a distal transradial amputee or complete loss of hand control in a transhumeral amputee. To address this, several groups have explored interfacing with the peripheral nerves in the residual limb of amputee patients for prosthetic hand control (Davis et al., 2016; Dhillon et al., 2004; Micera et al., 2010; Rossini et al., 2010). Utah Slanted Electrode Arrays (USEA), intrafascicular electrodes, have been implanted into the median and ulnar nerve of two subjects with previous transradial amputations (Davis et al., 2016). Using a Kalman filter, a linear regression based algorithm, Davis et al. (Davis et al., 2016) were able to continuously estimate finger position based on the firing rates of multiple neurons recorded from the USEA. Although promising, the group also reported a significant reduction in signal strength within the 1 month period of implantation. Most other groups using intrafascicular electrodes have not reported longer than 1 month signal stability. Thus, intrafascicular electrodes may not be a viable option for chronic neural control.

As a longer term method for obtaining peripheral nerve signals, our group has recently developed the Regenerative Peripheral Nerve Interface (RPNI). RPNIs are 2-3cm autologous muscle grafts that are neurotized with residual severed nerves or nerve branches. The RPNIs can generate recordable high-amplitude EMG activity, acting as bioamplifiers for efferent peripheral nerve signals (Kung et al., 2014; Ursu et al., 2016). We previously implanted RPNIs and intramuscular bipolar electrodes within two rhesus macaques, and reported the long-term safety and performance of RPNIs during a finger-level behavioral task (Irwin et al., 2016). That study demonstrated that RPNIs can be used as a control signal source for discrete classification of simple

finger movements. However, their capability for continuous estimation of finger movements has yet to be quantified.

Here, we build on this prior work by pursuing continuous fingertip control using indwelling bipolar intramuscular EMG electrodes (Memberg, Stage, & Kirsch, 2014). We record from both implanted RPNIs and intact muscles within two rhesus macaques. Using these signals, we evaluated the ability to control finger flexion and extension in a continuous fashion using the best-known approach from brain controlled prostheses (Kim, Simeral, Hochberg, Donoghue, & Black, 2008; Wu, Gao, Bienenstock, Donoghue, & Black, 2006), the Kalman filter, as well as a Wiener filter for comparison. Recorded EMG signals were used to train these algorithms to control a virtual hand both offline and in real-time. This is the first demonstration of chronic indwelling intramuscular electrodes being used for continuous position control of fingers, and the first use of a Kalman filter with EMG from RPNIs.

2.3 Materials & Methods

All procedures were approved by the University of Michigan Institutional Animal Care and Use Committee. The two animals used in this study were the same two animals used in Irwin *et al.* (Irwin et al., 2016).

2.3.1 System Design

RPNIs are neurotized free autologous muscle grafts that convert signals from transected residual peripheral nerves into high amplitude EMG signals (Kung et al., 2014). The EMG signals can then be recorded from intramuscular electrodes implanted into the belly of the muscle graft. Here, two surgeries were performed to implant all RPNIs and bipolar electrodes (IM-MES, Ardiem Medical). The first surgery consisted of implanting the majority of RPNIs. Typically, RPNIs takes

3-4 months to mature and reinnervate. Here, a whole year passed before implanting the IM-MES electrodes to assess health and safety of the RPNIs (Irwin et al., 2016). RPNI implantation takes ~2-4 hours, while the IM-MES implantation takes ~1-3 hours. A total of 9 RPNIs were implanted on separate branches of the median and radial nerves in the forearm of two rhesus macaques L and R. RPNI construction starts with harvesting a 1 x 3cm muscle graft from a healthy native donor muscle. Then, the distal end of a targeted peripheral nerve is isolated and dissected into individual fascicles or branches. The end of the isolated nerve is sutured to the center of the muscle graft and then the muscle graft is wrapped around the nerve and sutured shut to create an enclosed housing. This procedure is repeated as needed to create the desired number of RPNIs. For our purposes, the median and radial nerve branches of interest terminated on the extrinsic finger flexors and extensors in order to gain hand level control. We used only minor, redundant terminal motor nerve branches to preserve motor function. Specifically, the median nerve branches that controlled the flexion of digits 2-5 and 1-3, and the radial nerve branch that controlled the extension of digits 2-5. Further details of the RPNI graft construction and implantation can be seen in Irwin *et al.* (Irwin et al., 2016).

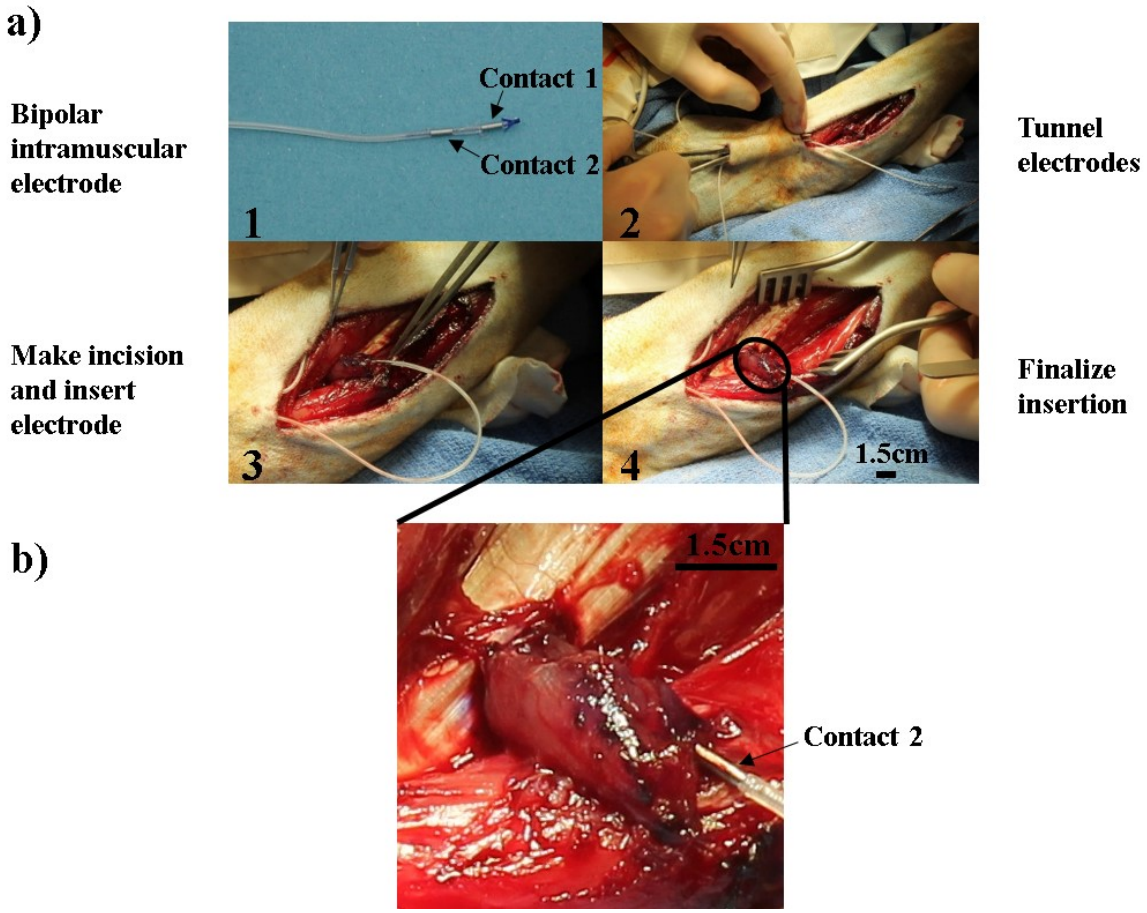

Figure 2.1 RPNI and electrode implantation procedure. (a) Bipolar electrode implantation procedure illustrated from *left* to *right*. *(1)* Representation of an IM-MES bipolar electrode (Ardiem Medical). *(2)* Electrodes are first tunneled through the skin until reaching the site of electrode insertion. *(3)* An incision is made in the belly of the RPNI graft or muscle of interest and the electrode is inserted. *(4)* Electrode insertion is complete and the remaining slack of the electrode wire is carefully tucked in between the intact muscles to minimize electrode shift. (b) A close up of a RPNI implanted with a bipolar intramuscular electrode.

2.3.2 Study Design and Device Validation

Post RPNI construction, we implanted IM-MES electrodes into RPNIs neurotized by nerves which originally innervated the flexor digitorum superficialis (FDS), flexor digitorum profundus (FDP), and extensor digitorum communis (EDC) muscles. We also implanted an IM-MES electrode into an intact extensor carpi radialis (ECR) muscle in monkey L as a control. For the remaining sections below, the RPNIs will be referred to by the muscle that was originally innervated by the transplanted nerve branch, i.e. FDS RPNI. Fig. 1(a) demonstrates the electrode

implantation process. These electrodes consist of two insulated stainless steel leads coiled in a double helix formation and potted in silicone tubing (Memberg, Stage, et al., 2014). Contacts are formed by exposing the leads and wrapping them around the tubing, and a polypropylene anchor at the distal end secures the electrode in the muscle. In the first animal, the two contacts on the electrode were 4 mm long with a diameter of 1.27 mm (the diameter of the silicone tubing), and were separated by 6 mm. After noting that in some cases, this was too large to fit both contacts within the muscle belly of an RPNI, a reduced contact size of 1.5 mm and inter-contact spacing of 2.5 mm was used for the second animal. A single IM-MES electrode was placed in the muscle belly of each RPNI, as well as in a healthy control muscle, by making a small incision and manually feeding the electrode anchor-first into the muscle. Leads were tunneled subcutaneously to a transcutaneous port on the animal's back and attached to a connector protected by a primate jacket. A fully-implanted RPNI is shown in Fig. 1(b).

2.3.3 Behavioral Task

We trained both monkeys to perform a finger movement task, illustrated in Fig. 2. A flex sensor (Spectra Symbol) was attached to the monkey's index finger, which fed finger position data to a real-time computer running xPC Target (Mathworks). Musculoskeletal Modeling Software (MSMS; (Hauschild, Davoodi, & Loeb, 2007)*) provided a virtual model of a monkey hand that was displayed in front of the monkey on a monitor, and mirrored the finger movements measured by the flex sensor. The xPC Target real-time system executes on a millisecond basis. Neural signals are collected at 30 ksp and are sent to the xPC Target via an Ethernet cable. Using a 1 Gbps Ethernet network card, data transmission time from the Cerebus to the xPC Target is trivial. Thus, the xPC Target collects 30 samples of neural data in 1 millisecond. The Kalman filter decoding algorithm can be manually set to update at arbitrary intervals. Here, we set the decoding algorithm

to update every 50 ms or 100 ms. Updated position values are then sent from the xPC Target to the MSMS virtual software over Ethernet. Again, transmission time from xPC Target to MSMS was unmeasured, but likely very small since it has very little software running. Using a 120 Hz monitor adds 8 ms.

The monkeys both performed movements with all four fingers simultaneously, with the position of all four indicated by the index flex sensor. Both monkeys L and R were trained with the virtual hand displaying only the index finger moving because this animation was the most robust and easiest to view during their earliest training sessions. However, the animal always moved all four fingers together, and all results that are present are for all four fingers moving simultaneously. Images are shown below in the way they were originally viewed by the animal. At the start of a trial, the xPC cued a spherical target to appear in the path of the virtual finger. The monkey was then required to move his fingers in order to hit the target on the screen. After holding the virtual finger in the target for a required hold time (usually set to 500-700 ms), the monkey was given a juice reward. Both monkeys performed a center out task with 50% flexion denoted as center. The xPC then chose randomly between 6 targets, 3 flexion and 3 extension targets, to display next after each center target was hit. The virtual hand could also be controlled by decoding the RPNI signals in real-time into predicted movement. As described below, the monkey would receive a reward only if the predicted movement was correct, and could act to correct the decode within the trial time limit in a closed-loop manner.

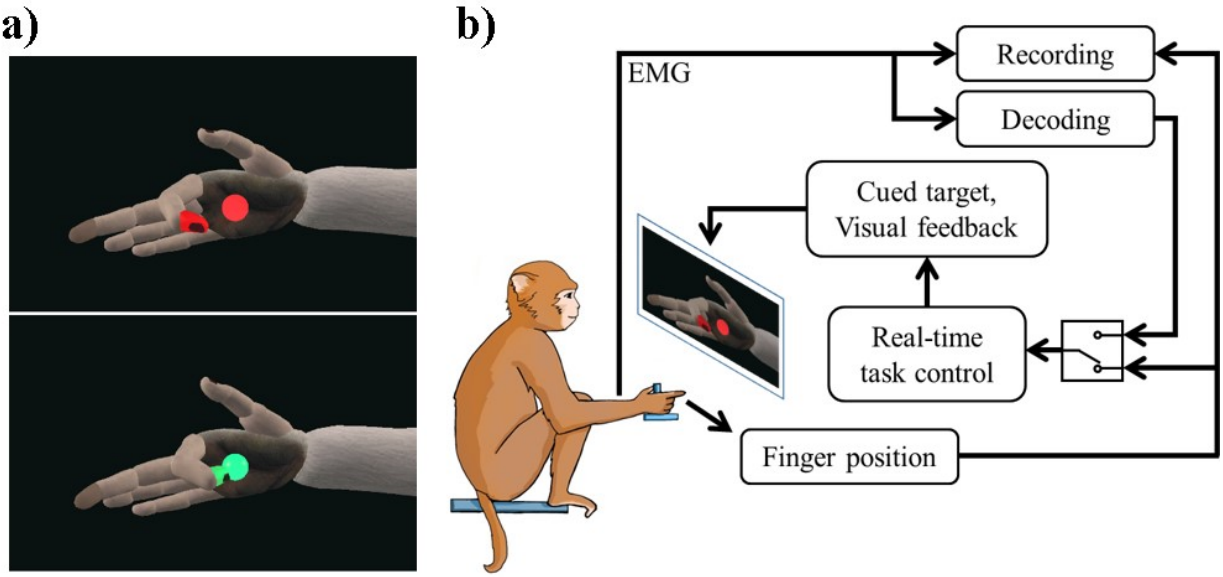

Figure 2.2 Monkey behavioral task.(a) The monkey hit virtual targets by moving his four fingers simultaneously. The index finger of the virtual hand moved in conjunction with the monkey's movements. (b) The virtual hand could be controlled either by the monkey's movements directly (as measured by flex sensors) or by EMG signals decoded into movement predictions in real-time, allowing either open-loop or closed-loop task performance [22] [16]. The "decoding" and "recording" blocks in parallel indicate that recorded EMG is both stored and sent to the decoding algorithm simultaneously, giving us the ability to flip between open-loop or closed-loop control instantly.

2.3.4 Electrophysiology Recording

During task performance, EMG signals from the RPNIs were input into either a DAM50 differential EMG amplifier (WPI), which filtered the signal between 10-1000 Hz with a gain of 1000x, or directly into a Cerebus neural signal processor (Blackrock Microsystems), which filtered the signal between .3-7000 Hz (unity gain). For real-time signal analysis, the Cerebus was used to record from multiple electrodes simultaneously. The DAM50 was used for lower-noise recordings from a single electrode. In both cases, the processed signal was digitized and saved to disk by the Cerebus at 30 ksps. The signal was further sent from the Cerebus to the behavioral rig via ethernet, where it could be processed in real-time.

2.3.5 Signal Analysis and Decoding

To isolate the EMG signal from motion and electrical artifacts, we filtered the data between 100-500 Hz using a second-order Butterworth filter. In offline analysis, the data were filtered forwards and backwards in order to eliminate phase shift.

To assess the EMG signal quality, we calculated both the maximum voluntary contraction (MVC) and the signal to noise ratio (SNR) for each recorded RPNI and intact muscle. MVC was calculated by isolating periods of maximum agonist behavior, corresponding to either full finger flexion or full finger extension movements, depending on the function of the RPNI nerve. Approximately 1000-1400 trials were conducted within each recording session. Movement periods were isolated and labeled by thresholding the finger position and velocity to ensure both maximum EMG activation and consistent behavior. The mean of the peak-to-peak amplitude during all such movements was taken as the MVC. SNR was calculated by simply dividing the MVC by the noise floor of the channel, which was extracted by manually selecting around 60-130 second quiescent periods in the signal and calculating the mean peak-to-peak amplitude.

To evaluate the stability of the IM-MES electrode over time, we measured the amplitude of recorded single motor unit activity from the EMG. Single unit activity was extracted manually by choosing the peak of the motor unit waveform during behavior segments where finger position remained constant and finger velocity was approximately zero. Two milliseconds of samples were taken before the peak and 6 ms after the peak. 100 examples of one motor unit were extracted per recording session approximately once a week, and the mean and variance of the motor unit amplitude were calculated. Each motor unit was chosen based on having the same shape. If the signal was perfectly stable, the amplitude of the motor unit would remain the same over time. Thus, by picking the same motor unit over time, we attempted to assess the variability of the recorded EMG signal and the stability of the IM-MES electrodes.

To assess the functional efficacy of the recorded RPNI signals, we used a Kalman filter to decode continuous finger position movements from the EMG signals. The Kalman filter is a recursive linear filter that tracks the state of a dynamical system throughout time using noisy measurements (Kalman, 1960; Kim et al., 2008; Wu et al., 2006) relying on a trajectory model and an observation model. Here, the trajectory model is a representation of the transition of the kinematic state of the fingers at time t to time $t+1$. We assume that the finger state vector x_t represents the position and velocity of the finger,

$$x_t = \left[pos_{t,}\, vel_t, 1\right]^T \qquad (1)$$

where pos_t is the finger position measured by the bend sensor and vel_t is the calculated difference of the position. The observation model represents the noisy transformation of the current finger state to recorded neural activity. Here, temporal characteristics of the EMG waveform represented the neural activity. We extracted two temporal characteristic features of the EMG waveform: (1) mean absolute value (MAV) and (2) waveform line length (LL) (Hudgins et al., 1993; Zhou et al., 2007). Mean finger kinematics and EMG features were computed in consecutive time bins. Decoding features were extracted from the flexor and extensor channel available for both monkeys. A total of two channels were input into the filter during offline and online analysis. In particular, these features were simultaneously obtained from the FDP and EDC RPNI in monkey L and the FDS RPNI and an intact extensor muscle in monkey R. For monkey R only the MAV was used as a feature. If we let $\vec{y}_t = [y_1 \ldots, y_k]^T$, where y_k is the temporal feature of the kth electrode, then the linear relationship between the finger state and neural measurements is:

$$\vec{x}_t = A\vec{x}_{t-1} + \vec{w}_t \qquad (2)$$
$$\vec{y}_t = C\vec{x}_t + \vec{q}_t \qquad (3)$$

where $A \in \boldsymbol{R}^{3\,x\,3}$ and $C \in \boldsymbol{R}^{k\,x\,3}$ represent the trajectory and observation models, and $\vec{w}_t$ and $\vec{q}_t$ are Gaussian distributed noise terms for the state trajectory transition and the observation

transformation, respectively. A is the linear transformation from the previous finger state to the current finger state (the trajectory model), while C is a mapping of the current finger state to the EMG temporal features (the observation model).

The above analysis was done both offline and in online closed-loop sessions. During closed-loop sessions, both monkeys performed a center-out task. After ~200 trials of normal task performance, the decoder was trained and the virtual hand was switched to mirror the Kalman filter output (predicted position values) instead of the flex sensor output. The Kalman filter updated every 50 ms, or 100 ms on some online sessions, allowing continuous control of the virtual hand.

For comparison in performance, a Wiener filter was also implemented both offline and online for monkey R and only offline for monkey L. A comparable study used Wiener filters as a baseline comparison for decoding performance between different algorithms (Smith et al., 2016). The Wiener filter equation is as follows:

$$\vec{x}_t = B\vec{y}_t + \vec{b}_0 \qquad (4)$$

where $\vec{x}_t$ represents the kinematic state of the system and $\vec{y}_t$ is the featured neural activity, where $\vec{y}_t$ equals $[y_1, y_2, \dots, y_k]^T$, representing a history of measurements up to time k. B is the linear transformation of the neural features to the kinematic state and $\vec{b}_0$ is a constant offset.

For offline performance evaluation, tenfold cross validation was implemented when training the Kalman filter and Wiener filter. Subsequently, accuracy of the reconstructed position trajectory was calculated via cross-correlation (CC) with the actual trajectory. Likewise, root mean squared error (RMSE) was calculated between the reconstructed and actual trajectories. Let $\hat{x}_t$ be the estimate for the true position x_t, then the CC and RMSE are defined as follows:

$$CC = \frac{\sum_t (x_t - \bar{x}_t)(\hat{x}_t - \bar{\hat{x}}_t)}{\sqrt{\sum_t (x_t - \bar{x}_t)^2 \sum_t (\hat{x}_t - \bar{\hat{x}}_t)^2}} \qquad (5)$$

$$RMSE = \sqrt{\frac{1}{T}\sum_{t=1}^{T}(x_t - \hat{x}_t)^2} \qquad (6)$$

where $\bar{x}_t$ represents the mean of the x position, $\bar{\hat{x}}_t$ represents the mean of the estimated position, and T represents the sample size of the predicted and actual position measurement.

For real-time performance metrics, we calculated throughput, described by Fitts's law (Soukoreff & MacKenzie, 2004; Thompson et al., 2014), and average success percentage. Fitts's law, which calculates an overall bit rate, has been shown to be a robust performance metric for continuous brain machine interfaces (BMIs) across different task parameters. The Fitts's equation used is shown below.

$$Throughput = \frac{\log_2\left(1 + \frac{D}{W}\right)}{Movement\ time}\ (bits\ per\ second) \qquad (7)$$

Here, D is the distance between targets and W the width of the target. In addition to performance, we evaluated the smoothness of the estimated path trajectory between targets. In both offline and online analysis, the jitter metric was calculated by counting the number of times the velocity of the estimated trace changed signs and normalizing that number to the total experiment time to obtain the number of sign changes (SC) per second.

To gauge the limits of recalibrating the decoding algorithms between recording sessions, Wiener filter parameters were trained offline on an initial EMG recording day and reused for decoding with subsequent EMG recording days. CC and RMSE values were calculated for each day to measure the performance. As a baseline for comparison, new Wiener filter parameters were trained on each day, used to decode that day's EMG, and CC and RMSE values were calculated.

Overall for decoding analysis, a total of 7 recording session datasets were used for offline and online analysis between both monkeys. For signal stability measures and further functional efficacy, 12 datasets were used over the span of 8 weeks to extract single units and train the Wiener filter parameters. Unless otherwise stated, paired t-tests were used to evaluate the differences in CC and RMSE measurements between the decoding filters within each monkey (n = 2). Additionally, unpaired t-tests were used to evaluate the differences of single unit waveform amplitude between days.

2.4 Results

2.4.1 Signal Quality Over Time from Indwelling Electrodes

A total of 8 muscles were recorded with indwelling electrodes, 4 in each monkey. For monkey L, the FDP and EDC RPNI were used for offline and online continuous decoding analysis, as they provided task-relevant finger flexion and extension information. The intact ECR was not used since it only contained wrist information. Additionally, due to connector breakage, the FDS RPNI did not show finger flexion information during online continuous decoding. However, the FDS RPNI signal did appear during previously-reported online discrete decoding using a percutaneous electrode (Irwin et al., 2016). For monkey R, the FDS RPNI and intact EDC were used for decoding. The IM-MES electrode in the intact EDC was originally placed in the EDC RPNI, but high amplitude was immediately recorded after implantation, which could not have been produced by a denervated muscle. Thus, the electrode was assumed to have slipped out of the RPNI and was recording from surrounding EDC muscle. Similar to monkey L, the FDP RPNI channel was not used due to connector breakage.

For both monkeys, the maximum voluntary contraction (MVC) and signal to noise ratio (SNR) of the EMG signals used for decoding are shown in table 1. Here it is important to note that each RPNI muscle graft surrounds a single small branch of the median and radial nerves, with an IM-MES electrode inside that graft. Consistent with this, the RPNI signals had an average SNR of 7.92, smaller than the intact EDC muscle with an SNR of 39.8 but greater than the SNRs reported for intrafascicular electrodes (Davis et al., 2016; Rossini et al., 2010). Fig. 2.3 shows the intramuscular raw EMG signals from both flexor and extensor RPNIs and intact EDC, bandpass

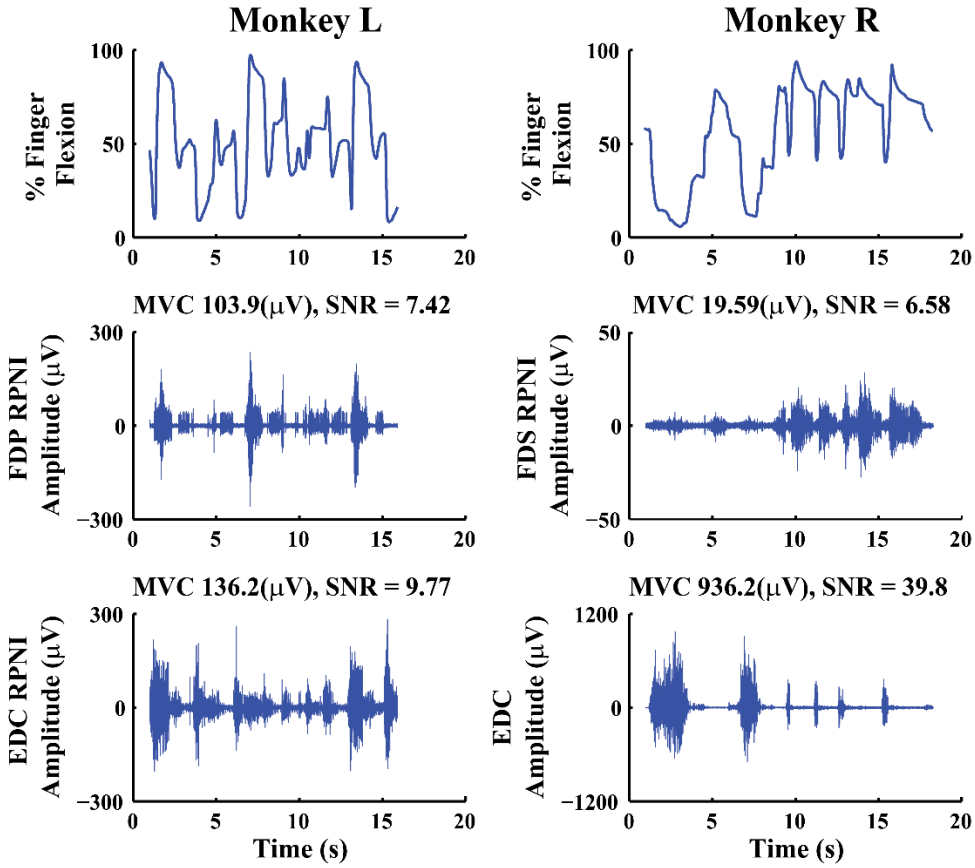

Figure 2.3 Example of recorded EMG from chronic IM-MES electrodes.The *top* trace in each column is finger position during task behavior. The *bottom* two rows in the *left* column are the EMG signals from the flexor and extensor RPNIs in monkey L. The *bottom* two rows in the *right* column are the EMG signals from the flexor RPNI and the intact EDC in monkey R. The displayed raw signals came from online continuous finger control recording sessions, which differ from the signals reported in Irwin *et al.* (Irwin et al., 2016).

filtered from 100-500 Hz. The top row represents each monkey's finger movements during the behavioral task (as a percentage of fully-flexed, with zero as fully-extended).

2.4.2 Offline Continuous Reconstruction

Using the Kalman filter, which uses only the past 50 ms bin for input, there was an overall average CC of 0.89 and 0.84, and RMSE of 0.112 and 0.140, for monkey L and R respectively. This performance is similar to another study using a linear regression algorithm with intramuscular EMG during an annulus target task (Smith et al., 2015). Overall, the Kalman filter had smooth transitions between targets but would occasionally overshoot near the minimum and maximum finger positions. This may be a result of un-modeled non-linearities in the relationship between EMG and finger position.

To compare performance with the Kalman filter, we applied the Wiener filter to the same training and testing datasets. Fig. 4 illustrates the reconstruction of true position offline using both Kalman and Wiener filters in monkeys L and R. Wiener filters have been used both offline and online in cortical brain machine interfaces (BMIs) for linear reconstruction (Wu et al., 2006). Additionally, Smith *et al.* (Smith et al., 2016; Smith et al., 2015) has used the Wiener filter as a baseline comparison to their algorithm's performance with intramuscular EMG. Here, the Wiener filter had an overall average CC of 0.91 and 0.83 and RMSE of 0.0883 and 0.121, for monkey L and R respectively.

Table 2.1 Maximum Voluntary Contraction and Signal-to-Noise of Implanted Electrodes

Monkey	Muscle	MVC (μV)	SNR
L	FDP RPNI	103.9	7.42
	EDC RPNI	136.2	9.77
R	FDS RPNI	19.59	6.58
	Intact EDC	936.2	39.8

Although this performance was not significantly different than the Kalman filter ($p = 0.643$), it was dependent on 500 ms of past EMG signal (10 bins). Without history, the overall average CC was 0.66 and 0.68 with an RMSE of 0.157 and 0.161 for monkey L and R respectively. This is a significant drop compared to the Kalman filter ($p < 0.001$). Additionally, the Kalman filter was smoother than the Wiener filter with or without history, with an average jitter of 1.7 and 1.4 in monkeys L and R, respectively, compared to 2.3 and 1.9 for the Wiener filter (2.2 and 2.1 for the Wiener filter without history).

Table 2.2 shows the performance metrics for all sessions conducted with monkeys L and R. The Wiener filter with and without history had significantly higher jitter than the Kalman filter ($p < 0.01$). This is expected due to the Kalman filter's trajectory model, which is based on a physics model of the kinematics of the finger. Thus, although the performance of the Wiener filter can be equal to that of the Kalman filter, it requires history. Other studies have previously shown

Table 2.2 Offline decoding performance metrics for Monkeys L and R

		Kalman Filter			**Wiener Filter with History**			**Wiener Filter without History**		
Monkey	**Session**	**CC**	**RMSE**	**Jitter (#SC/s)**	**CC**	**RMSE**	**Jitter (#SC/s)**	**CC**	**RMSE**	**Jitter (#SC/s)**
L	**1**	0.88	0.12	1.6	0.92	0.083	2.2	0.64	0.17	2.0
	2	0.89	0.10	1.7	0.90	0.082	2.4	0.64	0.15	1.8
	3	0.91	0.095	1.5	0.91	0.079	1.9	0.67	0.15	2.1
	4	0.87	0.14	1.9	0.89	0.11	2.5	0.69	0.17	2.8
	Mean	0.89	0.11	1.7	0.91	0.088	2.3	0.66	0.16	2.2
R	**1**	0.85	0.15	1.5	0.83	0.13	2.1	0.66	0.18	2.3
	2	0.84	0.13	1.3	0.85	0.11	1.7	0.70	0.15	2.0
	3	0.82	0.14	1.5	0.83	0.11	1.9	0.68	0.15	1.8
	Mean	0.84	0.14	1.4	0.83	0.12	1.9	0.68	0.16	2.1
Overall	**Mean**	0.87	0.12	1.6	0.88	0.10	2.1	0.67	0.16	2.1

that adding neural data from hundreds of milliseconds in the past can significantly lower performance (Cunningham et al., 2011).

2.4.3 Online Continuous Control

During online control sessions, both monkeys performed the center-out task in hand control (controlled by flex sensor) and neural control (controlled by EMG signals) form. A summary of the overall average success rate, average acquisition time, and throughput for Kalman and Weiner filters can be seen in tables 3 and 4. For monkey L, the Kalman filter in session 1 used 50ms bins of neural data, while session 2 used 100 ms bins. The target could randomly appear in 6 different locations, 3 flexion and 3 extension targets after the center target was hit. Animals had to hold their hand within the acquired target space for 500- 700ms to receive the reward. Fig. 2.5 shows a sample of the online neural control task performance with the Kalman filter for both monkeys and

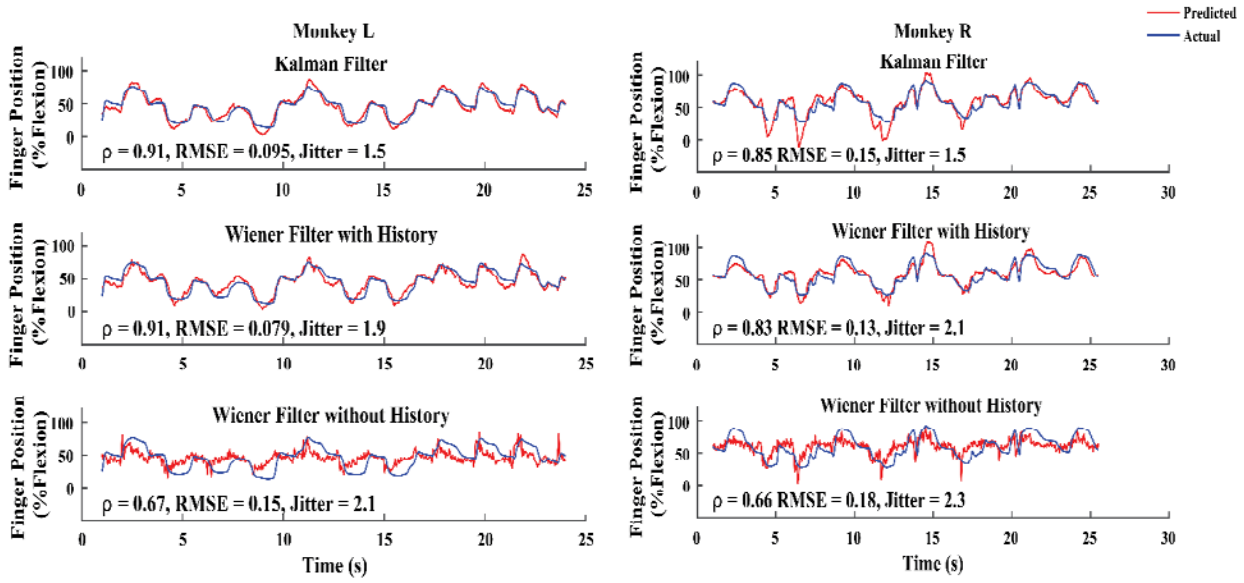

Figure 2.4 Offline continuous reconstruction. Traces were produced from one of the recording sessions from each monkey. CC, RMSE, and Jitter values are mean values for each filter across datasets. The *top* traces in each column are the offline predicted reconstructions (red) overlapping on the actual finger position (blue) for the Kalman filter. *Middle* traces illustrate the same reconstructions for the Wiener filter with 500ms of history and the *bottom* traces show the reconstruction for the Wiener filter without history (using a single 50 ms bin).

the Wiener filter for monkey R. Both the estimated finger position and the actual finger position are displayed over time.

For a comparison baseline, the animals had an overall average success rate of 98.50% using hand control, and an average time to target of 1.25 sec. The animals were able to acquire targets with a high success rate using an online Kalman filter, albeit at a slower pace with a significant difference between the time to success compared to hand control ($p < 0.001$). Specifically, their overall success rate was 96.70% with an average time to target of 1.61 sec. This was 77.64% as fast as hand control. The overall throughput was 0.77 bits/s, which was 93.90% of the throughput under hand control.

For one animal, the Wiener filter with history was also used online, and resulted in a statistically significant smaller average throughput of 0.69 bits/s, 79.65% of the throughput under Kalman filter control ($p < 0.001$). The average success rate and acquisition time were not statistically different ($p = 0.55$, 0.27, respectively). However, on average the acquisition time for the Wiener filter was longer than the Kalman filter, 1.84 to 1.49 sec, even though statistical

Table 2.3 Online Kalman filter task performance metrics for Monkeys L and R

		Success (%)		**Mean Time to Success (s)**		**Throughput (bits/s)**		**Jitter (# SC/s)**
Monkey	**Session**	**Hand Control**	**Neural Control**	**Hand Control**	**Neural Control**	**Hand Control**	**Neural Control**	**Neural Control**
L	**1**	100	96.3	1.21	1.66	0.79	0.68	3.5
	2	94.3	94.9	1.31	1.77	0.71	0.66	4.7
	Mean	97.1	95.6	1.26	1.72	0.75	0.67	4.1
R	**1**	100	99.4	1.23	1.49	0.86	0.85	2.6
	2	99.9	97.0	1.24	1.50	0.92	0.88	3.2
	3	99.7	97.0	1.22	1.48	0.87	0.85	3.7
	Mean	99.9	97.8	1.23	1.49	0.88	0.86	3.2
Overall	**Mean**	98.5	96.7	1.25	1.61	0.82	0.77	3.6

significance was not met. This would tend to lower the Wiener filter's throughput average, suggesting that the 500ms history did have some negative impact on the performance. Finally, similar to the cursor jitter measured offline, we found a significant difference between the Kalman filter and Wiener filter online in monkey R ($p = 0.043$). This suggests that orbiting behaviors may have played a role in longer target acquisition time, which resulted in lower throughput. For monkey L, only the online Kalman filter was implemented.

Table 2.4 Online Wiener filter task performance metrics for Monkey R

		Success (%)		**Mean Time to Success (s)**		**Throughput (bits/s)**		**Jitter (# SC/s)**
Monkey	**Session**	**Hand Control**	**Neural Control**	**Hand Control**	**Neural Control**	**Hand Control**	**Neural Control**	**Neural Control**
R	**1**	97.48	92.58	1.27	1.99	0.95	0.68	4.4
	2	99.55	98.20	1.14	1.68	0.96	0.69	4.7
	Mean	98.52	95.39	1.21	1.84	0.96	0.69	4.5

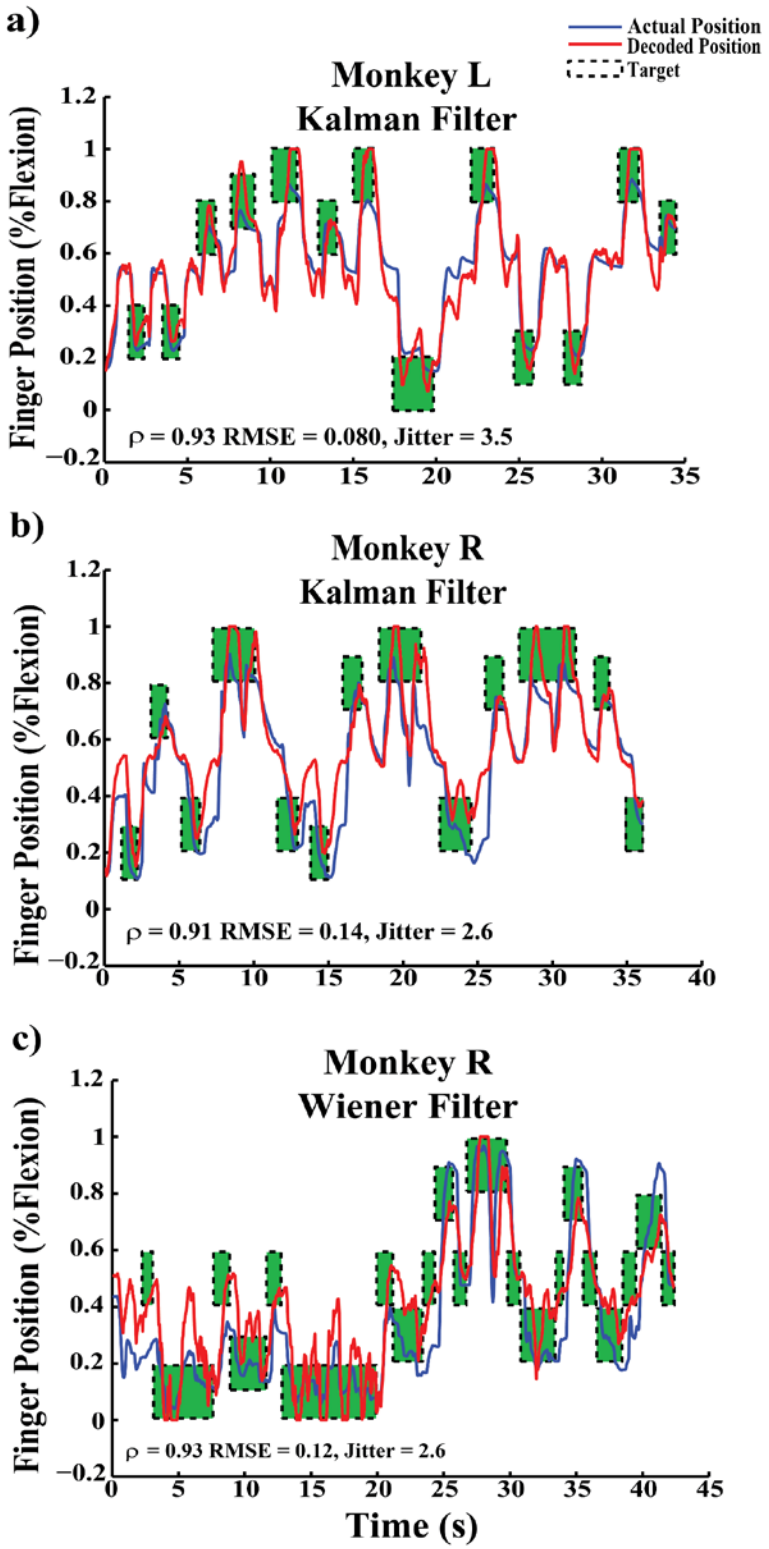

Figure 2.5 Online continuous control. (a), (b) Traces in each row are the online predictions (red) overlapping on the actual finger positions (blue) for the Kalman filter in monkey L (a) and the Kalman and Wiener filter with history in monkey R (b), (c), respectively. Each trace also displays the target area, where height of the area represents the size of the virtual target, while the width of the area represents how long the virtual target was displayed. Green target areas denotes a successful target hit.

2.4.4 Recalibration Longevity

Surface EMG is the standard control signal used in clinical myoelectric prostheses. However, surface EMG electrodes have some limitations that contribute to the rejection of myoelectric prosthetic use. Surface electrodes can shift on the skin, which can cause EMG instability (Young et al., 2011). Additionally, perspiration can alter the electrical impedance of the electrode such that the system's performance reduces (Farina et al., 2014). This reduction in functionality can cost time for the user and add frustration to the usage of the prosthetic. Thus, a system where the EMG signal remains stable would be desirable.

To assess the functional stability of the intramuscular EMG over time, the FDP and FDS RPNIs in monkey L were fed individually into a Wiener filter offline. This was done because the EDC RPNI was created at the same time as the IM-MES electrodes were implanted. Thus, a waiting period was required to allow the EDC RPNI to fully mature to produce EMG activity. Since the Kalman filter required both the extensor and flexor RPNI inputs to function, this prevented full evaluation of the recalibration longevity measurement. As an alternative, we used the Wiener filter to test the functional stability of individual flexor RPNIs.

The Wiener filter decoder parameters were trained on an initial EMG recording day and reused on subsequent EMG recording days. As a comparison, decoding parameters were also recalibrated on the same days and CC and RMSE values were measured for both conditions (uncalibrated vs. recalibrated). Fig. 2.6a illustrates the performance of each RPNI, showing the change of CC and RMSE values over time (blue line). The red line indicates measured performance based on recalibrated decode parameters.

For the FDP RPNI, CC values of the uncalibrated decoder were slightly lower compared to the calibrated decoder's CC values for each day. Contrarily, the FDS RPNI did not have a significant change in CC values between uncalibrated and calibrated decoders ($p = 0.165$).

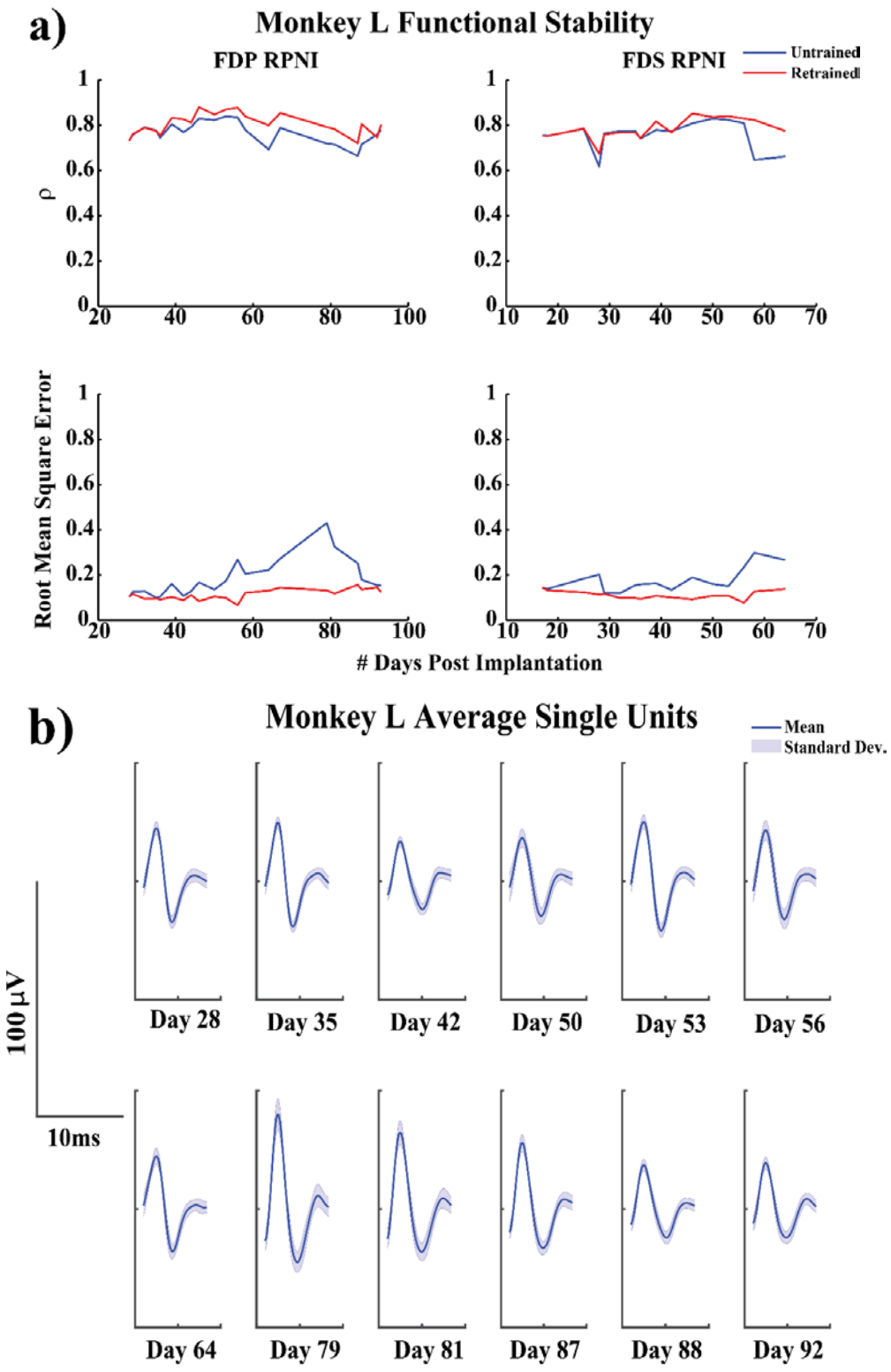

Figure 2.6 Functional stability and single unit activity. (a) Decoding parameters were trained on Day 28 for monkey L and reused to decode finger position on subsequent days. In (a) blue line denotes the decoding performance for the FDP and FDS RPNI over time for uncalibrated decoder parameters. Red line indicates decoding performance over time after recalibration. (b) 100 examples of one motor unit were extracted and averaged once a week for 8 weeks.

While correlation coefficients are not sensitive to large changes in amplitude, this result suggests that the timing of decoded flexion and extension was consistent across days without recalibration. While the signals may provide some form of stable functionality over time, they may also cause an undesired overshoot at the minimum and maximum finger positions. To investigate this further, the RMSE showed clear visible changes over time. Both the FDP and FDS had significant difference between RMSE values ($p < 0.05$).

Looking more closely at the data, there was an increase in error centered on day 79. Average single units from the FDP RPNI are shown across time throughout this period (Fig. 2.6b). 100 examples of a chosen motor unit during consistent near zero velocity and constant position behavior were extracted from the FDP RPNI. The extracted single unit's amplitude changed by a maximum factor of +18.65% and a minimum factor of –25.85% compared to its mean over the recorded time period, which was a significant change ($p < 0.05$). While we do not know for certain that this was the same unit, the changes correspond well to increased errors in the decode, with day 79 showing the most significant change. Overall, this suggests that intramuscular EMG signal amplitude varies over time, which may be due to either RPNIs still maturing 16+ months post-implantation, or the IM-MES electrodes shifting during the monkey's non-task related free time. This varying amplitude would not be desired in a practical myoelectric control system.

2.5 Discussion

In this study, we demonstrated continuous control of finger position using intramuscular EMG electrodes in RPNIs using a Kalman filter. To the best of our knowledge, this is the first demonstration of RPNI continuous control of all four finger movements using indwelling electrodes. Previous continuous decoding studies have either used percutaneous fine-wire electrodes or surface electrodes to obtain EMG signals (Ameri, Kamavuako, Scheme, Englehart,

& Parker, 2014; Hahne et al., 2014; Jiang et al., 2014; Smith et al., 2015), with few decoding isolated finger movements (Kamavuako, Englehart, Jensen, & Farina, 2012; Ngeo et al., 2014). Other studies using indwelling electrodes have only implemented classifiers or proportional control algorithms (Baker, Scheme, Englehart, Hutchinson, & Greger, 2010; Pasquina et al., 2015).

Overall offline, the Kalman filter had a smoother position output compared to the Wiener filter for both monkeys. Online we did not see a significant difference in the jitter between the Kalman and Wiener filter in monkey R, but qualitatively, we can see that control of the virtual hand was more difficult. This reflects the Wiener filter's significantly lower throughput compared to the Kalman filter's throughput. Thus, in a practical system, the Wiener filter with history would not provide the appropriate control for finger-level fine motor skills.

Though the Kalman filter demonstrated the ability to provide continuous finger control, there are some challenges that need to be addressed. Primarily, we limited the number of DOFs to a simple open-close to demonstrate the capabilities of RPNIs as a proof of concept. To add more movement types, more RPNIs would need to be created with separated fascicles from each nerve. Studies have shown that distinct somatotopic organization occurs within peripheral nerves (Stewart, 2003). For example, nerve fibers innervating a specific muscle remain grouped together throughout most of the nerve. This is promising for separating nerves into discrete functional RPNIs and then potentially recording independent signals, increasing the number of DOF control sources. Additionally, monkeys will need to be trained on a new behavioral task that encompasses different grasp movements. Future studies are needed to measure and compare performances between different grasp movements using multiple RPNIs, and the question of individuated finger movements may ultimately be easier to address in humans.

Secondly, the Kalman filter reconstruction caused overshoots during some periods of flex and extend movements. This may indicate that the assumptions of a linear relationship between EMG activity and finger kinematics are erroneous. Nonlinear methods such as artificial neural networks, support vector regression, and kernel-ridge regression have been evaluated using surface EMG (Ameri et al., 2014; Hahne et al., 2014; Muceli & Farina, 2012; Ngeo et al., 2014), but no physiological model of the EMG to kinematic states has been used for prosthetic control. The results from Ngeo et al., 2014, show that a Gaussian process regression had an average correlation coefficient of 0.84 using 8 surface electrodes. For a single DOF, their best estimate for the MCP, PIP, and DIP joints were 0.92, 0.85, and 0.79, respectively. Comparatively, the Kalman filter for a single DOF performs just as well as this decoder with 2 intramuscular bipolar electrodes. Although RPNIs may not offer higher regression accuracy, they are able to produce relevant EMG signals from peripheral nerves, which could ultimately lead to many more independent EMG signals associated with missing or deep musculature, unlike surface EMG. The small number of nonlinear studies may be attributed to the recent interest of muscle synergies and how muscle activity during movement can be broken down into linear combinations (d'Avella, Saltiel, & Bizzi, 2003). However, muscle synergies may not be as important in intramuscular EMG because of the single motor unit activity that can be picked up from intramuscular electrodes. Most studies have used Hill-based muscle models or other biomechanical models to predict forces of one or two DOFs (Cavallaro, Rosen, Perry, & Burns, 2006; Ding, Zhao, Xiong, & Han, 2011; Sartori, Reggiani, Mezzato, & Pagello, 2009). These studies have reported high motor performance, demonstrating that nonlinear algorithms could provide a better solution to current clinical control algorithms. Thus, more exploration is needed to investigate potential nonlinear relationships that may exist between intramuscular EMG and finger kinematics.

Furthermore, we investigated the recalibration longevity in order to assess the stability of intramuscular EMG. Surface EMG has numerous limitations, discussed earlier, which prevent it from being an ideal solution to myoelectric prosthesis control. In this study, we purposefully used only electrodes with a strong existing safety record in humans (Memberg, Stage, et al., 2014), to enable fast translation. These bipolar electrodes had large contact sizes and low impedance, but were limited to a small number of channels due to the wiring. To investigate cross-talk issues, one bipolar electrode was implanted into an intact extensor carpi radialis (ECR) muscle as a control. Signals compared between the EDC RPNI and intact ECR muscle showed different amplitudes and shape. Additionally, the EDC RPNI fired more frequently during the behavioral movements than the ECR. Thus, any existence of cross-talk between the bipolar electrodes appeared to be minimal.

The higher SNR reported here and by others (Ortiz-Catalan, Hakansson, & Branemark, 2014; Weir et al., 2009), motivates additional development in multi-channel intramuscular EMG electrodes, as it is very likely that additional channels could provide anatomically precise information about additional joints simultaneously. For example, multi-channel intramuscular thin film electrodes have been demonstrated in both animals and humans for multi-motor unit recordings (Farina, Yoshida, Stieglitz, & Koch, 2008; Muceli et al., 2015). Single units were generally visible on even these macroscopic electrodes, and remained high throughout 7 months of implantation in two animals. However, single unit waveforms were not identical from day to day. Quantitatively, they varied much less than Utah array waveforms (Chestek et al., 2011), and there were no systematic changes indicative of progressive scarring. However, as EMG electrodes get smaller and more numerous over time, the biological environment around them may shift similar to brain electrodes. This may require adaptive approaches to stabilize the control signal

(Bishop et al., 2014; Li, O'Doherty, Lebedev, & Nicolelis, 2011), or further investigation for different electrode designs to mitigate this effect.

Overall, these results suggest that future implantable systems may be more able to precisely control the position of individual joints. While many advanced prosthetic hands have fully articulated fingers and other joints (Touch Bionics, Deka), most are not natively capable of position-based control. Future designs may need to take the availability of these novel control signals into account, for example in making hands that can sense their current position for real time adjustment. For future studies, we would like to (1) increase the number of EMG electrodes that can be implanted simultaneously to obtain higher functionality, and (2) evaluate the use and controllability of multiple DOFs both individually and in combination. Combined with intramuscular recording of EMG, Kalman filter based positional control may provide patients with more naturalistic movements of their prosthetic limb.

CHAPTER III

Viability of Regenerative Peripheral Nerve Interfaces in Humans with Amputations

3.1 Abstract

Peripheral nerves provide a promising source of motor control signals for neuroprosthetic devices because they are relatively easy to access and functionally selective. Unfortunately, the clinical utility of current peripheral nerve interfaces is limited due to their lack of long-term stability and low amplitude signals. In contrast, the Regenerative Peripheral Nerve Interface (RPNI) is biologically stable and serves as a functionally selective, bioamplifier of efferent motor action potentials. The RPNI is created by suturing a small muscle graft on the residual end of a peripheral nerve or fascicle. The muscle graft is reinnervated, creating a stable bioamplifier of nerve signals. In this study, we demonstrate the viability of RPNIs to provide high fidelity efferent motor signals in three human participants.

Participant 1 (P1) underwent a proximal transradial amputation and implantation of nine RPNIs, while participant 2 (P2) and participant 3 (P3) had a distal transradial amputation with implantation of three and four RPNIs, respectively. Ultrasonography was used to visualize the RPNIs, and fine wire bipolar electrodes were percutaneously implanted in P1, P2, and P3. Later in a separate surgery, indwelling intramuscular bipolar electrodes were surgically implanted for P2

and P3. Efferent motor action potentials were then recorded from the RPNIs during volitional finger movements.

Ultrasound demonstrated strong contractions of P1 and P2's median RPNIs during flexion of the phantom thumb and P1's ulnar RPNIs during small finger flexion. In P1, the median RPNI and ulnar RPNIs produced signals with a signal-to-noise ratio (SNR) of 4.62 and 3.80, respectively. In P2, the median RPNI and ulnar RPNI had an average SNR of 107 and 35.9, respectively, while P3's median RPNI and ulnar RPNIs had an average SNR of 22.3 and 19.4, respectively.

This study provides evidence that the transected peripheral nerves have reinnervated the RPNI muscle grafts allowing RPNIs to transduce and amplify efferent motor action potentials during volitional individual finger movements. Thus, RPNIs show promise in enhancing prosthetic rehabilitation in patients with limb loss.

3.2 Introduction

Limb loss can dramatically alter an individual's lifestyle and impede the ability to perform activities of daily living. Building a direct interface to the peripheral nervous system may be a viable option for providing intuitive control of a prosthesis. However, current peripheral nerve interfaces have limitations, which minimize their clinical utility. Electrodes placed within a peripheral nerve can record distinct efferent motor action potentials but can experience a decline in signal amplitude over time (Davis et al., 2016). In contrast, electrodes placed around a nerve have been successfully used in humans for more than two years. These electrodes can be used to stimulate efferent motor axons to control distal innervated muscles and afferent sensory axons to provide patients with a sense of touch and pressure while using a prosthesis (Tan et al., 2014).

However, recording specific efferent motor action potentials is challenging, limiting the number of independent control signals (Dweiri et al., 2017).

Targeted muscle reinnervation (TMR) can provide multiple control signals by transferring divided peripheral nerves in a residual limb to intact local or regional muscles. Surface electromyography (EMG) is then used to record the efferent motor control signals (Zhou et al., 2007). With TMR, a normally innervated muscle must be partially denervated to provide a new target muscle for recording EMG signals from the implanted nerve. In addition, two or three nerves (median, radial, and ulnar) may be implanted into the same target muscle (e.g. pectoralis major muscle), making it difficult to record independent control signals from individual nerves or fascicles. Consequently, participants can control a limited number of independent, simultaneous movements (Cheesborough et al., 2015).

To achieve both greater signal specificity and long-term signal stability, we have developed the Regenerative Peripheral Nerve Interface (RPNI). An RPNI is composed of a transected peripheral nerve, or peripheral nerve fascicle, that is implanted into a free muscle graft. The free muscle graft undergoes a three month process of regeneration, revascularization, and reinnervation by the implanted peripheral nerve. This creates a stable, peripheral nerve bioamplifier that produces high amplitude EMG signals which can be used to control a prosthetic device (Irwin et al., 2016; Kung et al., 2014; Ursu et al., 2016; Vu et al., 2018). Additionally, RPNIs have been shown to prevent and treat neuroma pain and phantom pain after amputation (Woo et al., 2016; Kubiak, Kemp, Cederna & Kung, In press). Here, we present initial results in three participants with upper extremity limb loss who have undergone RPNI implantation.

3.3 Materials & Methods

The Institutional Review Board at the University of Michigan approved this study, and each participant provided written and informed consent.

3.3.1 RPNI Construction

In this pilot study, three participants underwent RPNI surgery to treat neuroma and phantom pain. A 3 x 1.5 x 0.5 cm muscle graft was harvested from a healthy native donor muscle. The distal end of a transected peripheral nerve in the residual limb was isolated. The end of the isolated nerve or nerve fascicle was implanted into the muscle graft and secured into position to create an enclosed biologic peripheral nerve interface. This procedure was then repeated to provide the desired number of RPNIs (Figure 3.1a).

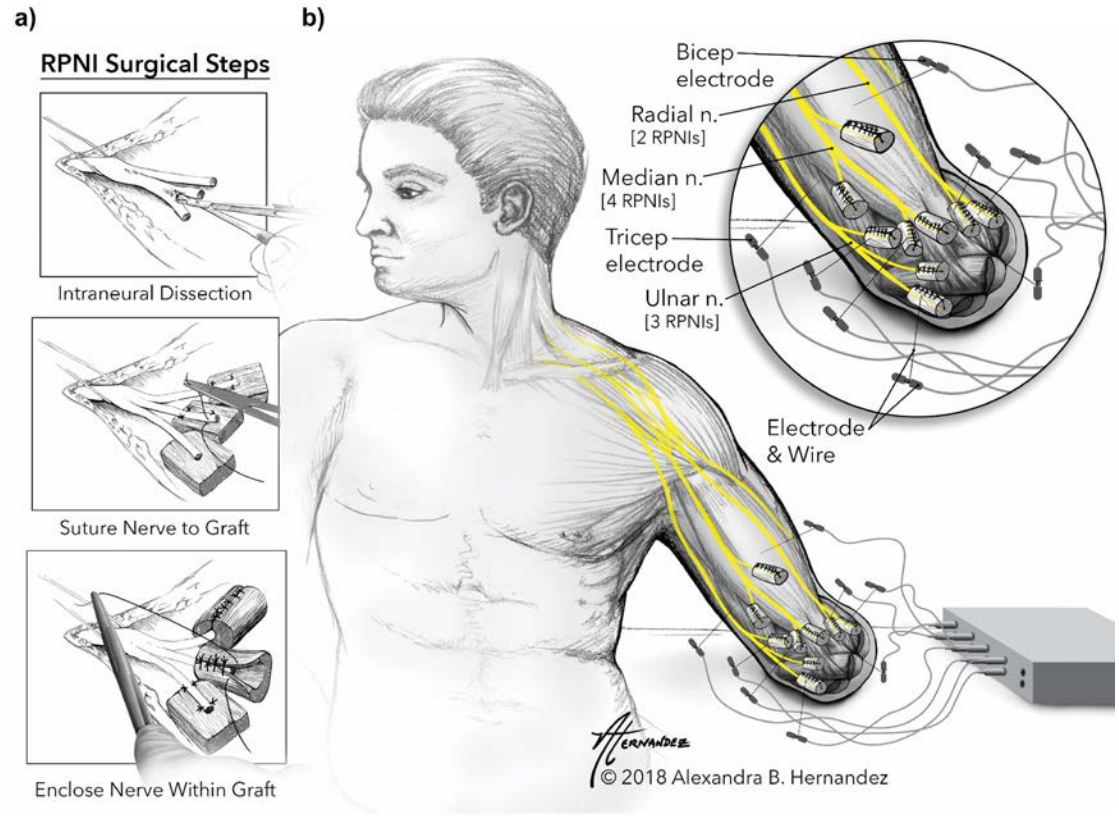

Figure 3.1 RPNI surgical construction and implantation, and P1's electrode insertion. (a) A peripheral nerve in the residual limb is identified and isolated. The nerve is either used whole or is dissected into individual nerve fascicles by performing intraneural dissection. A muscle graft is then harvested from a regional or distant site. The nerve or fascicle is then sutured to the muscle graft and the graft is wrapped around the nerve and sutured together to form am RPNI. (b) Illustration of percutaneous bipolar hook electrodes embedded into the RPNI muscle belly and the remaining bicep and triceps muscles of P1 during acute sessions. Following electrode placement, the lead wires were plugged into a neural recording system.

3.3.2 Participant 1 (P1)

P1 is a 45 year old male who sustained a left proximal transradial amputation. He presented 16 years postoperatively with severe, persistent neuroma pain that was inadequately treated using traditional techniques. In 2016, the patient underwent excision of his ulnar, median, and radial nerve neuromas at the level of his antecubital fossa. An intraneural dissection of the median, ulnar, and radial nerves was performed to isolate individual nerve fascicles. Four RPNIs were created on the median nerve, three RPNIs on the ulnar nerve, and two RPNIs on the radial nerve (Figure 3.1b, 3.2a). The RPNIs were created by harvesting free muscle grafts from the ipsilateral vastus lateralis muscle and then implanting the end of each divided nerve fascicle into a separate muscle graft.

3.3.3 Participant 2 (P2)

P2 is a 30 year old male who sustained a traumatic amputation of the right hand resulting in a right wrist disarticulation. He presented two years after his original injury with severe, persistent symptomatic neuromas of the median, ulnar, and dorsal radial sensory nerves. The pain limited his ability to wear his prosthesis. In 2015, P2 underwent resection of his median, ulnar and radial nerve neuromas in his distal forearm. One RPNI was created on each of these nerves using free skeletal muscle grafts from his ipsilateral vastus lateralis (Figure 3.2b).

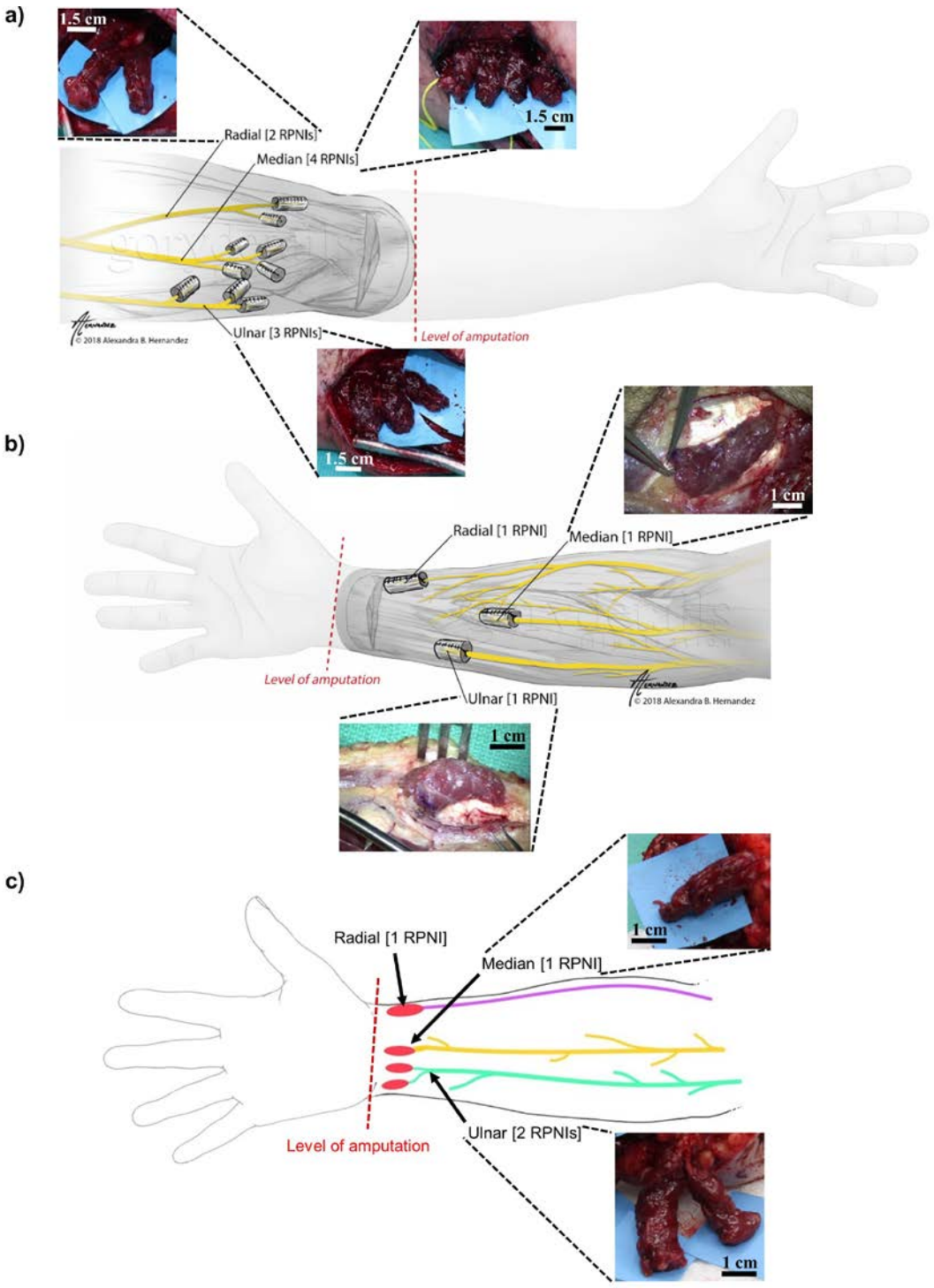
a)
1.5 cm
1.5 cm
Radial [2 RPNIs]
Median [4 RPNIs]
Ulnar [3 RPNIs]
Level of amputation
© 2018 Alexandra B. Hernandez
1.5 cm
b)
1 cm
Radial [1 RPNI]
Median [1 RPNI]
Level of amputation
Ulnar [1 RPNI]
© 2018 Alexandra B. Hernandez
1 cm
c)
1 cm
Radial [1 RPNI]
Median [1 RPNI]
Level of amputation
Ulnar [2 RPNIs]
1 cm

Figure 3.2 RPNI surgical implantation. (a) Anatomical layout of P1's RPNI surgical implantation. P1 had 9 RPNIs implanted: 4 for the median nerve, 3 for the ulnar nerve, and 2 for the radial nerve. (b) Anatomical layout of P2's RPNI surgical implantation. P2 had three RPNIs implanted, one on each of the median, ulnar, and dorsal radial sensory nerves. (c) Anatomical layout of P3's RPNI surgical implantation. P3 had four RPNIs implanted, one on each of the median and radial nerve, and two on the ulnar nerve.

3.3.4 Participant 3 (P3)

P3 is a 53 year old female who suffered a suspected urinary tract infection, leading to septic shock and acute renal failure. Her treatment was complicated by an IV extravasation of calcium into her right hand and forearm, leading to tissue necrosis and requiring a partial hand amputation. Her hand became contracted with limited flexion/extension, pronation/supination, and limited function. In 2017, P3 underwent a voluntary wrist disarticulation amputation. Free muscle grafts were extracted from the ipsilateral vastus lateralis. An RPNI was created on each of the median and radial nerves, while an intraneural dissection of the ulnar nerve was performed to create two RPNIs (Figure 3.2c).

3.3.5 Electrophysiology

P1, P2, and P3 participated in experimental sessions beginning four, six months, and eleven months post-RPNI surgery, respectively. Initiation of experimentation was based on patient availability and results from previous animal work which demonstrated that it took approximately three months for RPNIs to mature and stabilize (Irwin et al., 2016; Kung et al., 2014). During each experiment, ultrasound imaging was performed to identify the RPNIs and to guide percutaneous placement of fine wire electrodes into the RPNIs (Natus Medical P/N 019-475400). At the same time, fine wire electrodes were also placed percutaneously into innervated muscles in the residual limb (Figure 3.1b). The electrodes were removed at the completion of each session.

After obtaining RPNI signals and achieving prosthetic control with the fine wires, P2 and P3 elected to undergo surgical implantation of eight indwelling intramuscular bipolar electrodes (30.5 x 0.025 cm, Synapse Biomedical, Oberlin, OH, USA). The electrodes consist of two stainless steel leads coiled in a double helix formation and insulated with perfluoroalkoxy (PFA) material. For P2, electrode implantation was performed three years following the original RPNI surgery and five years following the original amputation. One electrode was implanted in each of the median and ulnar nerve RPNIs (Figure 3.3a) and six electrodes were implanted in residual muscle. For P3, electrode implantation was performed 12 months following the original RPNI and amputation surgery. P3 had three electrodes implanted in the RPNIs, and five were implanted in the residual muscle (see Table A.1 for details). No electrode was implanted into the dorsal radial sensory RPNI for either participant since it is a purely sensory nerve and transduces no efferent motor action potentials. A neural signal processor (NeuroPort, Blackrock Microsystems, Salt Lake City, UT, USA) filtered EMG signals from residual muscles and RPNIs between 3-7000 Hz (unity gain) and recorded the signals for offline analysis. For all three participants, EMG signal to noise ratio (SNR) was calculated offline. Specifically, the root mean square (RMS) of the EMG amplitude during maximal voluntary contraction (MVC) was divided by the RMS of the electrode's noise floor seen during rest. The calculated SNR and MVC are averaged across two sessions with fine wire electrodes in P1 and three sessions with indwelling electrodes in P2 and P3.

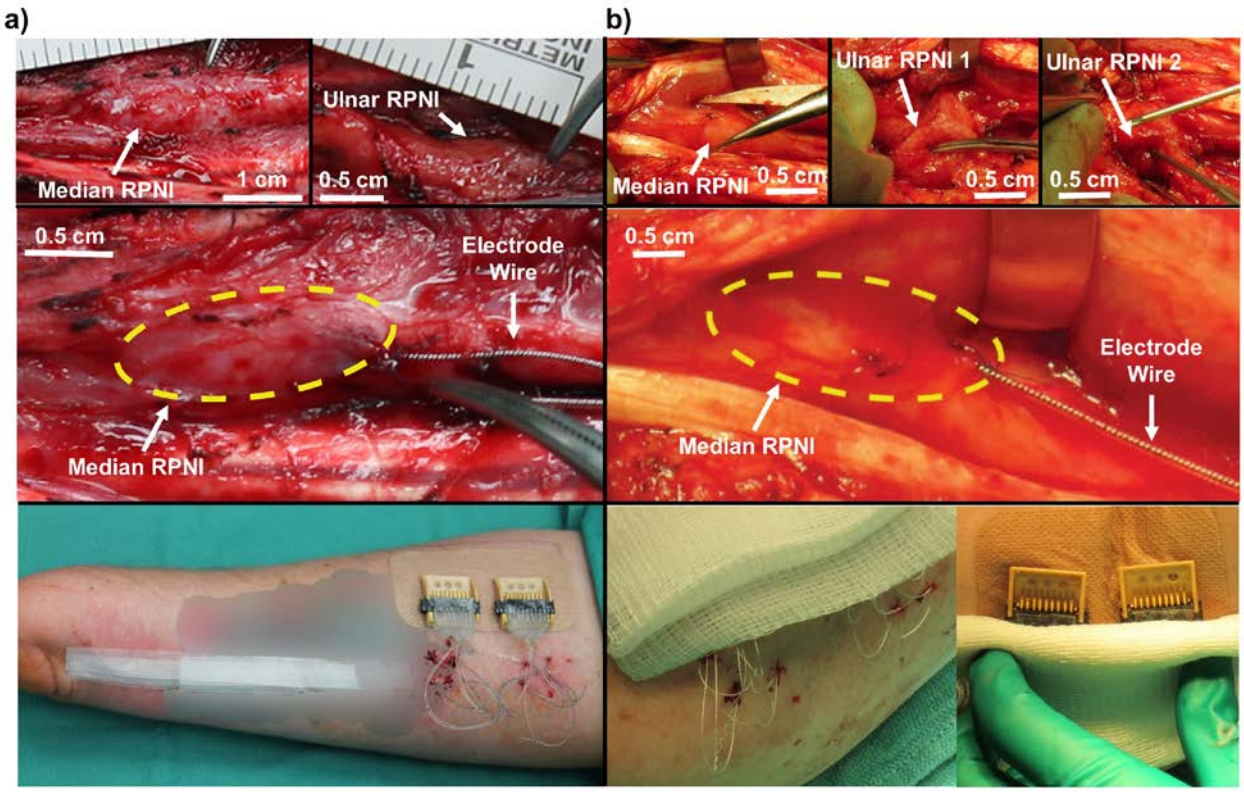

Figure 3.3 Electrode implantation for P2, and P3. (a) P2 underwent bipolar electrode implantation after several acute sessions. (Top) Surgical photos show the RPNIs three years post-implantation. (Middle) Example of wire insertion into the RPNI muscle graft (dashed line). (Bottom) Final connector setup after all electrodes have been implanted (Partially blurred to protect participant identification). (b) P3 underwent bipolar electrode implantation approximately 12 months post RPNI implantation. (Top) Surgical photos show the median RPNI, ulnar RPNI 1, and ulnar RPNI 2 before electrode implantation. (Middle) Example of wire insertion into the RPNI muscle graft (dashed line). (Bottom) Final connector setup after all electrodes have been implanted.

3.3.6 Ultrasound Imaging and Recording

In separate experimental sessions, a 15-6 MHz linear array ultrasound transducer (Sonosite X-Porte, Bothell, Washington, USA) was positioned along the transverse plane of the arm to locate and measure the size of the RPNIs in each participant. In addition, the subjects were asked to perform finger movements with their phantom hand, and the changes in the size and shape of the associated RPNIs were evaluated and visualized. P1 volitionally flexed and

extended his phantom thumb at a self-paced frequency of 1.5 Hz for a duration of approximately 13 seconds. Subsequently, he was asked to move his phantom index and then his phantom small finger in a similar manner. P2 had a distal transradial amputation and was asked to perform activities which required function of his absent intrinsic hand muscles. In particular, he volitionally flexed and extended his small finger metacarpal phalangeal (MCP) joint at ~0.5 Hz (self-paced) for approximately 16 seconds. Subsequently, he simultaneously flexed and extended his index and middle finger MCP joint, and then his thumb MCP joint. Each ultrasound video clip was evaluated qualitatively and quantitatively.

To quantify the contraction of the RPNIs, frames at rest and at maximum volitional contraction (MVC) of each video were analyzed and the percent difference of pixel mean intensity (MI) and standard deviation (SD) between frames was calculated. Using Matlab (MathWorks, Natick, Massachusetts), the selected frames were segregated and labeled as rest or MVC. Subsequently, the manually traced RPNI region was extracted from each frame and the remaining area was identified as the "surrounding tissue". Similar calculations of the pixel MI and SD were taken as well as the percent differences between frames. A Wilcoxon rank sum test was used to test for significance between the percent differences of the surrounding tissue and the percent differences of the traced RPNI regions. Ultrasound data was collected in two sessions in P1 and one session in P2.

3.4 Results

3.4.1 P1

P1's median nerve RPNI grafts, located near the short head of the biceps brachii, demonstrated independent muscle contractions during attempted thumb metacarpophalangeal

(MCP)/interphalangeal (IP) and index finger proximal interphalangeal (PIP)/distal interphalangeal (DIP) joint flexion of the phantom limb. In particular, median RPNI one contracted for thumb flexion, while a combination of median RPNI one, two, three, and four contracted for index finger flexion (Figure 3.4a, 3.4b). These movements correlated anatomically to the level of amputation (Table A.2). Ultrasound imaging showed isolated median RPNI contractions with minimal movement of the surrounding tissue. For RPNI one, pixel changes were significantly larger within the RPNI than in the surrounding tissue during thumb flexion (MI = 8.34% vs. 1.20% $p < .001$, SD = 10.80% vs. 0.28% $p < .001$). Recorded EMG signals from RPNI one during thumb flexion demonstrated a signal to noise ratio (SNR) of 4.62 (Figure 3.4c). A subregion of median RPNI one also contracted for index finger movement, significantly more than surrounding tissue (MI = 4.49% vs. 0.18% $p < .001$, SD = 6.74% vs. 0.25% $p = .002$). Median RPNIs 2 to 4 were observed to make smaller contractions compared to median RPNI one during median nerve appropriate finger flexion and had mixed significant pixel changes compared to surrounding tissue (See Table 3.1).

For both ulnar RPNI one and two, located near the long and medial heads of the triceps brachii, contractions were observed during attempted phantom small finger PIP/DIP joint flexion as expected. Pixel changes in ulnar RPNI one and two (MI = 12.8%, 1.24%, SD = 11.2%, 2.37%, respectively) were significantly larger than in the surrounding tissue (MI = 0.86%, 0.67% SD = 0.33%, 0.16% $p < .001$ for all comparisons). Acute EMG was recorded from all three ulnar RPNIs with an average SNR of 3.80 during voluntary small finger contractions (Figure 3.4f). A subsection of ulnar RPNI one contracted for thumb MCP/IP joint flexions, while a subsection of ulnar RPNI two contracted for both thumb MCP/IP and index PIP/DIP joint flexions (Figure 3.4d, 3.4e). Contractions of the ulnar nerve RPNIs are expected based on the ulnar nerve

innervation of both the adductor policis muscle and the deep head of the flexor policis brevis. The unexpected contraction for the index finger may be due to P1's 16 year period without a hand, and no training with the virtual hand or the prosthesis, making certain volitional movements difficult to generate independently.

3.4.2 P2

Unlike P1, P2 had RPNIs placed in areas with residual innervated muscles controlling finger movement, prompting more reliance on surgically placed EMG leads (rather than ultrasound guided lead placement) for analysis. Figure 3.5a and 3.5d show sonographs of the median and ulnar RPNI captured 31 months post-RPNI surgery. P2's median RPNI contracted appropriately during phantom thumb MCP joint flexion (Figure 3.5b). Specifically, the median RPNI changed shape independently of the adjacent residual tissue.

Stronger evidence of reinnervation for both the ulnar and median RPNIs came from the surgically implanted bipolar electrodes. For the median RPNI, EMG recordings during voluntary thumb movements showed average peak-to-peak amplitude of 2.88 mV, with an SNR of 107 (Figure 3.5c). During voluntary small finger movements, the average peak-to-peak amplitude from the ulnar RPNI was 501 μV, with an SNR of 35.9 (Figure 3.5e, 3.5f). As expected, minimal median RPNI EMG firing was detected during small finger flexion. For the ulnar RPNI, EMG firing appropriately occurred during flexion of the phantom thumb, while minimal activation occurred during index finger flexion as expected (Figure 3.6a). Additionally, both the median ulnar RPNIs activated for hand abduction and hand adduction, finger movements that are dominantly driven with intrinsic muscles. This suggest that RPNIs are receiving some level of efferent motor signals that would be absent due to amputation.

Table 3.1 Quantitative analysis of ultrasound videos for P1 and P2

Participant	Finger movement		Pixel mean intensity change (%)	Pixel standard deviation change (%)	Compared against surrounding tissue Mean intensity p – value, Standard deviation p – value
P1	Thumb MCP/IP flexion	Surrounding Tissue	1.20	0.28	N/A
		Median RPNI 1	8.34	10.80	p < .001, .001
		Median RPNI 2	2.33	0.61	p < .001, = .005
		Median RPNI 3	5.91	0.81	p = .03, < .001
		Median RPNI 4	1.45	0.20	p = .74, .02
		Surrounding Tissue	1.23	0.52	N/A
		Ulnar RPNI 1	6.08	11.6	p = .47, < .001
		Surrounding Tissue	0.33	0.11	N/A
		Ulnar RPNI 2	1.11	0.16	p < .001, .001
	Index finger PIP/DIP flexion	Surrounding Tissue	0.18	0.25	N/A
		Median RPNI 1	4.49	6.74	p < .001, .002
		Median RPNI 2	0.60	3.07	p = .52, < .001
		Median RPNI 3	7.90	11.8	p = .005, < .001
		Median RPNI 4	0.16	4.63	p = .18, .01
		Surrounding Tissue	0.28	0.09	N/A
		Ulnar RPNI 1	3.02	3.22	p = .06, .01
		Surrounding Tissue	0.08	0.62	N/A
		Ulnar RPNI 2	4.59	7.28	p < .001, .001

CMC – Carpometacarpal joint, MCP – metacarpophalangeal joint, PIP – proximal interphalangeal joint, DIP – distal interphalangeal joint, IP – interphalangeal joint

Table 3.1 Quantitative analysis of ultrasound videos for P1 and P2 (continued)

Participant	Finger movement		Pixel mean intensity change (%)	Pixel standard deviation change (%)	Compared against surrounding tissue Mean intensity p – value, Standard deviation p – value
P1	Small finger PIP/DIP flexion	Surrounding Tissue	0.02	0.24	N/A
		Median RPNI 1	2.01	1.02	p = .008, .48
		Median RPNI 2	1.41	2.20	p = .005, < .001
		Median RPNI 3	0.64	0.19	p = .009, .005
		Median RPNI 4	0.57	2.03	p = .50, .01
		Surrounding Tissue	0.86	0.33	N/A
		Ulnar RPNI 1	12.8	11.2	p < .001, .001
		Surrounding Tissue	0.67	0.16	N/A
		Ulnar RPNI 2	1.24	2.37	p < .001, .001
P2	Thumb CMC/MCP flexion	Surrounding Tissue	1.13	0.47	N/A
		Median RPNI	16.3	8.88	p = .001, .002
		Surrounding Tissue	2.08	6.66	N/A
		Ulnar RPNI	4.22	1.73	p = .02, .004
	Index and Middle finger MCP flexion	Surrounding Tissue	3.75	0.67	N/A
		Median RPNI	8.47	11.4	p = 0.07, 0.002
		Surrounding Tissue	3.94	0.93	N/A
		Ulnar RPNI	1.02	0.64	p = .004, .16
	Small finger MCP flexion	Surrounding Tissue	0.30	1.22	N/A
		Median RPNI	6.79	3.17	p = .01, .07
		Surrounding Tissue	0.86	0.67	N/A
		Ulnar RPNI	3.70	3.21	p < .001, .001

CMC – Carpometacarpal joint, MCP – metacarpophalangeal joint, PIP – proximal interphalangeal joint, DIP – distal interphalangeal joint, IP – interphalangeal joint

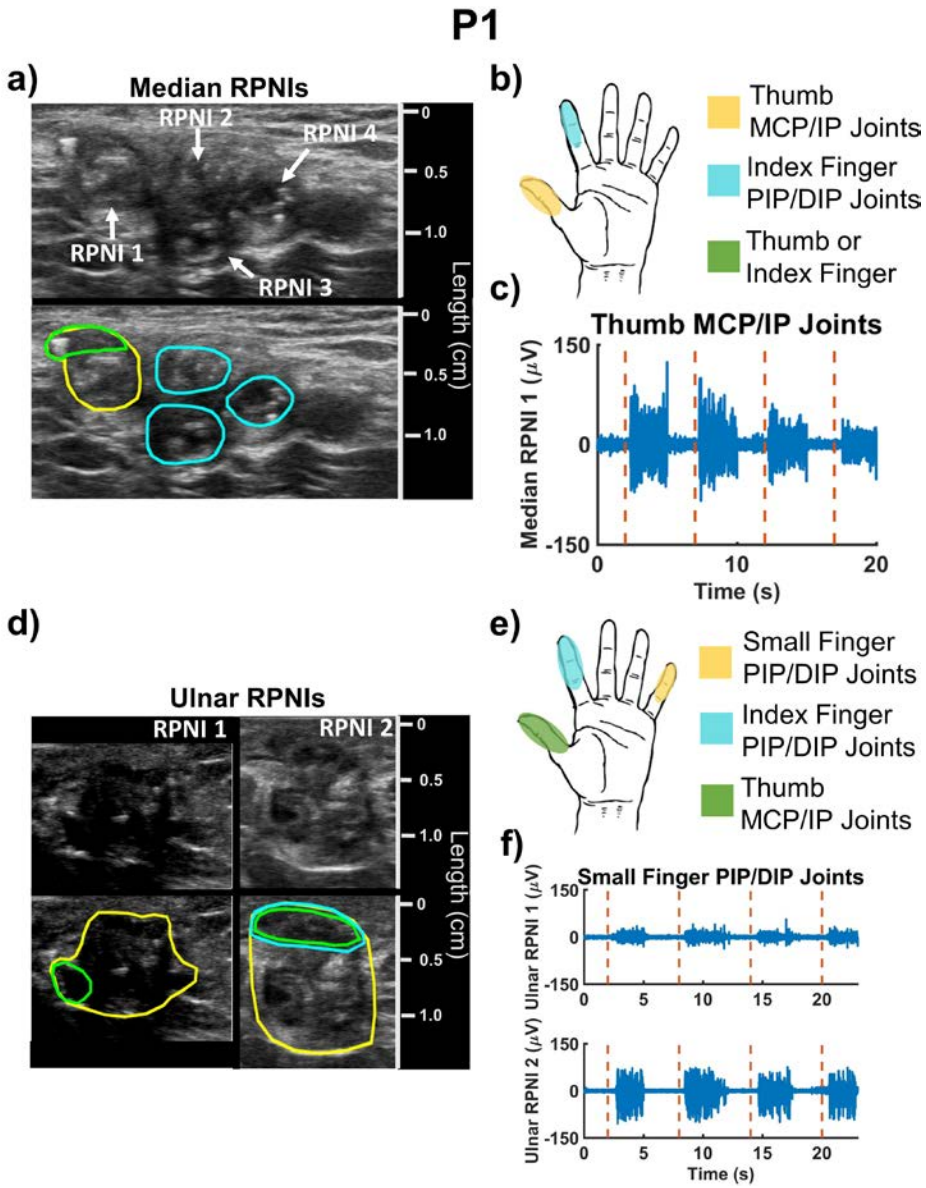

Figure 3.4 P1's RPNI sonograms, motor map, and electrophysiology. (a), (d) P1's median and ulnar RPNI sonograms captured 19 months post-RPNI surgery. Highlighted areas on the sonogram and hand map (b), (e) show which region of the RPNIs contracted and for what finger, respectively. (a), (b) The median RPNIs contracted during thumb MCP/IP and index finger PIP/DIP joint flexion. In particular, median RPNI 1 strongly contracted during thumb MCP/IP joint flexion (yellow), while different regions of median RPNI 1, 2, 3, and 4 contracted during index finger PIP/DIP joint flexion (cyan). A subsection of median RPNI 1, highlighted green, contracted for either thumb MCP/IP or index finger PIP/DIP joint flexion. (c) A sample of median RPNI 1's EMG signals (blue) recorded after cued thumb MCP/IP joint movement (red dashed line). (d), (e) The ulnar RPNI 1 and 2 contracted during small finger PIP/DIP joint flexion (yellow), while a subsection of both RPNI grafts contracted during thumb MCP/IP joint flexion (green). Additionally, a subsection of ulnar RPNI 2 contracted for index finger PIP/DIP joint flexion (cyan). (f) A sample of EMG signals (blue) recorded after cued small finger PIP/DIP movement (red dashed line).

3.4.3 P3

Similar to P2, evidence of RPNI reinnervation in P3 relied more on surgically implanted electrodes since P3's RPNIs were also placed within areas of residual muscles innervated for finger movement. All three RPNIs were located under ultrasound approximately 16 months post-RPNI surgery and 4 months post-indwelling electrode surgery Figure (3.5g, 3.5j). EMG was recorded on all three implanted RPNIs. Specifically, the median RPNI strongly activated for thumb IP joint flexion (Figure 3.5h), while ulnar RPNI 1 and 2 activated for small finger flexion (Figure 3.5k). On average, EMG recordings for the median RPNI had a peak-to-peak amplitude of 649 μV, and SNR of 22.3 (Figure 3.5i). For the ulnar RPNI 1 and 2 the average peak-to-peak amplitude was 386 μV and 474 μV with an SNR of 19.4 and 19.5, respectively (Figure 3.5l). As expected, minimal activation occurred during small finger flexion for the median RPNI, while both ulnar RPNIs had little to no activation during index finger movement (Figure 3.6b). Like P2, RPNI EMG activation occurred during cued hand abduction and hand adduction movements. Specifically, ulnar RPNI 2 strongly activated during hand adduction as well as hand abduction. Additionally, ulnar RPNI 2 activated for thumb CMC/MCP joint flexion, which further suggests that RPNIs are receiving missing intrinsic motor signals

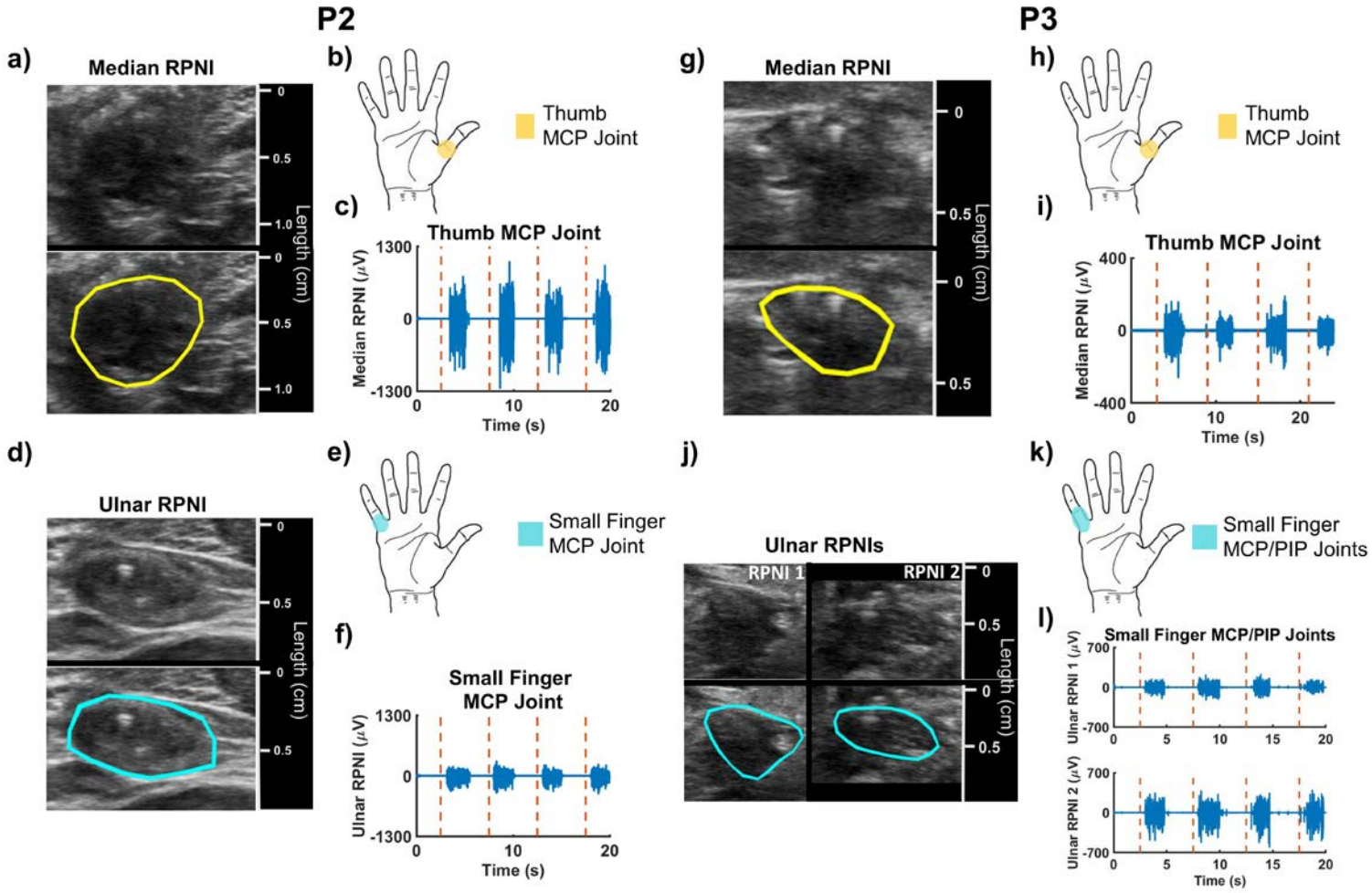

Figure 3.5 P2 and P3's RPNI sonograms, motor map, and electrophysiology. (a), (d) P2's median and ulnar RPNI sonograms captured 31 months post-RPNI surgery. (a), (b) The median RPNI contracted during thumb MCP joint flexion (yellow). (c) A sample of EMG signals recorded after cued thumb movement (red dashed line). (d), (e) Contraction of surrounding tissue obscured any obvious contractions of the ulnar RPNI during small finger MCP joint flexion (cyan). (f) However, a sample of ulnar RPNI EMG signals (blue) were recorded after cued small finger movement (red dashed line). (g), (j) P3's median and ulnar RPNI sonograms captured 16 months post-RPNI surgery and 4 months post-indwelling electrode surgery. (g), (h), (j), (k) Like P1's ulnar RPNI, contraction of surrounding tissue obscured any obvious contractions of P3's RPNIs. (i), (l) However, EMG signals (blue) were recorded after cued thumb movement and small finger movement (red dashed line) in the median and ulnar RPNIs, respectively.

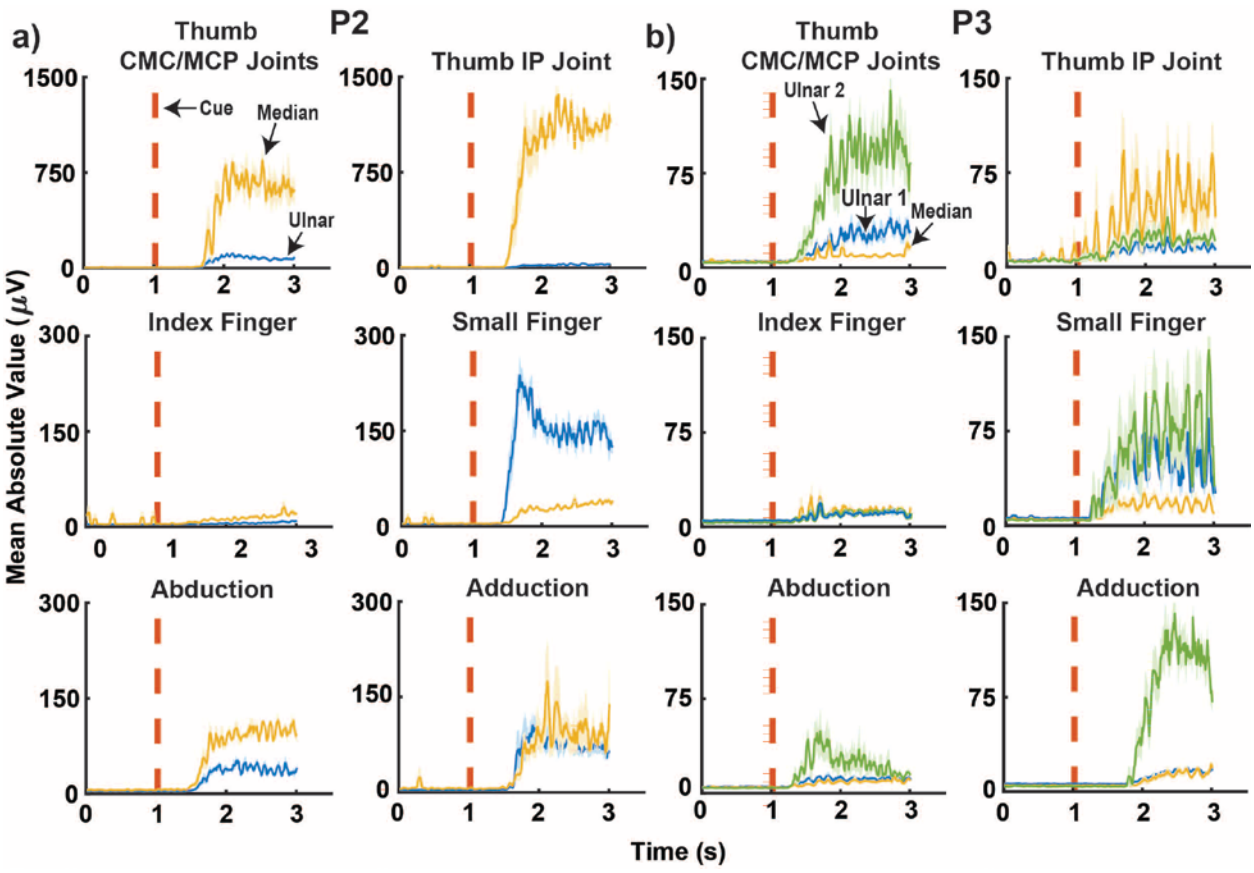

Figure 3.6 P2 and P3's RPNI mean absolute value (MAV) signals during six different finger movements. (a) P2's median and ulnar RPNI MAV signals during Thumb CMC/MCP joint flexions, Thumb IP joint flexion, index MCP/PIP/DIP joint flexions, small MCP/PIP/DIP joint flexions, hand abduction and adduction movements. Each median (maize) and ulnar (blue) trace is averaged across 5-6 trials from a single experimental block. P2's median and ulnar RPNIs activated the strongest during anatomically appropriate movements. (b) P3's median ulnar RPNI 1 and ulnar RPNI 2 MAV signals during Thumb CMC/MCP joint flexions, Thumb IP joint flexion, index MCP/PIP/DIP joint flexions, small MCP/PIP/DIP joint flexions, hand abduction and adduction movements. The median (blue), ulnar 1 (maize), and ulnar 2 (green) traces are averaged across 10 trials from a single experimental block. Like P2, P3's RPNIs activated for anatomically appropriate movements.

3.5 Discussion

We have demonstrated that RPNIs are an effective peripheral nerve interface to provide efferent motor signals for control of prosthetic devices. The RPNI amplifies efferent nerve signals to provide favorable SNRs for high fidelity control of both extrinsic and intrinsic hand

functions. The SNR of the recorded EMG had a mean of 4.21 in P1, a mean of 71.5 in P2, and a mean of 20.4 in P3. The wide SNR gap between P1 versus P2, P3 is mainly due to fine wires versus implanted indwelling wires, while the difference between P2 and P3's measured SNR may be due to the period of reinnervation. P2's nerves had two plus years to reinnervate his muscle grafts before electrode implantation. Nonetheless, P2 and P3's SNR were substantially larger for RPNIs with implanted bipolar electrodes than measured SNR in nerve cuff electrodes or intraneural probes (Sahin et al., 1997; Wendelken et al., 2017). Intraneural probes, such as the Utah Slanted Electrode Array, can provide larger signals, but they do not remain stable over time (Wendelken et al., 2017). In comparison, RPNIs have remained a stable peripheral nerve interface in P1, P2 and P3 for two, three and one year(s), respectively. The chronic bipolar electrodes used in this study are similar to those that have been previously observed to record stable EMG for up to 7.5 years (Memberg, Polasek, et al., 2014). As P2 and P3 remain implanted, we hypothesize that RPNI signals will continue to demonstrate stability over the course of their implantation.

With ultrasound guidance, we demonstrated at the proximal transradial level that different subregions of each RPNI contracted for different volitional movements. This is not surprising since the reinnervated muscle of the RPNI will have different single motor units reinnervating distinct portions of the free muscle graft. With surgically implanted indwelling electrodes at the distal transradial level, we have shown that RPNI EMG activation occurred during specific intrinsic hand movements. Together, this suggests that RPNIs are functionally selective to a certain degree. To gain even greater selectivity for prosthetic control, electrodes with more recording sites within RPNIs can theoretically provide enhanced signaling. In contrast to intraneural electrodes, which require numerous recording sites a few hundred microns apart,

electrodes in RPNIs could have recording sites millimeters apart to record different efferent motor control signals.

In the past, investigators have provided prosthetic control signals by interfacing with muscles in the residual limb. This strategy has provided reasonable signal amplitude and demonstrations of some control of a prosthetic limb in patients undergoing transradial amputations (Ajiboye & Weir, 2005; Cipriani et al., 2011; Jiang et al., 2014; Li, Schultz, & Kuiken, 2010; Smith et al., 2015). However, when intrinsic hand muscles and extrinsic flexors and extensors of the fingers are absent, there is no effective way to obtain these control signals without directly interfacing with the peripheral nerves. RPNIs have provided an alternative where extracting efferent motor action potentials from the peripheral nerve is possible. Furthermore, we did not need to divide any motor branches to any of the residual muscles of the upper arm, and thus did not create any new denervated muscle, as is necessary in targeted muscle reinnervation (Kuiken et al., 2009).

We have demonstrated that RPNIs can be used to record efferent motor nerve action potentials at both the intrinsic and extrinsic levels. RPNIs have shown proficiency in amplifying motor nerve signals, enabling motor selectivity, and remain a stable interface over time. Thus, the RPNI technique combined with a wireless recording/stimulation device may provide a viable option for future clinical prosthetic technology and greatly improve the quality of life for patients with limb loss.

CHAPTER IV

Real-Time Myoelectric Prosthesis Control with Regenerative Peripheral Nerve Interfaces in Humans with Amputations

4.1 Abstract

Normal hand function requires articulation of multiple degree of freedom (DOF) joint control at high accuracy and precision. Current state of the art prosthetic hand controllers in the past decade have greatly increased hand functionality for prosthetic users. However, these controllers can only move the hand in sequential and discrete patterns. Proportional control and regression-based algorithms have been applied to allow simultaneous and continuous control, but the number of controllable DOFs dwindles as the number of available control sites disappear due to amputation. Thus, a combination of dynamic continuous controllers along with stable peripheral nerve interfaces are needed to be able to reach the level of normal hand functionality. Here, we address these issues by investigating the use of regenerative peripheral nerve interface (RPNI) signals for simultaneous and continues control of one degree of freedom finger and two degree of freedom thumb movement across two participants with transradial amputations. Participants reported in this chapter are P2 and P3 from chapter III. Both participants successfully hit targets during a center-out target task with 92.4 ± 2.3% accuracy, controlling RPNI-driven one DOF finger movements. Comparably, non-RPNI driven finger movement had similar accuracy and

performance. Without recalibrating parameter coefficients, no decreasing trend in motor performance was seen for all one DOF finger control across 300 days for P2 and 40 days for P3, suggesting that RPNIs can generate robust control signals from day to day. Lastly, using RPNI-driven control, P2 and P3 successfully manipulated a two DOF virtual and physical thumb with 96.4 ± 2.5% accuracy. This study demonstrates that RPNIs are capable of robust continuous control of one and two degree of freedom finger and thumb movements. RPNIs may be a viable option to advance peripheral nerve interfaces into clinical reality and enhance neuroprosthetic technology for people with limb loss.

4.2 Introduction

The gold standard for upper-limb neural prostheses is to replace the capabilities and functionalities of an intact human hand and arm. The human hand has 27 degrees of freedom, 4 in each finger, 5 for the thumb and 6 for the wrist (ElKoura & Singh, 2003). Beginning in the 1950s, the first neural-based controlled hand prosthesis was introduced. The myoelectric prosthesis, which utilizes the user's muscle activity as the control source, allowed users to more intuitively control their prosthetic hand (Battye et al., 1955). However, the technology was severely limited to one degree of freedom hand open/close. Since then, the advancement of myoelectric prostheses have gradually increased and has become a commercialized standard option for upper-limb amputations. Unfortunately, like body-powered hooks, myoelectric prostheses have limitations that have prevented them from reaching the gold standard of full hand restoration. Particularly, myoelectric interfaces are restricted to gross movements, and lack robust capabilities to control multiple independent finger movements. This is mainly due to the myoelectric interface setup and the interface-dependent control architecture

The control architecture of the 1960s involved using an EMG signal's amplitude, or rate of change of one to two channels to directly control a simple one degree of freedom movement (e.g. hand open/closed) and to switch between other states of movement (Scott and Dorcas, 1966; Childress 1980). Once a movement is selected, the velocity was either fixed at a certain rate or proportionally controlled. By the 1990s, the paradigm shifted to machine learning techniques, which was data driven but provided users with increased functionality and more intuitive control (Hudgins et al., 1993). As described in chapter 2.2, these algorithms can be either discrete or continuous, with continuous algorithms allowing simultaneous and proportional control. However, discrete algorithms have gain more popularity in the past two decades because of its more robust feature. As a result, they have shifted from use in a research lab to more use in a clinical research setting. One of many reasons why discrete algorithms are now the state of the art technology is that myoelectric interfaces continue to limit the advancement of the control architecture.

As described in chapter 3.2, advancement in peripheral nerve interface technology has shown promising avenues to greater prosthetic functionality in the clinical setting. For example, discrete algorithms in combination with TMR surgery has shown greater performance in prosthesis functionality than conventional control (Hargrove et al., 2017). Another study has tested TMR with more physiologically based algorithms to gain simultaneous and proportional control of multi-degree of freedom arm and hand control (Farina et al., 2017). Similarly, intraneural electrodes combined with regression-based machine learning techniques have shown to achieve simultaneous and proportional multi-DOF control but at the finger level (Wendelken et al., 2017). However, as mentioned before, these peripheral interface technologies have their shortcomings in providing both signal selectivity and signal stability at the same time. Like myoelectric interfaces, this limits their capabilities of reaching the gold standard of prosthesis technology. In this chapter,

we address these issues by investigating the efficacy of RPNIs signals to simultaneously and continuously predict end point finger dynamics in real-time. In particular, two participants with implanted RPNIs controlled one DOF finger and two DOF thumb movements with high accuracy with a virtual and physical prosthesis. Additionally, no recalibration motor performance remained high up to 12 months, demonstrating robust signal stability and fidelity. Thus, RPNIs may be a viable option to propel peripheral nerve interfaces to have a greater impact on people with limb loss.

4.3 Materials & Methods

This study was approved by the Institutional Review Board at the University of Michigan and each participant provided written and informed consent.

4.3.1 RPNI Construction, Implantation and Participants

Refer to chapter 3.3.1 for details on RPNI construction and subject implantation. Participants P2 and P3 will be reported in this chapter.

4.3.2 Electrophysiology

Refer to chapter 3.3.2 for details on the implantation of indwelling bipolar electrodes and the recording system used to obtain EMG signals.

4.3.3 Online Prosthesis Control

A continuous task was conducted to measure motor performance. Each task was split between two phases, a training phase and a decoding phase.

For the continuous task training phase, participants performed a bilateral mirrored behavioral task in which finger position from their intact hand and EMG data from their amputated

limb were recorded (Muceli & Farina, 2012). Participants donned a glove embedded with five flex sensors (Spectra Symbol) on their intact hand to measure finger position. Using the glove, they controlled a virtual prosthetic hand generated by MuJoCo software and followed a visual target during a center-out target task (Figure 4b) (Todorov, Erez, & Tassa, 2012). Participants followed the visual target for 2-5 min (~50-200 trials), and held the fingers of their intact hand and phantom hand within the target for one second. The target color would turn green if the participant successfully placed the virtual finger within the target radius. Additionally, each trial was labeled success if the participant successfully held the finger within the target.

To train one degree of freedom (DOF) finger control, P2 and P3 were asked to volitionally move the following joints: thumb interphalangeal (IP) joint, thumb carpometacarpal (CMC)/metacarpophalangeal (MCP) joints (opposition/reposition), index MCP/proximal interphalangeal (PIP)/distal interphalangeal (DIP) joints, and small MCP/PIP/DIP joints. To train two DOF thumb control, P2 and P3 were asked to volitionally move their thumb CMC/MCP and IP joints separately, then all together. Because the glove did not measure thumb opposition, a real-time computer (Matlab xPC Target) controlled the movement of the virtual finger and P2 and P3 were instructed to follow along. Additionally, P3 followed this training protocol for all her training phases for each finger, while P2 followed this protocol for some of his training phases. All participants performed at least one session of contralateral hand glove control of the virtual task for motor performance comparison.

During this training phase, a neural signal processor (NeuroPort, Blackrock Microsystems, Salt Lake City, UT, USA) filtered EMG signals from residual muscles and RPNIs between 3 to 7000 Hz (unity gain) and recorded the signals for offline analysis. The signals were then sent to xPC Target where they were further filtered from 100-500 Hz. The real-time computer calculated

the mean absolute value (MAV) from the EMG waveform (Zhou et al., 2007). Additionally, the real-time computer received and smoothed the finger position data from the glove. Both the temporal features and the finger position data were stored in Matlab to train a position/velocity Kalman filter (described in detail in Chapter 2.3), a machine learning algorithm previously shown to effectively decode RPNI signals (Vu et al., 2018). A separate computer smoothed the stored MAV feature and finger position in successive 50 ms bins for P2, and 100 ms bins for P3 and calculated Kalman filter matrix coefficients. Offline Kalman filter analysis showed that 100 ms bins gave P3 the best decoding performance. The coefficients were then uploaded to the real-time computer for use during the decoding phase. For one degree of freedom (DOF), P2 and P3's decoding features were extracted from one RPNI and an extensor channel, while for two DOF control, decoding features were extracted from all RPNIs, and all extensor channels available (Table 4.1).

During the decoding phase, the Kalman filter allowed participants to volitionally control the virtual prosthetic finger in real-time during the center-out target task. The participants performed the same task but without the data glove. The neural signal processor sent the filtered EMG signals from the residual muscles and RPNIs to the xPC target where the MAV features were calculated, smoothed, and used to decode (predict) the participant's volitional movement in real time. Participants used this decoder to control the virtual prosthetic finger between 20 to 100 trials. For one degree of freedom movements, participants were required to hold the finger within 2 cm targets for 1 second. During the two degree of freedom control, participants were required to hold within 3 cm targets for 500 ms. The physical LUKE arm (DEKA, Manchester, NH, USA) was used in place of the virtual prosthesis for some of P2's trials.

For real-time performance metrics, we calculated throughput, described by Fitts's law (Soukoreff & MacKenzie, 2004; Thompson et al., 2014), average time to success, and average success percentage (see Chapter 2.3 for detailed equations of Fitt's law). Performance data shown comes from three experimental blocks in P2 and four experimental blocks in P3.

To measure signal stability of the indwelling wires, Kalman filter matrix coefficients were calculated for one DOF finger movements as the baseline training session and reused across days. P2 and P3 performed the same target hitting task, and the real-time performance metrics mentioned above were calculated for each day. Data shown comes from nine sessions in P2 and six sessions in P3 across 300 and 40 days, respectively. Two-sample t-tests were used to evaluate differences between no recalibration and recalibration motor performance, and a Mann-Kendall test was used to evaluate increasing or decreasing trends across days. Significance was evaluated at $\alpha = 0.05$ for all t-tests. Means are reported as ± standard error. Error bars in figures represent standard error.

Table 4.1 Muscles Used to Train One DOF and Two DOF Movement Decode Parameters

ONE DOF MOVEMENT			
Participant	**Finger**	**Agonist Muscle**	**Antagonist Muscle**
P2	Thumb IP joint	Median RPNI	EPL
	Thumb CMC/MCP joints	Ulnar RPNI	EPL
	Index finger joints	FDP Index	EDC
	Small finger joints	Ulnar RPNI	EDC
P3	Thumb IP joint	Median RPNI	EDC
	Thumb CMC/MCP joints	Ulnar RPNI 2	EDC
	Index finger joints	FDP Index	EDC or EPL
	Small finger joints	Ulnar RPNI 1	EPL
TWO DOF MOVEMENT			
Participant	**Finger**	**Agonist Muscle**	**Antagonist Muscle**
P2	Thumb CMC/MCP/IP joints	Median and Ulnar RPNI	EDC and EPL
P3	Thumb CMC/MCP/IP joints	Median, Ulnar 1, and Ulnar 2 RPNIs	EDC and EPL

4.4 Results

4.4.1 Real-Time One DOF Finger Control

In chapter 3, we verified that RPNI grafts implanted in humans generate EMG signals during anatomically correct movements. Here, we wish to further characterize these signals and determine if RPNI generated signals can continuously predict finger position along the full range of motion of a single degree of freedom virtual prosthesis.

Overall, P2 and P3 successfully controlled the virtual thumb IP joint and thumb CMC/MCP joints continuously when the median or ulnar RPNI acted as the agonist muscle (Table 4.1). Across both subjects, the averaged throughput was 1.09 ± 0.096 bits/s and 1.02 ± 0.064 bits/s controlling the virtual thumb IP joint and thumb CMC/MCP, respectively (Table 4.2). These bit rates represent how efficiently subjects moved each finger within the virtual finger's full range of motion. Similar success was also observed for continuous small finger movements when the ulnar RPNIs acted as

Table 4.2 Motor Performance Averages Across Experimental Blocks for One DOF Control

Participant	Finger	Throughput (bits/s)	Time to Success (s)	Percent Correct (%)
P2	Thumb IP joint	1.28 ± 0.084	0.85 ± 0.024	98.9 ± 1.1
	Thumb CMC/MCP joints	1.26 ± 0.048	1.04 ± 0.054	96.0 ± 2.2
	Index finger joints	0.964 ± 0.14	1.44 ± 0.20	99.2 ± 0.81
	Small finger joints	1.04 ± 0.058	1.19 ± 0.048	98.7 ± 1.3
P3	Thumb IP joint	0.898 ± 0.11	1.69 ± 0.11	96.4 ± 0.50
	Thumb CMC/MCP joints	0.787 ± 0.079	2.20 ± 0.24	84.6 ± 4.6
	Index finger joints	0.581 ± 0.032	1.95 ± 0.15	92.8 ± 1.8
	Small finger joints	0.558 ± 0.035	2.62 ± 0.21	79.9 ± 4.0
Overall One DOF Mean		0.921 ± 0.073	1.62 ± 0.13	93.3 ± 2.0

the agonist muscle. The averaged throughput was 0.80 ± 0.047 bits/s controlling the virtual small finger. In comparison to non-RPNI finger control, the average throughput was 0.773 ± 0.086 bits/s. RPNI-driven fingers completed the task in 1.60 ± 0.11 s on average and were able to hit targets with 92.4 ± 2.3% accuracy. In comparison, the non-RPNI-driven finger completed the task in 1.70 ± 0.17 s and hit targets with 96.0 ± 1.3% accuracy. No significant difference was seen in motor performance between RPNI-driven and non-RPNI driven control (Two sample t-test, $p = 0.42$, 0.86, 0.59 for throughput, time to success, and percent correct, respectively). In other words, RPNI grafts performed just as well as existing innervated muscles in transradial amputations. Examples of real-time predicted trajectories for all finger movements are shown in figure 4.1.

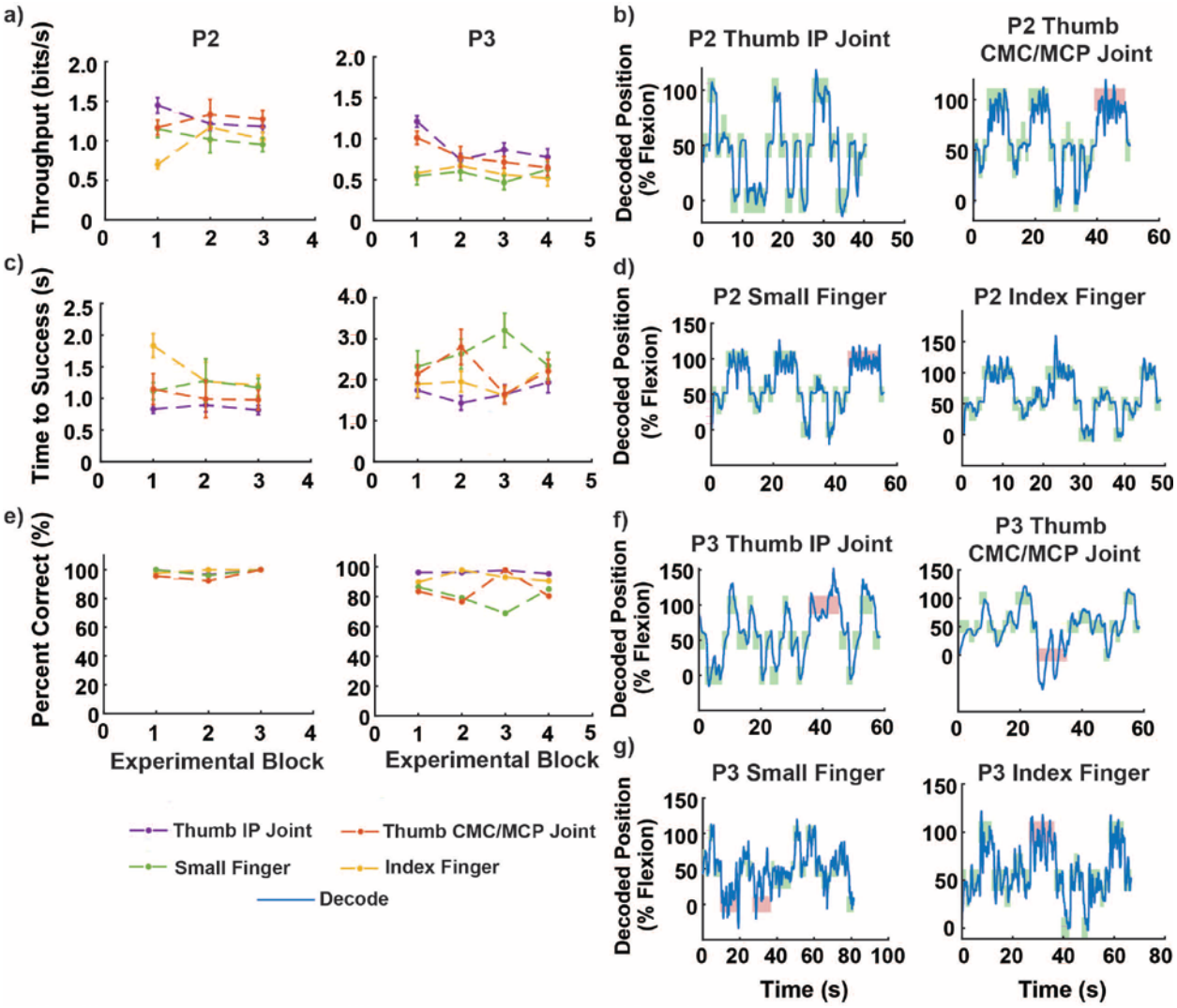

Figure 4.1 Real-time one DOF continuous decoding for P2, and P3. (a), (c), (e), P2 and P3's throughput (bits/s), time to success (s), and trial success (%) for thumb IP joint, thumb CMC/MCP joint, small finger, and index finger movements across three and four experimental blocks, respectively. (b),(d) Examples of P2's real-time predicted trajectories (blue) for all four finger movements.. Each green rectangle indicates the target was successfully hit. Red rectangles indicate unsuccessful trials. The width of the rectangle represents how long the virtual target was displayed, while the height represents the size of the virtual target. (f), (g) Examples of P3's real-time predicted trajectories for all four finger movements.

4.4.2 Motor Performance Stability for One DOF Control

In order for peripheral interfaces to reach clinical reality, they must have robust features in order to minimize error in prosthetic function. Here, we evaluate the stability of recorded RPNI and non-RPNI EMG signals from the implanted indwelling bipolar electrodes to control one DOF finger movements. One-time calculated parameter sets were reused for each finger over several experimental days. The results below represent motor performance measured up to 300 days post-implantable electrode surgery for P2, and 40 days for P3. Both subjects successfully controlled one DOF finger movements without recalibration, showing no significant increasing or decreasing trends of motor performance for either subject (Mann-Kendell test, $p > 0.05$) (Figure 4.2). Though performance varied slightly from day to day, there were no days on which the subjects felt recalibration was absolutely necessary. Additionally, there were no days in which the success rate fell below 80% (Figure 4.2b). The overall throughput was 0.955 ± 0.068 bits/s with a time to success of 1.49 ± 0.10 s and a target hit rate of 96.0 ± 1.2% (Table 4.3). In comparison to parameter recalibration motor performance (Table 4.2), there was no significant

Table 4.3 Motor Performance Averages Across Days for One DOF Control

Participant	Finger	Throughput (bits/s)	Time to Success (s)	Percent Correct (%)
P2	Thumb IP joint	1.21 ± 0.067	0.998 ± 0.096	97.5 ± 1.7
	Thumb CMC/MCP joints	1.17 ± 0.015	1.04 ± 0.072	97.5 ± 1.0
	Index finger joints	0.805 ± 0.043	1.62 ± 0.097	99.5 ± 0.49
	Small finger joints	1.04 ± 0.061	1.22 ± 0.085	99.6 ± 0.38
P3	Thumb IP joint	0.705 ± 0.11	2.04 ± 0.15	93.1 ± 1.5
	Thumb CMC/MCP joints	0.797 ± 0.11	2.04 ± 0.11	88.9 ± 2.0
Overall One DOF Mean		0.955 ± 0.068	1.49 ± 0.10	96.0 ± 1.2

difference between either method across all metrics (Two sample t-test, p = 0.81, 0.68, 0.43 for throughput, time to success, and percent correct, respectively). This suggests that (1) implantable bipolar electrodes can steadily record EMG signals, and (2) RPNI grafts can generate stable EMG signals that do not adversely affect prosthetic motor performance across time.

4.4.3 Real-Time Two DOF Thumb Control

Beyond one DOF control, normal hand function requires the use of multiple DOFs especially the thumb, which has five degrees of freedom. Here, the virtual thumb IP joint and thumb CMC/MCP joints were combined to form a continuous two degree of axis thumb control. A combination of median and ulnar RPNIs were used as agonist muscles since all grafts showed proficiency controlling one DOF movements (Table 4.1). P2 and P3 performed the same target hitting task, hitting eight different targets in a 2D space with 96.4 ± 2.5% accuracy. Their average throughput was 0.610 ± 0.041 bits/s with an average time to success of 1.66 ± 0.16 s (Figure 4.3a). Bit rate averages fell within the range (0.25 bits/s to 0.90 bits/s) of reported two DOF control for transradial amputations (Smith et al., 2015). Figure 4.3b shows an example of P2's predicted trajectories of continuous thumb control. In addition to the virtual target task, P2 was asked to use the physical prosthesis (LUKE arm, DEKA, Manchester, NH, USA) to touch the tip of a wand, placed at different locations, with the tip of the physical thumb (Figure 4.3c). The high accuracy of the thumb control seen during the virtual task easily translated to the physical prosthesis.

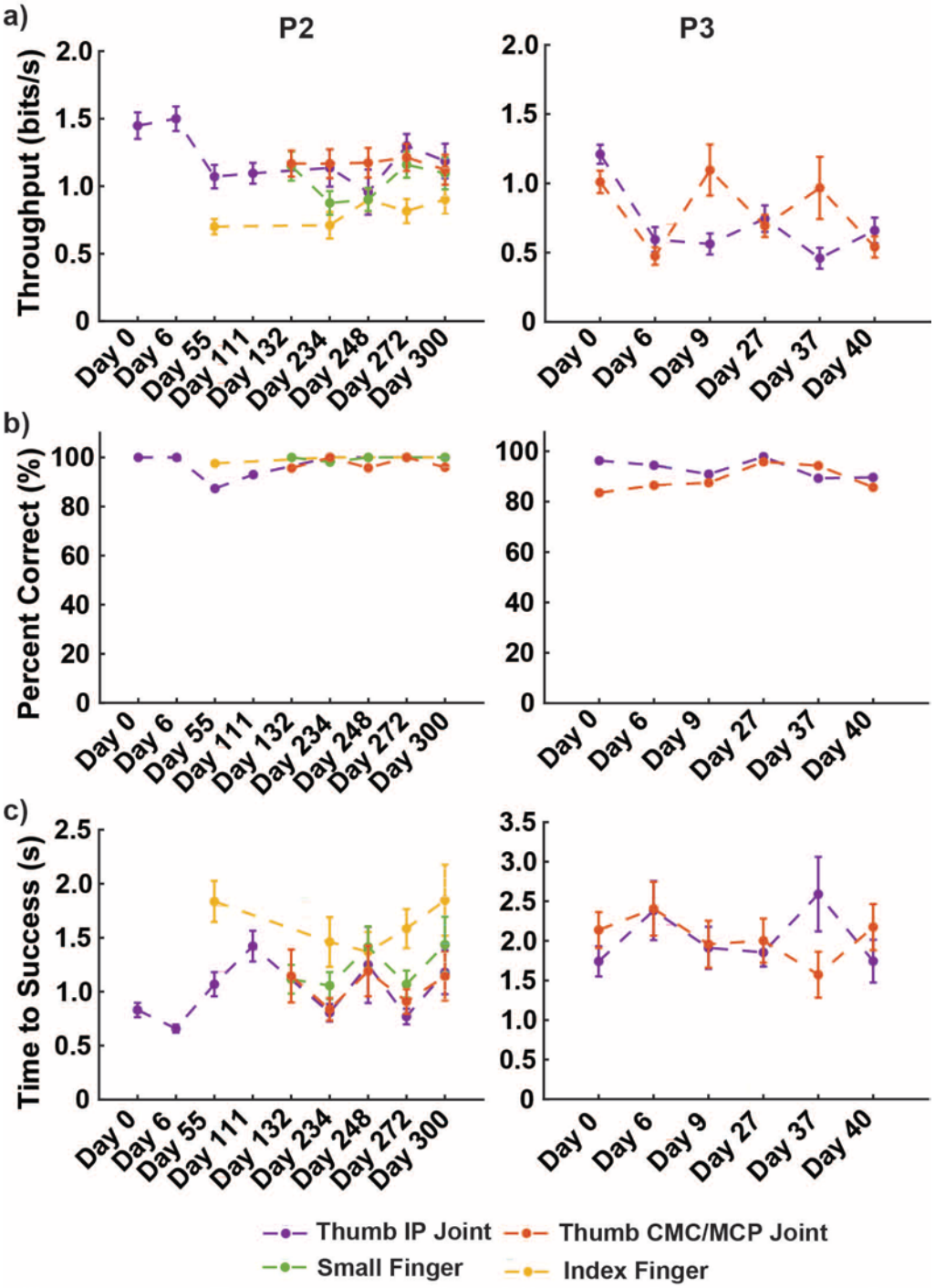

Figure 4.2 Motor performance stability of one DOF movements across time for P2, and P3. (a), (b), (c) P2 and P3's throughput (bits/s), trial success (%), and time to success (s) for thumb IP joint, thumb CMC/MCP joint, small finger, and index finger movements across 300 and 40 days, respectively. No increasing or decreasing motor performance trends were found across time (Mann-Kendell Test, $p > 0.05$).

4.5 Discussion

We have demonstrated that RPNI graft signals are capable of driving one DOF finger and two DOF thumb movements continuously and simultaneously in real-time. RPNI-driven motor performance was as effective as non-RPNI-driven motor performance, achieving target hitting accuracies greater than 90%. Across a 300 and 40 day period, P2 and P3 successfully controlled one DOF movements without recalibration, respectively. As mentioned in 3.5, the chronic bipolar electrodes used in this study are similar to those that have been previously observed to record stable EMG for up to 7.5 years (Memberg, Polasek, et al., 2014). As both P2 and P3 remain implanted, we anticipate that their motor performances will continue to remain stable over time.

As mentioned earlier, intraneural peripheral nerve interfaces have had difficulty in maintaining signal stability over time (Davis et al., 2016; Wendelken et al., 2017). Here, we demonstrated that with indwelling bipolar electrodes, RPNI signals can maintain equivalent motor performances as intact residual muscle up to 10 months. This may be attributed to the very high SNR found on all bipolar electrode channels. Compared to epineural or intraneural peripheral interfaces whose SNR ranges from 4-15 (Davis et al., 2016; Dweiri et al., 2017; Struijk, Thomsen, Larsen, & Sinkjaer, 1999), RPNIs can produce SNR levels of 30-100 (see chapter III for details). This is an important distinction as noisier control signals can lead to turbulent trajectories.

Unlike current myoelectric interfaces which use surface electrodes, implanted intramuscular electrodes have shown to be an effective method in obtaining more localized EMG signals. Surface electrodes are severely limited by cross-talk, which adversely affects the number of available independent control signals (Farina et al., 2014). This is readily apparent in targeted

muscle reinnervation, which uses high density surface electrodes to record EMG (Kuiken et al., 2009). Although the surgical technique by design creates new control sites, the new control sites are typically located in one or two intact muscles. This then influences the type of control architecture being implemented. Thus, TMR has shown to be only effective in utilizing pattern recognition algorithms for prosthetic function (Cheesborough et al., 2015; Hargrove et al., 2017; Simon, Hargrove, Lock, & Kuiken, 2011; Zhou et al., 2007). In contrast, multiple RPNIs can theoretically be created with the finite limiting factor dependent on the number of ways the intact nerve can be split. This would allow multiple independent control sites to be created for multiple degrees of functionality. Some evidence of this selectivity has been shown in chapter III, where P3's ulnar RPNI 1 and 2 activated for different intrinsic hand functions.

The most promising finding of intrinsic hand functionality was the ability for P2 and P3 to control the intrinsic muscles of their thumb using both their ulnar and median RPNIs. This is anatomically appropriate since both the median and ulnar nerves innervate the flexor pollicis brevis, which assists in flexing the thumb CMC/MCP joints. Past studies of simultaneous control of multiple degrees of freedom have focused on controlling the wrist and hand open/closed (Jiang et al., 2014; Sartori et al., 2018; Smith et al., 2015). In this study, RPNIs enabled P2 and P3 to have intuitive two degree of axis thumb control including thumb flexion/extension and thumb opposition/reposition. Similarly, the ulnar RPNI in P2 and ulnar RPNI 1 in P3 generated signals for small finger movements. Naturally, the ulnar nerve innervates the flexor digiti minimi brevis, which assists in flexing the small finger at the MCP joint. These additional control signals combined with existing residual muscle may help gain more dexterous control of the prosthetic

hand as many studies are limited to only existing musculature (Ameri et al., 2014; Smith et al., 2015; Tenore et al., 2009; Twardowski et al., 2019).

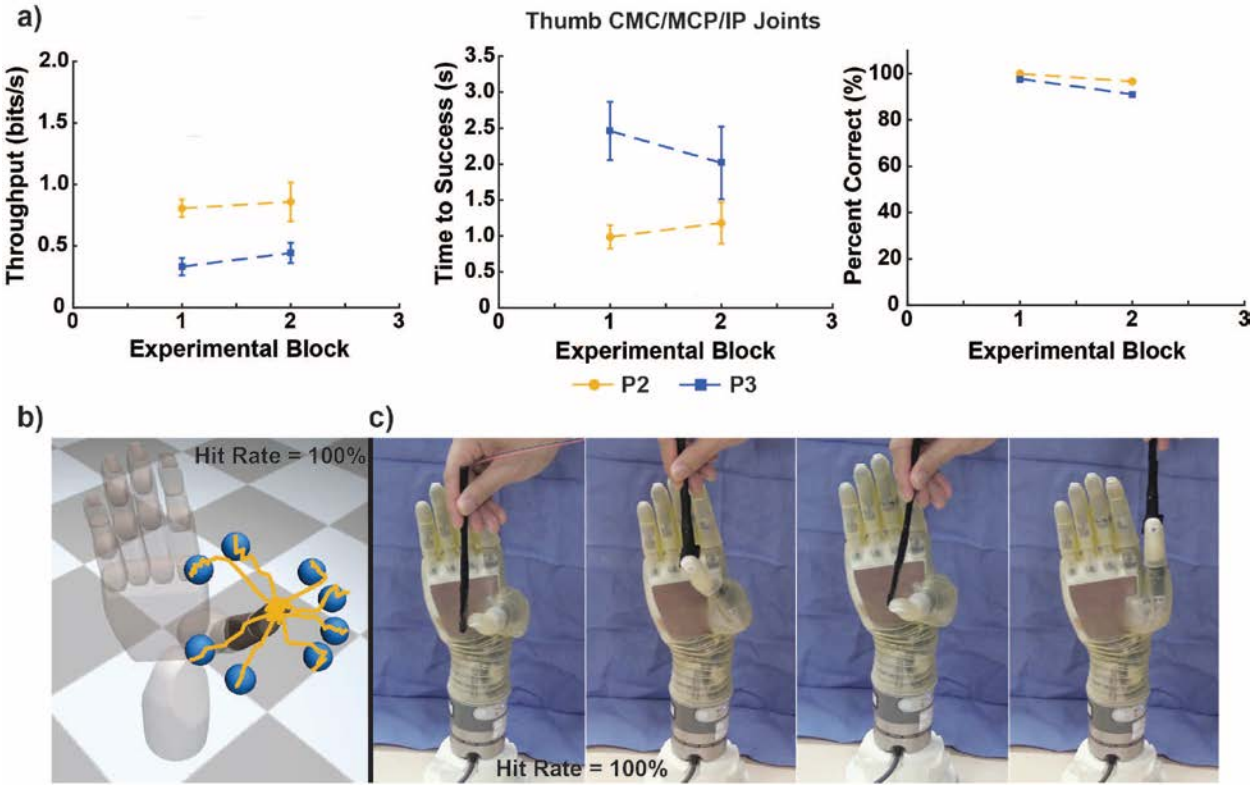

Figure 4.3 Real-time two DOF continuous decoding for P2, and P3. (a) P2 (Maize) and P3's (Blue) throughput (bits/s), time to success (s), and trial success (%) across two experimental blocks. (b) Example of P2's predicted trajectories during the virtual target task. A center-out task displayed eight targets within a 2D space. (c) An equivalent target hitting task moved to a physical prosthesis (DEKA LUKE arm). P2 had to hit the wand in four locations to complete the task.

The most promising finding of intrinsic hand functionality was the ability for P2 and P3 to control the intrinsic muscles of their thumb using both their ulnar and median RPNIs. This is anatomically appropriate since both the median and ulnar nerves innervate the flexor pollicis brevis, which assists in flexing the thumb CMC/MCP joints. Past studies of simultaneous control of multiple degrees of freedom have focused on controlling the wrist and hand open/closed (Jiang et al., 2014; Massimo Sartori et al., 2018; Smith et al., 2015). In this study, RPNIs enabled P2 and P3 to have intuitive two degree of axis thumb control including thumb flexion/extension and thumb

opposition/reposition. Similarly, the ulnar RPNI in P2 and ulnar RPNI 1 in P3 generated signals for small finger movements. Naturally, the ulnar nerve innervates the flexor digiti minimi brevis, which assists in flexing the small finger at the MCP joint. These additional control signals combined with existing residual muscle may help gain more dexterous control of the prosthetic hand as many studies are limited to only existing musculature (Ameri et al., 2014; Smith et al., 2015; Tenore et al., 2009; Twardowski et al., 2019).

We have demonstrated that RPNIs can be used to record efferent motor nerve action potentials from missing intrinsic muscles to provide high fidelity prosthetic control. In particular, RPNIs have shown proficiency in decoding one DOF and two DOF finger control in an artificial hand, and future studies will explore expanding the number of DOFs to controlling multiple fingers simultaneously and continuously. The RPNI technique may provide a viable option for future clinical prosthetic technology and greatly improve the quality of life for patients with limb loss at any amputation level.

CHAPTER V

Discussion

5.1 Conclusion

Integrating with the body's peripheral nervous system to extract intuitive prosthetic control signals has demonstrated great potential in restoring intuitive hand function to people with upper-limb amputations. However, many challenges still remain before the technology can be robust enough and widely accepted for translation into a commercial setting. This thesis provides several studies that attempts to address these challenges to bring peripheral nerve interfaces closer to clinical translation.

Chapter II investigated the ability of the regenerative peripheral nerve interface to be used for continuous control of hand movement. Agonist and antagonist RPNI muscle signals allowed real-time continuous control of hand-level movement with an overall throughput of 0.77 bits/s and a success rate of 96.7% using a postion/velocity Kalman filter. This motor performance was on par with that of an intact hand, and provided a level of control equal to that of current myoelectric prostheses. Additionally, signal robustness was measurements showed that signal amplitude varied significantly across time, which may be an issue for future implantable myoelectric systems. Nonetheless, this study has provided initial data on the capabilities of RPNIs to provide simultaneous and continuous prosthesis control for future human implementation.

Previous studies have shown RPNIs can safely be implemented in animals for signal extraction and prosthetic control (Irwin et al., 2016; Ursu et al., 2016). Chapter III explored the implementation and viability of RPNIs in people with upper-limb amputations. Using ultrasound to track the size and shape of the RPNIs post-implantation, we were able to view dynamic contractions of the RPNIs in two patients. Particularly the RPNIs in P1, who's missing a majority of his forearm muscles, displayed strong contractions for individual thumb and finger movements. Further evidence of viability was shown in P2 and P3, where high amplitude signals ranging from 300 μV to 2.5 mV and SNR ranging from 30-100 were recorded with surgically implanted bipolar electrodes. What's more promising is that RPNIs were able to generate efferent motor signals during movements that required missing intrinsic and extrinsic muscles. These results demonstrate that the RPNI technique is effective and safe within the human population and can increase the number of available control sources that could be implemented for prosthesis control.

To expand upon the results in the previous chapter, chapter IV further characterized RPNIs and tested their motor control capabilities in humans. In particular, one and two DOF finger control was achieved in three participants who had little to no experience in controlling a myoelectric prosthesis. In general, intuitive single degree of freedom continuous control was achieved for multiple fingers with accuracies > 85%. Additionally, two degree of freedom thumb control was possible for two transradial amputees who are missing all of their intrinsic thumb muscles. Lastly, motor performance remained stable for up to 300 days for one DOF finger movements. We speculate that motor performance will continue to remain stable for the remainder of P2 and P3's implantation period. Overall, RPNIs have provided a bridge to tap into the severed communication line of the peripheral nerve, indicating that this technique represents a viable option to enhance myoelectric prosthetic functionality for people with limb loss.

5.1.1 Thesis Contributions

This thesis has demonstrated several new characterizations of the RPNI. Aim 1 demonstrated that RPNIs can generate sufficient EMG signals that can be used to continuously control a prosthetic hand in non-human primates, an important characterization for future translation in humans with amputations. Aim 2 was the first study to test the translation of RPNIs into humans with upper-limb amputations and showed that RPNIs can safely be implemented and can physically contract and generate EMG signals during finger movements. Lastly, aim 3 took the translation one step further, and showed that RPNIs can provide humans with upper-limb amputations with robust continuous control of one DOF finger movements and continuous control of two DOF thumb movements in real-time.

5.2 Future Directions

Despite the promising results presented in this work, there still remains many challenges and improvements needed before peripheral nerve technology can be readily available for the prosthetic market. Advances in this technology will require further studies in both animals and humans. Below, I will briefly expand upon several promising avenues that could address some of the most critical challenges facing peripheral nerve technology's translation towards a viable clinical system.

Previous pilot and clinical trial human studies of two different peripheral nerve interfaces (intraneural electrodes and TMR, respectively) have demonstrated great promise in adding greater prosthetic functionality (Davis et al., 2016; Hargrove et al., 2017). However, both techniques come with a few shortcomings, particularly the signal stability of intraneural electrodes and the signal selectivity of TMR. The RPNI technique presented in this thesis, addresses both of these issues. To date, the RPNIs in P2 have been implanted for 4 years and we have successfully recorded

signals from his RPNIs 1 year following his electrode implantation. For P3, her RPNIs were implanted 1 year ago and we have successfully recorded signals 5 months post-electrode implantation. We have then presented initial results of RPNIs activating for specific finger movements in people who are missing the appropriate musculature to perform such movements. This suggests that RPNIs can add unique signal sources that could be used to increase motor functionality to myoelectric users.

Further studies are needed to characterize the degree of motor selectivity in RPNIs. To do this, multi-contact electrodes are necessary to obtain a higher spatial resolution. Current intramuscular electrodes contain one or two contact sites, which would then require multiple electrode insertions to record from different portions of the muscle (Héroux, Dakin, Luu, Inglis, & Blouin, 2013). To address this issue, several studies have proposed and implemented a thin-film multi-channel electrode for intramuscular recordings in humans (Luu et al., 2017; Muceli et al., 2019, 2015). Integration of this technology with RPNIs may be well suited to mapping different regions of the RPNI graft. Alternatively, multi-channel intraneural peripheral probes, like the 96 channel Utah Slanted Electrode Array (USEA; [Branner et al., 2001]), could be repurposed for intramuscular recordings since the RPNI grafts are typically 1-3 cm in length.

The next challenge to address is the interpretation and implementation of these additional signal sources to gain full independent control of a prosthetic hand. Regression-based machine learning algorithms have shown to allow simultaneous and proportional control of multi-DOF finger control (Smith et al., 2015; Wendelken et al., 2017). However, these approaches are highly sensitive to external conditions that may cause muscle co-contractions or tonic firing, producing unintended movement error. Deep learning and convolutional neural networks have recently had success in applications of speech recognition and computer vision, which by design must be robust

against external variability (Goodfellow et al., 2016). Thus, these methods may be applicable to reducing error rate and solving the nonlinearities between muscle activations and end-point finger kinematics in prosthetic control.

Alternatively, more physiological approaches have been implemented that may warrant more attention in the neuroprosthetic community. To generate dexterous hand control, the central nervous system needs to coordinate multiple degrees of freedom of the musculoskeletal limb (Bernstein, 1967). This in turn produces muscle synergies that follow a specific pattern to generate natural limb behavior (d'Avella et al., 2006). Depending on the level of amputation, the natural production of muscle synergies is ultimately lost. RPNIs show promise in restoring these lost synergy patterns in order regain full control of the hand. Future human studies need to combine RPNIs with EMG-drive musculoskeletal models that rely on synergy patterns for control. Implementation of musculoskeletal models has been recently demonstrated in TMR subjects and a normal transradial amputee, showing promise in improving state of the art decoders (Farina et al., 2017; Sartori et al., 2018).

Finally, if an optimal solution can be reached to provide simultaneous and continuous control of multiple degrees of freedom, then the next step would be to implement a fully implantable system. The system will need to be able to receive incoming neural signals, predict the user intention, and output the commands to the artificial limb all below the maximum 200 ms delay specification for prosthesis response time. One possible option for a fully implantable system with RPNIs is osseointegration. Osseointegration is a surgical technique where an abutment and a fixture are placed within the intramedullary cavity of the bone at the stump. The abutment then serves as an anchor for the prosthetic limb and feedthrough connectors can be embedded within the abutment to allow bidirectional electrical communication (Ortiz-Catalan et al., 2014). This

system would then be fully proficient for take home trials to assess activities of daily living and overall user satisfaction.

Much more work is required before peripheral nerve interfaces can have a widespread impact in the prosthetic community. However, combining the work presented here with the recent progress in prosthetic limb technology mentioned above may bring us one step closer to reaching that gold standard of fully restoring normal limb function.

APPENDIX

Supplemental Material for Chapter III and IV

Table A.1 Summary of implanted RPNI grafts, the recording electrode, and the finger movement correlated to each RPNI or residual contraction.

Participant	RPNI or residual muscle name	Nerve	Electrode type	RPNI or residual muscle contraction correlated with
P1	Median RPNI 1	Median	Fine wire	Thumb MCP/IP joint flexion, Index finger PIP/DIP joint flexion
	Median RPNI 2	Median	Fine wire	Index finger PIP/DIP joint flexion
	Median RPNI 3	Median	Fine wire	Index finger PIP/DIP joint flexion
	Median RPNI 4	Median	Fine wire	Index finger PIP/DIP joint flexion
	Ulnar RPNI 1	Ulnar	Fine wire	Small finger PIP/DIP joint flexion, Thumb MCP/IP joint flexion
	Ulnar RPNI 2	Ulnar	Fine wire	Small finger PIP/DIP joint flexion, Thumb MCP/IP joint flexion, Index finger PIP/DIP joint flexion
P2	Median RPNI	Median	Intramuscular	Thumb MCP joint flexion
	Ulnar RPNI	Ulnar	Intramuscular	Small finger MCP joint flexion
	Flexor Digitorum Profundus Index	Median	Intramuscular	Index finger PIP/DIP joint flexion
	Flexor Digitorum Profundus Small	Ulnar	Intramuscular	Small finger PIP/DIP joint flexion
	Extensor Digitorum Communis	Radial	Intramuscular	Extension of all four fingers at the MCP joint
	Extensor Pollicis Longus	Radial	Intramuscular	Thumb MCP/IP joint extension
	Flexor Carpi Radialis	Median	Intramuscular	Wrist flexion

CMC – Carpometacarpal joint, MCP – metacarpophalangeal joint, PIP – proximal interphalangeal joint, DIP – distal interphalangeal joint, IP – interphalangeal joint

Table A.1 Summary of implanted RPNI grafts, the recording electrode, and the finger movement correlated to each RPNI or residual contraction (Continued).

Participant	RPNI or residual muscle name	Nerve	Electrode type	RPNI or residual muscle contraction correlated with
P3	Median RPNI	Median	Intramuscular	Thumb MCP joint flexion
	Ulnar RPNI 1	Ulnar	Intramuscular	Small finger MCP joint flexion
	Ulnar RPNI 2	Ulnar	Intramuscular	Small finger MCP joint flexion
	Flexor Digitorum Profundus Index	Median	Intramuscular	Index finger PIP/DIP joint flexion
	Extensor Digitorum Communis	Radial	Intramuscular	Extension of all four fingers at the MCP joint
	Extensor Pollicis Longus	Radial	Intramuscular	Thumb MCP/IP joint extension
	Flexor Carpi Radialis	Median	Intramuscular	Wrist flexion

Table A.2 Details of a subset of muscles missing in each participant and their function

Participant	Level of Amputation	Missing Muscles	Nerve	Function
P1*	Proximal transradial	Flexor Digitorum Superficialis	Median	Flex digits 2-5 at MCP/PIP joints
		Flexor Digitorum Profundus	Median and Ulnar	Median half: Flex digits 2-3 at DIP joint, Ulnar half: Flex digits 4-5 at DIP joint
		Flexor Pollicis Longus	Median	Flex digit 1 at IP joint
P2	Wrist disarticulation	Abductor Pollicis Brevis	Median	Abduct digit 1– assists to oppose and extend digit 1
		Flexor Pollicis Brevis	Median and Ulnar	Flex digit 1 at MCP/CMC joints – assists to oppose digit 1
		Opponens Pollicis	Median	Flex digit 1 at CMC joint – assists to oppose digit 1
		Lumbricals 1 and 2	Median	Simultaneously flex digit 2 and 3 at MCP joint and extend 2 or 3 at PIP joint
		Flexor Digiti Minimi Brevis	Ulnar	Flex digit 5 at MCP joint
		Opponens Digiti Minimi	Ulnar	Oppose digit 5 – flex/rotate 5th metacarpal
		Lumbicals 3 and 4	Ulnar	Simultaneously flex digit 4 or 5 at MCP joint and extend digit 4 or 5 at PIP joint
P3	Wrist disarticulation	Abductor Pollicis Brevis	Median	Abduct digit 1– assists to oppose and extend digit 1
		Flexor Pollicis Brevis	Median and Ulnar	Flex digit 1 at MCP/CMC joints – assists to oppose digit 1
		Opponens Pollicis	Median	Flex digit 1 at CMC joint – assists to oppose digit 1
		Lumbricals 1 and 2	Median	Simultaneously flex digit 2 and 3 at MCP joint and extend 2 or 3 at PIP joint
		Flexor Digiti Minimi Brevis	Ulnar	Flex digit 5 at MCP joint
		Opponens Digiti Minimi	Ulnar	Oppose digit 5 – flex/rotate 5th metacarpal
		Lumbicals 3 and 4	Ulnar	Simultaneously flex digit 4 or 5 at MCP joint and extend digit 4 or 5 at PIP joint

MCP – metacarpophalangeal joint, PIP – proximal interphalangeal joint, DIP – distal interphalangeal joint, IP – interphalangeal joint, CMC – Carpometacarpal joint

*P1 is also missing all the muscles missing in P2 and P3

BIBLIOGRAPHY

Ajiboye, A. B., & Weir, R. F. (2005). A heuristic fuzzy logic approach to EMG pattern recognition for multifunctional prosthesis control. *IEEE Transactions on Neural Systems and Rehabilitation Engineering*, *13*(3), 280–291. https://doi.org/10.1109/TNSRE.2005.847357

Ameri, A., Kamavuako, E. N., Scheme, E. J., Englehart, K. B., & Parker, P. A. (2014). Support Vector Regression for Improved Real-Time, Simultaneous Myoelectric Control. *IEEE Transactions on Neural Systems and Rehabilitation Engineering*, *22*(6), 1198–1209. https://doi.org/10.1109/TNSRE.2014.2323576

Baker, J. J., Scheme, E., Englehart, K., Hutchinson, D. T., & Greger, B. (2010). Continuous Detection and Decoding of Dexterous Finger Flexions With Implantable MyoElectric Sensors. *IEEE Transactions on Neural Systems and Rehabilitation Engineering*, *18*(4), 424–432. https://doi.org/10.1109/TNSRE.2010.2047590

Barsakcioglu, D. Y., & Farina, D. (2018). A real-time surface EMG decomposition system for non-invasive human-machine interfaces. In *2018 IEEE Biomedical Circuits and Systems Conference (BioCAS)* (pp. 1–4). https://doi.org/10.1109/BIOCAS.2018.8584659

Barsotti, M., Dupan, S., Vujaklija, I., Došen, S., Frisoli, A., & Farina, D. (2019). Online Finger Control Using High-Density EMG and Minimal Training Data for Robotic Applications. *IEEE Robotics and Automation Letters*, *4*(2), 217–223. https://doi.org/10.1109/LRA.2018.2885753

Battye, C. K., Nightingale, A., & Whillis, J. (1955). The use of myo-electric currents in the operation of prostheses. *The Journal of Bone and Joint Surgery. British Volume*, *37-B*(3), 506–510. https://doi.org/10.1302/0301-620X.37B3.506

Bernstein, N. (1967) *The co-ordination and Regulation of Movement* (Pergamon, Oxford).

Biddiss, E. A., & Chau, T. T. (2007). Upper limb prosthesis use and abandonment: A survey of the last 25 years. *Prosthetics and Orthotics International*, *31*(3), 236–257. https://doi.org/10.1080/03093640600994581

Birdwell, J. A., Hargrove, L. J., Kuiken, T. A., & Weir, R. F. ff. (2013). Activation of individual extrinsic thumb muscles and compartments of extrinsic finger muscles. *Journal of Neurophysiology*, *110*(6), 1385–1392. https://doi.org/10.1152/jn.00748.2012

Bishop, W., Chestek, C. C., Gilja, V., Nuyujukian, P., Foster, J. D., Ryu, S. I., … Yu, B. M. (2014). Self-recalibrating classifiers for intracortical brain–computer interfaces. *Journal of Neural Engineering*, *11*(2), 026001. https://doi.org/10.1088/1741-2560/11/2/026001

Boretius, T., Badia, J., Pascual-Font, A., Schuettler, M., Navarro, X., Yoshida, K., & Stieglitz, T. (2010). A transverse intrafascicular multichannel electrode (TIME) to interface with the peripheral nerve. *Biosensors and Bioelectronics*, *26*(1), 62–69. https://doi.org/10.1016/j.bios.2010.05.010

Branner, A., Stein, R. B., & Normann, R. A. (2001). Selective Stimulation of Cat Sciatic Nerve Using an Array of Varying-Length Microelectrodes. *Journal of Neurophysiology*, *85*(4), 1585–1594. https://doi.org/10.1152/jn.2001.85.4.1585

Buchanan, T. S., Lloyd, D. G., Manal, K., & Besier, T. F. (2004). Neuromusculoskeletal Modeling: Estimation of Muscle Forces and Joint Moments and Movements from Measurements of Neural Command. *Journal of Applied Biomechanics*, *20*(4), 367–395. https://doi.org/10.1123/jab.20.4.367

Calvetti, D., Wodlinger, B., Durand, D. M., & Somersalo, E. (2011). Hierarchical beamformer and cross-talk reduction in electroneurography. *Journal of Neural Engineering*, *8*(5), 056002. https://doi.org/10.1088/1741-2560/8/5/056002

Cavallaro, E. E., Rosen, J., Perry, J. C., & Burns, S. (2006). Real-Time Myoprocessors for a Neural Controlled Powered Exoskeleton Arm. *IEEE Transactions on Biomedical Engineering*, *53*(11), 2387–2396. https://doi.org/10.1109/TBME.2006.880883

Cheesborough, J. E., Smith, L. H., Kuiken, T. A., & Dumanian, G. A. (2015). Targeted Muscle Reinnervation and Advanced Prosthetic Arms. *Seminars in Plastic Surgery*, *29*(1), 62–72. https://doi.org/10.1055/s-0035-1544166

Chestek, C. A., Gilja, V., Nuyujukian, P., Foster, J. D., Fan, J. M., Kaufman, M. T., … Shenoy, K. V. (2011). Long-term stability of neural prosthetic control signals from silicon cortical arrays in rhesus macaque motor cortex. *Journal of Neural Engineering*, *8*(4), 045005. https://doi.org/10.1088/1741-2560/8/4/045005

Childress, D. S. (1980). Closed-loop control in prosthetic systems: Historical perspective. *Annals of Biomedical Engineering*, *8*(4–6), 293–303. https://doi.org/10.1007/BF02363433

Christensen, M. B., Wark, H. A. C., & Hutchinson, D. T. (2016). A histological analysis of human median and ulnar nerves following implantation of Utah slanted electrode arrays. *Biomaterials*, *77*, 235–242. https://doi.org/10.1016/j.biomaterials.2015.11.012

Cipriani, C., Antfolk, C., Controzzi, M., Lundborg, G., Rosen, B., Carrozza, M. C., & Sebelius, F. (2011). Online Myoelectric Control of a Dexterous Hand Prosthesis by Transradial Amputees. *IEEE Transactions on Neural Systems and Rehabilitation Engineering*, *19*(3), 260–270. https://doi.org/10.1109/TNSRE.2011.2108667

Cunningham, J. P., Nuyujukian, P., Gilja, V., Chestek, C. A., Ryu, S. I., & Shenoy, K. V. (2011). A closed-loop human simulator for investigating the role of feedback control in brain-machine interfaces. *Journal of Neurophysiology*, *105*(4), 1932–1949. https://doi.org/10.1152/jn.00503.2010

d'Avella, A., Portone, A., Fernandez, L., & Lacquaniti, F. (2006). Control of Fast-Reaching Movements by Muscle Synergy Combinations. *Journal of Neuroscience*, *26*(30), 7791–7810. https://doi.org/10.1523/JNEUROSCI.0830-06.2006

d'Avella, A., Saltiel, P., & Bizzi, E. (2003). Combinations of muscle synergies in the construction of a natural motor behavior. *Nature Neuroscience*, *6*(3), 300–308. https://doi.org/10.1038/nn1010

Davis, T. S., Wark, H. A. C., Hutchinson, D. T., Warren, D. J., O'Neill, K., Scheinblum, T., Greger, B. (2016). Restoring motor control and sensory feedback in people with upper extremity amputations using arrays of 96 microelectrodes implanted in the median and ulnar nerves. *Journal of Neural Engineering*, *13*(3), 036001. https://doi.org/10.1088/1741-2560/13/3/036001

Delgado-Martínez, I., Badia, J., Pascual-Font, A., Rodríguez-Baeza, A., & Navarro, X. (2016). Fascicular Topography of the Human Median Nerve for Neuroprosthetic Surgery. *Frontiers in Neuroscience*, *10*. https://doi.org/10.3389/fnins.2016.00286

Dhillon, G. S., & Horch, K. W. (2005). Direct neural sensory feedback and control of a prosthetic arm. *IEEE Transactions on Neural Systems and Rehabilitation Engineering*, *13*(4), 468–472. https://doi.org/10.1109/TNSRE.2005.856072

Dhillon, Gurpreet S, Lawrence, S. M., Hutchinson, D. T., & Horch, K. W. (2004). Residual function in peripheral nerve stumps of amputees: implications for neural control of artificial limbs1. *The Journal of Hand Surgery*, *29*(4), 605–615. https://doi.org/10.1016/j.jhsa.2004.02.006

Dillingham, T. R., Pezzin, L. E., & Mackenzie, E. J. (2002). Limb Amputation and Limb Deficiency: Epidemiology and Recent Trends in the United States. *Journal*, *95*(8), 875–883.

Ding, Q., Zhao, X., Xiong, A., & Han, J. (2011). A Novel Motion Estimate Method of Human Joint with EMG-Driven Model. In *2011 5th International Conference on Bioinformatics and Biomedical Engineering* (pp. 1–5). https://doi.org/10.1109/icbbe.2011.5780185

Dumanian, G. A., Potter, B. K., Mioton, L. M., Ko, J. H., Cheesborough, J. E., Souza, J. M., … Jordan, S. W. (2019). Targeted Muscle Reinnervation Treats Neuroma and Phantom Pain in Major Limb Amputees: A Randomized Clinical Trial. *Annals of Surgery*, *Publish Ahead of Print*. https://doi.org/10.1097/SLA.0000000000003088

Dweiri, Y. M., Eggers, T. E., Gonzalez-Reyes, L. E., Drain, J., McCallum, G. A., & Durand, D. M. (2017). Stable Detection of Movement Intent From Peripheral Nerves: Chronic Study in Dogs. *Proceedings of the IEEE*, *105*(1), 50–65. https://doi.org/10.1109/JPROC.2016.2607520

Eggers, T. E., Dweiri, Y. M., McCallum, G. A., & Durand, D. M. (2017). Model-based Bayesian signal extraction algorithm for peripheral nerves. *Journal of Neural Engineering*, *14*(5), 056009. https://doi.org/10.1088/1741-2552/aa7d94

ElKoura, G., & Singh, K. (2003). Handrix: Animating the Human Hand. In *Proceedings of the 2003 ACM SIGGRAPH/Eurographics Symposium on Computer Animation* (pp. 110–119). Aire-la-Ville, Switzerland, Switzerland: Eurographics Association. Retrieved from http://dl.acm.org/citation.cfm?id=846276.846291

Englehart, K., Hudgin, B., & Parker, P. A. (2001). A wavelet-based continuous classification scheme for multifunction myoelectric control. *IEEE Transactions on Biomedical Engineering*, *48*(3), 302–311. https://doi.org/10.1109/10.914793

Farina, D., Jiang, N., Rehbaum, H., Holobar, A., Graimann, B., Dietl, H., & Aszmann, O. C. (2014). The Extraction of Neural Information from the Surface EMG for the Control of Upper-Limb Prostheses: Emerging Avenues and Challenges. *IEEE Transactions on Neural Systems and Rehabilitation Engineering*, *22*(4), 797–809. https://doi.org/10.1109/TNSRE.2014.2305111

Farina, D., & Negro, F. (2012). Accessing the Neural Drive to Muscle and Translation to Neurorehabilitation Technologies. *IEEE Reviews in Biomedical Engineering*, *5*, 3–14. https://doi.org/10.1109/RBME.2012.2183586

Farina, Dario, Vujaklija, I., Sartori, M., Kapelner, T., Negro, F., Jiang, N., Aszmann, O. C. (2017). Man/machine interface based on the discharge timings of spinal motor neurons after targeted muscle reinnervation. *Nature Biomedical Engineering*, *1*(2), 0025. https://doi.org/10.1038/s41551-016-0025

Farina, Dario, Yoshida, K., Stieglitz, T., & Koch, K. P. (2008). Multichannel thin-film electrode for intramuscular electromyographic recordings. *Journal of Applied Physiology*, *104*(3), 821–827. https://doi.org/10.1152/japplphysiol.00788.2007

Florestal, J. R., Mathieu, P. A., & Malanda, A. (2006). Automated decomposition of intramuscular electromyographic signals. *IEEE Transactions on Biomedical Engineering*, *53*(5), 832–839. https://doi.org/10.1109/TBME.2005.863893

Fougner, A., Scheme, E., Chan, A. D. C., Englehart, K., & Stavdahl, Ø. (2011). Resolving the Limb Position Effect in Myoelectric Pattern Recognition. *IEEE Transactions on Neural Systems and Rehabilitation Engineering*, *19*(6), 644–651. https://doi.org/10.1109/TNSRE.2011.2163529

Gasson, M., Hutt, B., Goodhew, I., Kyberd, P., & Warwick, K. (2005). Invasive neural prosthesis for neural signal detection and nerve stimulation. *International Journal of Adaptive Control and Signal Processing*, *19*(5), 365–375. https://doi.org/10.1002/acs.854

Goodfellow, I., Bengio, Y., & Courville, A. (2016). *Deep Learning*. MIT Press.

Hahne, J. M., Biebmann, F., Jiang, N., Rehbaum, H., Farina, D., Meinecke, F. C., Parra, L. C. (2014). Linear and Nonlinear Regression Techniques for Simultaneous and Proportional Myoelectric Control. *IEEE Transactions on Neural Systems and Rehabilitation Engineering*, *22*(2), 269–279. https://doi.org/10.1109/TNSRE.2014.2305520

Hargrove, L. J., Englehart, K., & Hudgins, B. (2007). A Comparison of Surface and Intramuscular Myoelectric Signal Classification. *IEEE Transactions on Biomedical Engineering*, *54*(5), 847–853. https://doi.org/10.1109/TBME.2006.889192

Hargrove, L. J., Miller, L. A., Turner, K., & Kuiken, T. A. (2017). Myoelectric Pattern Recognition Outperforms Direct Control for Transhumeral Amputees with Targeted Muscle Reinnervation: A Randomized Clinical Trial. *Scientific Reports*, *7*(1), 13840. https://doi.org/10.1038/s41598-017-14386-w

Hauschild, M., Davoodi, R., & Loeb, G. E. (2007). A Virtual Reality Environment for Designing and Fitting Neural Prosthetic Limbs. *IEEE Transactions on Neural Systems and Rehabilitation Engineering*, *15*(1), 9–15. https://doi.org/10.1109/TNSRE.2007.891369

Heckman, C. J., & Enoka, R. M. (2004). Physiology of the motor neuron and the motor unit. In A. Eisen (Ed.), *Handbook of Clinical Neurophysiology* (Vol. 4, pp. 119–147). Elsevier. https://doi.org/10.1016/S1567-4231(04)04006-7

Héroux, M. E., Dakin, C. J., Luu, B. L., Inglis, J. T., & Blouin, J.-S. (2013). Absence of lateral gastrocnemius activity and differential motor unit behavior in soleus and medial gastrocnemius during standing balance. *Journal of Applied Physiology*, *116*(2), 140–148. https://doi.org/10.1152/japplphysiol.00906.2013

Holobar, A., Minetto, M. A., Botter, A., Negro, F., & Farina, D. (2010). Experimental Analysis of Accuracy in the Identification of Motor Unit Spike Trains From High-Density Surface EMG. *IEEE Transactions on Neural Systems and Rehabilitation Engineering*, *18*(3), 221–229. https://doi.org/10.1109/TNSRE.2010.2041593

Holobar, A., & Zazula, D. (2007). Multichannel Blind Source Separation Using Convolution Kernel Compensation. *IEEE Transactions on Signal Processing*, *55*(9), 4487–4496. https://doi.org/10.1109/TSP.2007.896108

Horch, K., Meek, S., Taylor, T. G., & Hutchinson, D. T. (2011). Object Discrimination With an Artificial Hand Using Electrical Stimulation of Peripheral Tactile and Proprioceptive Pathways With Intrafascicular Electrodes. *IEEE Transactions on Neural Systems and Rehabilitation Engineering*, *19*(5), 483–489. https://doi.org/10.1109/TNSRE.2011.2162635

Hudgins, B., Parker, P., & Scott, R. N. (1993). A new strategy for multifunction myoelectric control. *IEEE Transactions on Biomedical Engineering*, *40*(1), 82–94. https://doi.org/10.1109/10.204774

Irwin, Z. T., Schroeder, K. E., Vu, P. P., Tat, D. M., Bullard, A. J., Woo, S. L., Chestek, C. A. (2016). Chronic recording of hand prosthesis control signals via a regenerative peripheral nerve interface

in a rhesus macaque. *Journal of Neural Engineering*, *13*(4), 046007. https://doi.org/10.1088/1741-2560/13/4/046007

Jia, X., Koenig, M. A., Zhang, X., Zhang, J., Chen, T., & Chen, Z. (2007). Residual Motor Signal in Long-Term Human Severed Peripheral Nerves and Feasibility of Neural Signal-Controlled Artificial Limb. *The Journal of Hand Surgery*, *32*(5), 657–666. https://doi.org/10.1016/j.jhsa.2007.02.021

Jiang, N., Rehbaum, H., Vujaklija, I., Graimann, B., & Farina, D. (2014). Intuitive, Online, Simultaneous, and Proportional Myoelectric Control Over Two Degrees-of-Freedom in Upper Limb Amputees. *IEEE Transactions on Neural Systems and Rehabilitation Engineering*, *22*(3), 501–510. https://doi.org/10.1109/TNSRE.2013.2278411

Jun-Uk Chu, Inhyuk Moon, & Mu-Seong Mun. (2006). A Real-Time EMG Pattern Recognition System Based on Linear-Nonlinear Feature Projection for a Multifunction Myoelectric Hand. *IEEE Transactions on Biomedical Engineering*, *53*(11), 2232–2239. https://doi.org/10.1109/TBME.2006.883695

Kalman, R. E. (1960). A New Approach to Linear Filtering and Prediction Problems. *Journal of Basic Engineering*, *82*(1), 35–45. https://doi.org/10.1115/1.3662552

Kamavuako, E. N., Englehart, K. B., Jensen, W., & Farina, D. (2012). Simultaneous and Proportional Force Estimation in Multiple Degrees of Freedom From Intramuscular EMG. *IEEE Transactions on Biomedical Engineering*, *59*(7), 1804–1807. https://doi.org/10.1109/TBME.2012.2197210

Khushaba, R. N., Kodagoda, S., Takruri, M., & Dissanayake, G. (2012). Toward improved control of prosthetic fingers using surface electromyogram (EMG) signals. *Expert Systems with Applications*, *39*(12), 10731–10738. https://doi.org/10.1016/j.eswa.2012.02.192

Kim, S.-P., Simeral, J. D., Hochberg, L. R., Donoghue, J. P., & Black, M. J. (2008). Neural control of computer cursor velocity by decoding motor cortical spiking activity in humans with tetraplegia. *Journal of Neural Engineering*, *5*(4), 455. https://doi.org/10.1088/1741-2560/5/4/010

Kubiak CA, Kemp SWP, Cederna PS, Kung TA. "Prophylactic Regenerative Peripheral Nerve Interfaces (RPNIs) to Prevent Postamputation Pain" Plas Recon Surg. In press.

Kuiken, Li G, Lock BA, & et al. (2009). Targeted muscle reinnervation for real-time myoelectric control of multifunction artificial arms. *JAMA*, *301*(6), 619–628. https://doi.org/10.1001/jama.2009.116

Kuiken, T. A., Dumanian, G. A., Lipschutz, R. D., Miller, L. A., & Stubblefield, K. A. (2004). The use of targeted muscle reinnervation for improved myoelectric prosthesis control in a bilateral shoulder disarticulation amputee. *Prosthetics and Orthotics International*, *28*(3), 245–253. https://doi.org/10.3109/03093640409167756

Kung, T. A., Langhals, N. B., Martin, D. C., Johnson, P. J., Cederna, P. S., & Urbanchek, M. G. (2014). Regenerative Peripheral Nerve Interface Viability and Signal Transduction with an Implanted

Electrode: *Plastic and Reconstructive Surgery*, *133*(6), 1380–1394. https://doi.org/10.1097/PRS.0000000000000168

Lawrence, S. M., Dhillon, G. S., Jensen, W., Yoshida, K., & Horch, K. W. (2004). Acute Peripheral Nerve Recording Characteristics of Polymer-Based Longitudinal Intrafascicular Electrodes. *IEEE Transactions on Neural Systems and Rehabilitation Engineering*, *12*(3), 345–348. https://doi.org/10.1109/TNSRE.2004.831491

Lee, W. A. (1984). Neuromotor Synergies as a Basis for Coordinated Intentional Action. *Journal of Motor Behavior*, *16*(2), 135–170. https://doi.org/10.1080/00222895.1984.10735316

Li, G., Schultz, A. E., & Kuiken, T. A. (2010). Quantifying Pattern Recognition—Based Myoelectric Control of Multifunctional Transradial Prostheses. *IEEE Transactions on Neural Systems and Rehabilitation Engineering*, *18*(2), 185–192. https://doi.org/10.1109/TNSRE.2009.2039619

Li, Z., O'Doherty, J. E., Lebedev, M. A., & Nicolelis, M. A. L. (2011). Adaptive Decoding for Brain-Machine Interfaces Through Bayesian Parameter Updates. *Neural Computation*, *23*(12), 3162–3204. https://doi.org/10.1162/NECO_a_00207

Lin, C., Wang, B., Jiang, N., & Farina, D. (2018). Robust extraction of basis functions for simultaneous and proportional myoelectric control via sparse non-negative matrix factorization. *Journal of Neural Engineering*, *15*(2), 026017. https://doi.org/10.1088/1741-2552/aa9666

Luu, B. L., Muceli, S., Saboisky, J. P., Farina, D., Héroux, M. E., Bilston, L. E., Butler, J. E. (2017). Motor unit territories in human genioglossus estimated with multichannel intramuscular electrodes. *Journal of Applied Physiology*, *124*(3), 664–671. https://doi.org/10.1152/japplphysiol.00889.2017

Manal, K., Gonzalez, R. V., Lloyd, D. G., & Buchanan, T. S. (2002). A real-time EMG-driven virtual arm. *Computers in Biology and Medicine*, *32*(1), 25–36. https://doi.org/10.1016/S0010-4825(01)00024-5

Marateb, H. R., Muceli, S., McGill, K. C., Merletti, R., & Farina, D. (2011). Robust decomposition of single-channel intramuscular EMG signals at low force levels. *Journal of Neural Engineering*, *8*(6), 066015. https://doi.org/10.1088/1741-2560/8/6/066015

McGill, K. C., Lateva, Z. C., & Marateb, H. R. (2005). EMGLAB: An interactive EMG decomposition program. *Journal of Neuroscience Methods*, *149*(2), 121–133. https://doi.org/10.1016/j.jneumeth.2005.05.015

Memberg, W. D., Polasek, K. H., Hart, R. L., Bryden, A. M., Kilgore, K. L., Nemunaitis, G. A., … Kirsch, R. F. (2014). Implanted Neuroprosthesis for Restoring Arm and Hand Function in People With High Level Tetraplegia. *Archives of Physical Medicine and Rehabilitation*, *95*(6), 1201-1211.e1. https://doi.org/10.1016/j.apmr.2014.01.028

Memberg, W. D., Stage, T. G., & Kirsch, R. F. (2014). A Fully Implanted Intramuscular Bipolar Myoelectric Signal Recording Electrode. *Neuromodulation: Technology at the Neural Interface*, *17*(8), 794–799. https://doi.org/10.1111/ner.12165

Micera, S., Citi, L., Rigosa, J., Carpaneto, J., Raspopovic, S., Pino, G. D., Rossini, P. M. (2010). Decoding Information From Neural Signals Recorded Using Intraneural Electrodes: Toward the Development of a Neurocontrolled Hand Prosthesis. *Proceedings of the IEEE*, *98*(3), 407–417. https://doi.org/10.1109/JPROC.2009.2038726

Micera, Silvestro, Rossini, P. M., Rigosa, J., Citi, L., Carpaneto, J., Raspopovic, S., Dario, P. (2011). Decoding of grasping information from neural signals recorded using peripheral intrafascicular interfaces. *Journal of NeuroEngineering and Rehabilitation*, *8*(1), 53. https://doi.org/10.1186/1743-0003-8-53

Miller, L. A., Feuser, A. E. S., & Kuiken, T. A. (2013). *Targeted Muscle Reinnervation: A Neural Interface for Artificial Limbs*. Taylor & Francis.

Muceli, S., & Farina, D. (2012). Simultaneous and Proportional Estimation of Hand Kinematics From EMG During Mirrored Movements at Multiple Degrees-of-Freedom. *IEEE Transactions on Neural Systems and Rehabilitation Engineering*, *20*(3), 371–378. https://doi.org/10.1109/TNSRE.2011.2178039

Muceli, S., Jiang, N., & Farina, D. (2014). Extracting Signals Robust to Electrode Number and Shift for Online Simultaneous and Proportional Myoelectric Control by Factorization Algorithms. *IEEE Transactions on Neural Systems and Rehabilitation Engineering*, *22*(3), 623–633. https://doi.org/10.1109/TNSRE.2013.2282898

Muceli, Silvia, Poppendieck, W., Negro, F., Yoshida, K., Hoffmann, K. P., Butler, J. E., Farina, D. (2015). Accurate and representative decoding of the neural drive to muscles in humans with multi-channel intramuscular thin-film electrodes. *The Journal of Physiology*, *593*(17), 3789–3804. https://doi.org/10.1113/JP270902

Muceli, S., Bergmeister, K. D., Hoffmann, K.-P., Aman, M., Vukajlija, I., Aszmann, O. C., & Farina, D. (2019). Decoding motor neuron activity from epimysial thin-film electrode recordings following targeted muscle reinnervation. *Journal of Neural Engineering*, *16*(1), 016010. https://doi.org/10.1088/1741-2552/aaed85

Naples, G. G., Mortimer, J. T., Scheiner, A., & Sweeney, J. D. (1988). A spiral nerve cuff electrode for peripheral nerve stimulation. *IEEE Transactions on Biomedical Engineering*, *35*(11), 905–916. https://doi.org/10.1109/10.8670

Negro, F., Muceli, S., Castronovo, A. M., Holobar, A., & Farina, D. (2016). Multi-channel intramuscular and surface EMG decomposition by convolutive blind source separation. *Journal of Neural Engineering*, *13*(2), 026027. https://doi.org/10.1088/1741-2560/13/2/026027

Ngeo, J. G., Tamei, T., & Shibata, T. (2014). Continuous and simultaneous estimation of finger kinematics using inputs from an EMG-to-muscle activation model. *Journal of NeuroEngineering and Rehabilitation*, *11*(1), 122. https://doi.org/10.1186/1743-0003-11-122

Nielsen, J. L. G., Holmgaard, S., Jiang, N., Englehart, K. B., Farina, D., & Parker, P. A. (2011). Simultaneous and Proportional Force Estimation for Multifunction Myoelectric Prostheses Using Mirrored Bilateral Training. *IEEE Transactions on Biomedical Engineering*, *58*(3), 681–688. https://doi.org/10.1109/TBME.2010.2068298

Ortiz-Catalan, M., Hakansson, B., & Branemark, R. (2014). An osseointegrated human-machine gateway for long-term sensory feedback and motor control of artificial limbs. *Science Translational Medicine*, *6*(257), 257re6-257re6. https://doi.org/10.1126/scitranslmed.3008933

Pasquina, P. F., Evangelista, M., Carvalho, A. J., Lockhart, J., Griffin, S., Nanos, G., Hankin, D. (2015). First-in-man demonstration of a fully implanted myoelectric sensors system to control an advanced electromechanical prosthetic hand. *Journal of Neuroscience Methods*, *244*, 85–93. https://doi.org/10.1016/j.jneumeth.2014.07.016

Popov, B. (1965). The bio-electrically controlled prosthesis. *The Journal of Bone and Joint Surgery. British Volume*, *47-B*(3), 421–424. https://doi.org/10.1302/0301-620X.47B3.421

Popovic, D. B., Stein, R. B., Jovanovic, K. L., Dai, R., Kostov, A., & Armstrong, W. W. (1993). Sensory nerve recording for closed-loop control to restore motor functions. *IEEE Transactions on Biomedical Engineering*, *40*(10), 1024–1031. https://doi.org/10.1109/10.247801

Prahm, C., Paassen, B., Schulz, A., Hammer, B., & Aszmann, O. (2017). Transfer Learning for Rapid Re-calibration of a Myoelectric Prosthesis After Electrode Shift. In J. Ibáñez, J. González-Vargas, J. M. Azorín, M. Akay, & J. L. Pons (Eds.), *Converging Clinical and Engineering Research on Neurorehabilitation II* (pp. 153–157). Springer International Publishing.

Raspopovic, S., Capogrosso, M., Petrini, F. M., Bonizzato, M., Rigosa, J., Pino, G. D., Micera, S. (2014). Restoring Natural Sensory Feedback in Real-Time Bidirectional Hand Prostheses. *Science Translational Medicine*, *6*(222), 222ra19-222ra19. https://doi.org/10.1126/scitranslmed.3006820

Roche, A. D., Rehbaum, H., Farina, D., & Aszmann, O. C. (2014). Prosthetic Myoelectric Control Strategies: A Clinical Perspective. *Current Surgery Reports*, *2*(3), 1–11. https://doi.org/10.1007/s40137-013-0044-8

Rossini, P. M., Micera, S., Benvenuto, A., Carpaneto, J., Cavallo, G., Citi, L., Dario, P. (2010). Double nerve intraneural interface implant on a human amputee for robotic hand control. *Clinical Neurophysiology*, *121*(5), 777–783. https://doi.org/10.1016/j.clinph.2010.01.001

Sahin, M., & Durand, D. M. (1998). Improved nerve cuff electrode recordings with subthreshold anodic currents. *IEEE Transactions on Biomedical Engineering*, *45*(8), 1044–1050. https://doi.org/10.1109/10.704873

Sahin, Mesut, Haxhiu, M. A., Durand, D. M., & Dreshaj, I. A. (1997). Spiral nerve cuff electrode for recordings of respiratory output. *Journal of Applied Physiology*, *83*(1), 317–322. https://doi.org/10.1152/jappl.1997.83.1.317

Saridis, G. N., & Gootee, T. P. (1982). EMG Pattern Analysis and Classification for a Prosthetic Arm. *IEEE Transactions on Biomedical Engineering*, *BME-29*(6), 403–412. https://doi.org/10.1109/TBME.1982.324954

Sartori, M., Reggiani, M., Mezzato, C., & Pagello, E. (2009). A lower limb EMG-driven biomechanical model for applications in rehabilitation robotics. In *2009 International Conference on Advanced Robotics* (pp. 1–7).

Sartori, M., Durandau, G., Došen, S., & Farina, D. (2018). Robust simultaneous myoelectric control of multiple degrees of freedom in wrist-hand prostheses by real-time neuromusculoskeletal modeling. *Journal of Neural Engineering*, *15*(6), 066026. https://doi.org/10.1088/1741-2552/aae26b

Sartori, M., Farina, D., & Lloyd, D. G. (2014). Hybrid neuromusculoskeletal modeling to best track joint moments using a balance between muscle excitations derived from electromyograms and optimization. *Journal of Biomechanics*, *47*(15), 3613–3621. https://doi.org/10.1016/j.jbiomech.2014.10.009

Sartori, M., Reggiani, M., Farina, D., & Lloyd, D. G. (2012). EMG-Driven Forward-Dynamic Estimation of Muscle Force and Joint Moment about Multiple Degrees of Freedom in the Human Lower Extremity. *PLOS ONE*, *7*(12), e52618. https://doi.org/10.1371/journal.pone.0052618

Schultz, A. E., & Kuiken, T. A. (2011). Neural Interfaces for Control of Upper Limb Prostheses: The State of the Art and Future Possibilities. *PM&R*, *3*(1), 55–67. https://doi.org/10.1016/j.pmrj.2010.06.016

Scott, R. N., & Dorcas, D. S. (1966). A three-state myoelectric control system. *Med Biol Eng*, *4*, 367.

Simon, A. M., Hargrove, L. J., Lock, B. A., & Kuiken, T. A. (2011). Target Achievement Control Test: Evaluating real-time myoelectric pattern-recognition control of multifunctional upper-limb prostheses. *The Journal of Rehabilitation Research and Development*, *48*(6), 619. https://doi.org/10.1682/JRRD.2010.08.0149

Smith, L. H., Kuiken, T. A., & Hargrove, L. J. (2016). Evaluation of Linear Regression Simultaneous Myoelectric Control Using Intramuscular EMG. *IEEE Transactions on Biomedical Engineering*, *63*(4), 737–746. https://doi.org/10.1109/TBME.2015.2469741

Smith, L. H., Kuiken, T. A., & Hargrove, L. J. (2015). Use of probabilistic weights to enhance linear regression myoelectric control. *Journal of Neural Engineering*, *12*(6), 066030. https://doi.org/10.1088/1741-2560/12/6/066030

Smith, R. J., Huberdeau, D., Tenore, F., & Thakor, N. V. (2009). Real-time myoelectric decoding of individual finger movements for a virtual target task. In *2009 Annual International Conference of the IEEE Engineering in Medicine and Biology Society* (pp. 2376–2379). https://doi.org/10.1109/IEMBS.2009.5334981

Soukoreff, R. W., & MacKenzie, I. S. (2004). Towards a standard for pointing device evaluation, perspectives on 27 years of Fitts' law research in HCI. *International Journal of Human-Computer Studies*, *61*(6), 751–789. https://doi.org/10.1016/j.ijhcs.2004.09.001

Stango, A., Negro, F., & Farina, D. (2015). Spatial Correlation of High Density EMG Signals Provides Features Robust to Electrode Number and Shift in Pattern Recognition for Myocontrol. *IEEE Transactions on Neural Systems and Rehabilitation Engineering*, *23*(2), 189–198. https://doi.org/10.1109/TNSRE.2014.2366752

Stewart, J. D. (2003). Peripheral nerve fascicles: Anatomy and clinical relevance. *Muscle & Nerve*, *28*(5), 525–541. https://doi.org/10.1002/mus.10454

Struijk, J. J., Thomsen, M., Larsen, J. O., & Sinkjaer, T. (1999). Cuff electrodes for long-term recording of natural sensory information. *IEEE Engineering in Medicine and Biology Magazine*, *18*(3), 91–98. https://doi.org/10.1109/51.765194

Stubblefield, K. A., Miller, L. A., Lipschutz, R. D., & Kuiken, T. A. (2009). Occupational therapy protocol for amputees with targeted muscle reinnervation. *Journal of Rehabilitation Research and Development*, *46*(4), 481–488.

Tan, D. W., Schiefer, M. A., Keith, M. W., Anderson, J. R., Tyler, J., & Tyler, D. J. (2014). A neural interface provides long-term stable natural touch perception. *Science Translational Medicine*, *6*(257), 257ra138-257ra138. https://doi.org/10.1126/scitranslmed.3008669

Tang, Y., Wodlinger, B., & Durand, D. M. (2014). Bayesian Spatial Filters for Source Signal Extraction: A Study in the Peripheral Nerve. *IEEE Transactions on Neural Systems and Rehabilitation Engineering*, *22*(2), 302–311. https://doi.org/10.1109/TNSRE.2014.2303472

Tenore, F. V. G., Ramos, A., Fahmy, A., Acharya, S., Etienne-Cummings, R., & Thakor, N. V. (2009). Decoding of Individuated Finger Movements Using Surface Electromyography. *IEEE Transactions on Biomedical Engineering*, *56*(5), 1427–1434. https://doi.org/10.1109/TBME.2008.2005485

Thompson, D. E., Quitadamo, L. R., Mainardi, L., Laghari, K. ur R., Gao, S., Pieter-Jan Kindermans, Huggins, J. E. (2014). Performance measurement for brain–computer or brain–machine interfaces: a tutorial. *Journal of Neural Engineering*, *11*(3), 035001. https://doi.org/10.1088/1741-2560/11/3/035001

Ting, L. H., & Macpherson, J. M. (2005). A Limited Set of Muscle Synergies for Force Control During a Postural Task. *Journal of Neurophysiology*, *93*(1), 609–613. https://doi.org/10.1152/jn.00681.2004

Todorov, E., Erez, T., & Tassa, Y. (2012). MuJoCo: A physics engine for model-based control. In *2012 IEEE/RSJ International Conference on Intelligent Robots and Systems* (pp. 5026–5033). https://doi.org/10.1109/IROS.2012.6386109

Tsenov, G., Zeghbib, A. H., Palis, F., Shoylev, N., & Mladenov, V. (2006). Neural Networks for Online Classification of Hand and Finger Movements Using Surface EMG signals. In *2006 8th Seminar on Neural Network Applications in Electrical Engineering* (pp. 167–171). https://doi.org/10.1109/NEUREL.2006.341203

Twardowski, M. D., Roy, S. H., Li, Z., Contessa, P., Luca, G. D., & Kline, J. C. (2019). Motor unit drive: a neural interface for real-time upper limb prosthetic control. *Journal of Neural Engineering*, *16*(1), 016012. https://doi.org/10.1088/1741-2552/aaeb0f

Tyler, D. J., & Durand, D. M. (2002). Functionally selective peripheral nerve stimulation with a flat interface nerve electrode. *IEEE Transactions on Neural Systems and Rehabilitation Engineering*, *10*(4), 294–303. https://doi.org/10.1109/TNSRE.2002.806840

Ursu, D. C., Urbanchek, M. G., Nedic, A., Cederna, P. S., & Gillespie, R. B. (2016). In vivo characterization of regenerative peripheral nerve interface function. *Journal of Neural Engineering*, *13*(2), 026012. https://doi.org/10.1088/1741-2560/13/2/026012

Vidovic, M. M.-, Hwang, H., Amsüss, S., Hahne, J. M., Farina, D., & Müller, K. (2016). Improving the Robustness of Myoelectric Pattern Recognition for Upper Limb Prostheses by Covariate Shift Adaptation. *IEEE Transactions on Neural Systems and Rehabilitation Engineering*, *24*(9), 961–970. https://doi.org/10.1109/TNSRE.2015.2492619

Vu, P. P., Irwin, Z. T., Bullard, A. J., Ambani, S. W., Sando, I. C., Urbanchek, M. G., … Chestek, C. A. (2018). Closed-Loop Continuous Hand Control via Chronic Recording of Regenerative Peripheral Nerve Interfaces. *IEEE Transactions on Neural Systems and Rehabilitation Engineering*, *26*(2), 515–526. https://doi.org/10.1109/TNSRE.2017.2772961

Weir, R. F., Troyk, P. R., DeMichele, G. A., Kerns, D. A., Schorsch, J. F., & Maas, H. (2009). Implantable Myoelectric Sensors (IMESs) for Intramuscular Electromyogram Recording. *IEEE Transactions on Biomedical Engineering*, *56*(1), 159–171. https://doi.org/10.1109/TBME.2008.2005942

Wendelken, S., Page, D. M., Davis, T., Wark, H. A. C., Kluger, D. T., Duncan, C., Clark, G. A. (2017). Restoration of motor control and proprioceptive and cutaneous sensation in humans with prior upper-limb amputation via multiple Utah Slanted Electrode Arrays (USEAs) implanted in residual peripheral arm nerves. *Journal of NeuroEngineering and Rehabilitation*, *14*, 121. https://doi.org/10.1186/s12984-017-0320-4

Wodlinger, B., & Durand, D. M. (2009). Localization and Recovery of Peripheral Neural Sources With Beamforming Algorithms. *IEEE Transactions on Neural Systems and Rehabilitation Engineering*, *17*(5), 461–468. https://doi.org/10.1109/TNSRE.2009.2034072

Woo, S. L., Kung, T. A., Brown, D. L., Leonard, J. A., Kelly, B. M., & Cederna, P. S. (2016). Regenerative Peripheral Nerve Interfaces for the Treatment of Postamputation Neuroma Pain: A Pilot Study. *Plastic and Reconstructive Surgery Global Open*, *4*(12). https://doi.org/10.1097/GOX.0000000000001038

Wu, W., Gao, Y., Bienenstock, E., Donoghue, J. P., & Black, M. J. (2006). Bayesian Population Decoding of Motor Cortical Activity Using a Kalman Filter. *Neural Computation*, *18*(1), 80–118. https://doi.org/10.1162/089976606774841585

Young, A. J., Hargrove, L. J., & Kuiken, T. A. (2011). The Effects of Electrode Size and Orientation on the Sensitivity of Myoelectric Pattern Recognition Systems to Electrode Shift. *IEEE Transactions on Biomedical Engineering*, *58*(9), 2537–2544. https://doi.org/10.1109/TBME.2011.2159216

Zhou, P., Lowery, M. M., Englehart, K. B., Huang, H., Li, G., Hargrove, L., Kuiken, T. A. (2007). Decoding a New Neural–Machine Interface for Control of Artificial Limbs. *Journal of Neurophysiology*, *98*(5), 2974–2982. https://doi.org/10.1152/jn.00178.2007

Ziegler-Graham, K., MacKenzie, E. J., Ephraim, P. L., Travison, T. G., & Brookmeyer, R. (2008). Estimating the Prevalence of Limb Loss in the United States: 2005 to 2050. *Archives of Physical Medicine and Rehabilitation*, *89*(3), 422–429. https://doi.org/10.1016/j.apmr.2007.11.005